

07582-6001-R000  
Volume I

NT NO 07582-6001-R000  
Vol 1

# FEASIBILITY STUDY OF POSITIVE GAUGING SYSTEMS

## PHASE I REPORT PRELIMINARY ANALYSES

CONTRACT NO. NAS9-6750

SEPTEMBER 1967

FACILITY FORM 602	<u>N70-72371</u> (ACCESSION NUMBER)	(THRU)
	<u>171</u> (PAGES)	<u>None</u> (CODE)
	<u>C8-92063</u> (NASA CR OR TMX OR AD NUMBER)	(CATEGORY)

**TRW**  
SYSTEMS GROUP

FEASIBILITY STUDY OF  
POSITIVE GAUGING SYSTEMS  
PHASE I - PRELIMINARY ANALYSES

Contract NAS9-6750

September 1967


**TRW**  
SYSTEMS GROUP

Prepared for  
NATIONAL AERONAUTICS AND SPACE ADMINISTRATION  
MANNED SPACECRAFT CENTER  
Houston, Texas

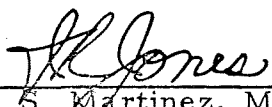
Prepared by:

S. Lieberman  
E. J. McGrath  
B. Siegel

Under the direction of

  
B. Siegel  
Program Manager

Approved by

  
for J. S. Martinez, Manager  
Technology Laboratory

## ABSTRACT

This report describes the work performed during the first phase of the Feasibility Study of Positive Gauging Systems for NASA/Manned Spacecraft Center under Contract NAS9-6750.

The primary objective of this program is to demonstrate the feasibility of an advanced storable propellant mass gauging system capable of operating independently of the propellant location or magnitude of a gravity field. The program is divided into two phases. The first phase consists of a systematic study of various possible gauging systems followed by analyses to establish their capability and feasibility. The second phase consists of an extensive investigation of the system deemed most promising by TRW, with NASA in concurrence.

During Phase I, a systematic effort was undertaken to identify and evaluate all possible gauging concepts. Over 50 separate concepts for gauging propellants were identified during this period: Preliminary analyses of the more promising approaches were then performed. As a result of these analyses, a Resonant Infrasonic Gauging System (RIGS) was selected for study in Phase II. A helium balance system, the RHO gauge, also appeared to offer appreciable promise.

# CONTENTS

	<u>Page</u>
1. INTRODUCTION . . . . .	1-1
2. GENERAL GAUGING SYSTEM CONSIDERATIONS . . . . .	2-1
2.1 Functions of a Propellant Gauging System. . . . .	2-1
2.1.1 Characteristics of an Ideal Gauging System . . . . .	2-3
2.1.2 System Characteristics . . . . .	2-4
2.1.3 Gauging Under Normal Gravity Conditions. . . . .	2-6
2.1.4 Gauging in a Bladder Tank Under Low Gravity . . . . .	2-8
2.1.5 Gauging in a Low Gravity Environment. . .	2-11
2.2 Propellant Characteristics. . . . .	2-20
2.2.1 Physical Properties of Propellants . . . . .	2-20
2.2.2 Transmission Characteristics of Propellants . . . . .	2-21
3. OUTLINE OF POSSIBLE GAUGING TECHNIQUES . . . . .	3-1
3.1 Acoustical Techniques. . . . .	3-1
3.1.1 Infrasonic Systems . . . . .	3-2
3.2 Interaction with an Electromagnetic Field. . . . .	3-17
3.2.1 Radio Frequency Techniques . . . . .	3-21
3.2.2 Interaction with Light Beams . . . . .	3-24
3.2.3 Gamma and X-Ray Techniques . . . . .	3-31
3.3 Interaction with Other Fields and Beams . . . . .	3-32
3.3.1 Gravitational Field Measurement . . . . .	3-32
3.3.2 Electric Field Interaction . . . . .	3-33
3.3.3 Magnetic Fields Interactions . . . . .	3-37
3.3.4 Interaction with Neutron Beams . . . . .	3-39
3.4 Other Direct Measuring Techniques. . . . .	3-42
3.4.1 Inertial Measuring Techniques . . . . .	3-42
3.4.2 Titration Techniques. . . . .	3-44
3.5 Ullage Volume Measuring Systems . . . . .	3-45
3.5.1 Pressurant Gas Balance Systems. . . . .	3-45
3.5.2 Tracer Gas Dilution Systems . . . . .	3-49

## CONTENTS (Continued)

	<u>Page</u>
4. PRELIMINARY ANALYSIS OF GAUGING SYSTEMS	
4.1 Infrasonic Systems . . . . .	4-1
4.1.1 Phase Sensitive Infrasonic System. . . . .	4-1
4.1.2 Resonant Infrasonic Gauging System . . . . .	4-13
4.1.3 Preliminary Error Analysis of the RIGS System . . . . .	4-24
4.2 Helium Balance System . . . . .	4-28
4.2.1 Analysis of the RHO Gauge System . . . . .	4-28
4.2.2 Application of the RHO Gauge to Zero Gravity Gauging . . . . .	4-42
4.3 Analysis of a Radiotracer Gas Dilution Gague in a Bladderless Tank . . . . .	4-45
4.3.1 System Description. . . . .	4-45
4.3.2 Discussion . . . . .	4-45
4.3.3 Conclusions. . . . .	4-52
5. SUMMARY AND RECOMMENDATIONS. . . . .	5-1
5.1 Introduction. . . . .	5-1
5.2 Results of General Survey . . . . .	5-1
5.3 Results of Preliminary Analysis . . . . .	5-5
5.3.1 Light Interaction Systems . . . . .	5-5
5.3.2 Infrasonic Systems . . . . .	5-6
5.3.3 Helium Balance System . . . . .	5-7
5.3.4 Ullage Gas Tracer Systems . . . . .	5-8
5.4 Recommendations . . . . .	5-8
APPENDIX A. . . . .	A-1
APPENDIX B. . . . .	B-1

## ILLUSTRATIONS

		Page
2-1	Effect of Gravity on a Level Gauge . . . . .	2-7
2-2	Level Increase Versus Acceleration . . . . .	2-7
2-3	Geometry of Tank . . . . .	2-14
2-4	Diffusion-Limited Mixing Process . . . . .	2-19
2-5	Rate of $N_2O_4$ Diffusion into Helium . . . . .	2-19
2-6	Light Attenuation Characteristics . . . . .	2-21
2-7	Photon Transmission in $N_2O_4$ Oxidizer . . . . .	2-24
2-8	Photon Transmission in Aerozine-50 Fuel . . . . .	2-24
2-9	Neutron Transmission, 8 Mev "Removal" . . . . .	2-24
3-1	Simple Piston System . . . . .	3-3
3-2	Piston System with Reference Volume . . . . .	3-4
3-3	Variation of Gamma with $N_2O_4$ Concentration and Temperature . . . . .	3-5
3-4	Acoustical, Electrical and Mechanical Analogues . . . . .	3-6
3-5	Helmholtz Resonator . . . . .	3-7
3-6	Acoustica Propellant Gauge . . . . .	3-8
3-7	Phase Sensitive Infrasonic System . . . . .	3-10
3-8	Resonant Infrasonic Gauging System, RIGS . . . . .	3-11
3-9	RIGS Response . . . . .	3-11
3-10	Submerged Gas Pocket Analogues . . . . .	3-12
3-11	Effect of Frequency of Gas Pocket Attenuation . . . . .	3-13
3-12	Typical Mode Pattern in Propellant Tank . . . . .	3-16
3-13	Electromagnetic Radiation Spectrum . . . . .	3-18
3-14	Dielectric Effect of a Polar Molecule . . . . .	3-19
3-15	Loss Factor for Fuel Versus Frequency . . . . .	3-20





# Illustrations (Continued)

	Page
4-14 Effect of Resistance on Phase Angle, $V = 0.3 \text{ ft}^3$ . . . . .	4-23
4-15 Effect of Resistance on Phase Angle, $V = 2 \text{ ft}^3$ . . . . .	4-23
4-16 Effect of Resistance on Phase Angle, $V = 12 \text{ ft}^3$ . . . . .	4-23
4-17 Variation $\lambda$ With Firing Time . . . . .	4-26
4-18 Effect of Firing on $\lambda$ Correction . . . . .	4-26
4-19 Mass Attenuation, Coefficients for the Elements — H, He, O, N, and C . . . . .	4-31
4-20 Mass Attenuation Coefficients for He, $\text{N}_2\text{O}_4$ , and Aerozine-50 . . . . .	4-33
4-21 Assumed Gas Mixture Characteristics . . . . .	4-37
4-22 Effect of Temperature on the Attenuation of Radiation by the He- $\text{N}_2\text{O}_4$ Ullage at a Constant Pressure of 200 psi . . . . .	4-38
4-23 Effect of Temperature on Attenuation of Radiation by the Assumed He-Aerozine-50 Ullage at a Constant Pressure of 200 psi . . . . .	4-39
4-24 Henry's Constant for Aerozine-50 and Nitrogen Tetroxide .	4-49
4-25 Performance of Hypothetical Helium Radiotracer Propellant Gauging System . . . . .	4-50
4-26 Performance of $^{39}\text{A}$ Radiotracer Propellant Gauging System . . . . .	4-50
4-27 Performance of $^{85}\text{Kr}$ Radiotracer Propellant Gaging System . . . . .	4-51
4-28 Performance of $^{39}\text{A}$ Radiotracer System for Different Temperature . . . . .	4-51
4-29 Effect of Increment Size of Gauging System Performance, Fuel Expelled in Equal Increments . . . . .	4-53
B-1 Schematic of Infrasonic Propellant Gauge . . . . .	B-2
B-2 Schematic of RIGS . . . . .	B-14

# TABLES

	Page
2-1 Evaluation Criteria for a Positive Propellant Gauging System . . . . .	2-2
2-2 Existing High Gravity Gauging System . . . . .	2-5
2-3 Gauging Systems for Bladder Tanks . . . . .	2-9
2-4 Gas Diffusion Rates (200 psi) . . . . .	2-10
2-5 Properties of Nitrogen Tetroxide, (NTO), $N_2O_4$ . . . . .	2-22
2-6 Properties of Aerozine-50 (A-50, 50/50, UDMH/Hydrazine), $(CH_2)N_2H_2/N_2H_4$ . . . . .	2-23
4-1 RIGS Error Analysis Estimate . . . . .	4-27
4-2 Helium Balance Error Estimate . . . . .	4-44
4-3 Ratio of Moles in Gas Versus Volume . . . . .	4-52
5-1 Summary of Gauging Principles . . . . .	5-2
A-1 General Survey Participants and Backgrounds . . . . .	A-2
B-1 Nomenclature for Appendix B . . . . .	B-3

## 1. INTRODUCTION

Accurate measurement of propellant quantity in liquid propulsion systems has become increasingly important as manned missions become longer and more demanding. Until recently, the major emphasis has been on gauging systems capable of performing the propellant utilization function. Since the propellant is predictably oriented during engine firing, this function is adequately performed by gauges which measure the propellant level in the tanks. However, future missions will include lengthy coast periods and require the measurement of randomly-oriented propellant quantities during extended periods of zero gravity.

The Feasibility Study of Positive Gauging Systems is divided into two phases. The first phase is a preliminary analysis of concepts for propellant gauging systems capable of operation under zero gravity. The second phase is a detailed investigation of the most promising concept identified during Phase I.

This report presents the results of the first phase of the program during which a concerted effort was undertaken to identify and evaluate all possible gauging system concepts. Two techniques were employed to originate new systems. A morphological survey of the properties of the propellants and pressurant gas was made to determine which properties might form the basis of a propellant gauging system. The second approach consisted of bringing together, in a series of brainstorming sessions, knowledgeable experts from diverse fields to identify and evaluate new propellant gauging concepts. Over 50 separate concepts for gauging propellants were uncovered by this approach. The relative advantages, limitations, and characteristics of these systems were studied. The main criterion for evaluating these systems was their capability to gauge the quantity of storable propellants under zero gravity in a tank without a bladder. The propellants specified for the study were Aerozine-50 and nitrogen tetroxide. Other criteria used in the evaluation are delineated in Section 2 and summarized in Table 2-1. The results of the Phase I evaluations indicated that a Resonant Infrasonic Gauging System (RIGS) appeared to be the most promising system. A helium balance system, the RHO gauge, also appeared to offer appreciable promise. However, these conclusions might differ for other propellant combinations.

A brief description of some of the systems considered will be found in Section 3 of the report. Section 4 contains a preliminary analysis of the more promising systems. Section 5 summarizes the results of this phase of the study and presents the logic leading up to the selection of the RIGS for Phase II of this study.

## 2. GENERAL GAUGING SYSTEM CONSIDERATIONS

In a general study of this type, it is necessary to clearly establish detailed evaluation criteria in order to provide a common basis of comparison for all the proposed systems. The evaluation criteria (summarized in Table 2-1) were derived from consideration of the functional use of the system, the performance requirements, the proposed application, and the mission requirements. These criteria were used in the General Survey of Phase I for rapid, systematic evaluation of the various concepts. Systems not capable of meeting many of the criteria were eliminated from consideration before a major effort had been expended.

One additional constraint was placed on the systems evaluated during the general survey—all systems, in order to merit further study, must offer a potential for gauging under zero and low gravity conditions in a bladderless tank. Inability to measure propellant quantity under high gravity, while counting against the system, was not sufficient to eliminate it from further study.

### 2.1 FUNCTIONS OF A PROPELLANT GAUGING SYSTEM

The purpose of a propellant gauging system is to measure the quantity of propellant available for use in the propulsion device.

This information is required for a variety of reasons:

- Determination of remaining total impulse capability
- Leak detection
- Mixture ratio control
- Center of gravity control
- Malfunction analysis
- Verification of propellant loading

It will be noted that of these functions two are performed under the influence of a gravity field: mixture ratio control is accomplished during engine firing and propellant loading is performed on the ground. The determination of the remaining available impulse, leak detection, and

Table 2-1. Evaluation Criteria for a Positive Propellant Gauging System

Criteria Specified by RFP	
<ul style="list-style-type: none"> <li>• Able to detect and monitor the propellant with an accuracy of <math>\pm 0.5\%</math> full load, varying linearly to <math>\pm 0.25\%</math> tank empty while in the following environment:               <ul style="list-style-type: none"> <li>• During extended periods of zero gravity and vacuum conditions</li> <li>• During loading and unloading of propellants</li> <li>• During boost phase of mission</li> <li>• During engine operation</li> </ul> </li> </ul>	<ul style="list-style-type: none"> <li>• Insensitive to temperature changes within the propellants or ability to compensate for these changes</li> <li>• Compatible with Apollo propellants (<math>N_2O_4</math> oxidizer, 50% UDMH/50% hydrazine fuel)</li> <li>• Weight (<math>\leq 50</math> lbs); Power — minimum possible</li> <li>• Present no hazards to human life (nuclear gauging systems will not create radiation dose levels at 50 inches greater than 0.1 mrem/hr)</li> <li>• Capable of ease of installation and require no hardware modifications (special tank fabrication)</li> </ul>
Additional Criteria	
<ul style="list-style-type: none"> <li>• Compatible with man-rated application (safety, hazards, redundancy, etc.)</li> <li>• Capable of providing data on an individual propellant tank basis for use in spacecraft center of gravity control</li> <li>• Capable of high response rate with continuous readout capability</li> <li>• Capable of accurate operation in propulsion system environment (launch, hard vacuum, temperature extremes) and insensitive to effects of changes</li> <li>• Provide propellant leak-detection capability for use with spacecraft malfunction detection system</li> <li>• Compatible with and possibly capable of determining pressurant leakage in either the propellant tank ullage space or the gas pressurization system</li> <li>• Capable of maintaining accuracy despite occasional propellant tank venting</li> <li>• Not degraded by propellant-to-pressurant and pressurant-to-propellant diffusion</li> <li>• Should not require independent recalibration</li> </ul>	<ul style="list-style-type: none"> <li>• Capable of use in a propellant utilization system</li> <li>• Capable of use in a propellant loading system</li> <li>• Simple data collection, data processing, and computation equipment</li> <li>• Simple calibration and system checkout requirements</li> <li>• Potential for in-space maintenance and repair</li> <li>• Insensitive to electromagnetic interference</li> <li>• Minimum interference with tank design</li> <li>• Insensitive to propellant containment or settling approach</li> <li>• Insensitive to mission duration</li> <li>• Insensitive to engine duty cycle</li> <li>• Insensitive to stratification of propellant or pressurant</li> </ul>

center of gravity control are primarily required during the coast or low g portion of the flight, while malfunction analysis may be needed at any time.

Each of the different functions has different accuracy requirements. For example, mixture ratio control or propellant utilization places very stringent accuracy requirements on the gauging system. On the other hand, determination of the remaining impulse capabilities during zero gravity flight usually presents a less stringent requirement. The accuracy required is also a function of the mission. As a particular mission becomes more difficult, or even marginal, greater accuracy is usually demanded of the propellant gauging system.

#### 2.1.1 Characteristics of an Ideal Gauging System

An ideal positive gauging system should indicate the quantity of propellant remaining in the propellant tanks at all times. The majority of the present propellant gauging systems in spacecraft use cannot do this. For example, the Apollo SPS propellant gauging and utilization system is basically a level sensing device which measures the quantity of propellant remaining in the propellant tank only when the engine is firing. Between engine firings, it merely indicates the propellant quantity present at the end of the last firing. This is not satisfactory for some missions. The astronaut does not have information early enough to permit a change of plans if, for example, a propellant leak were to occur between firings. The ideal positive propellant gauging system should be capable of indicating the quantity of propellant present during cruise operation under zero and low gravity conditions, and during engine operation. Accuracy should not be degraded during any of these phases.

The gauging system should require minimum interfaces and present minimum interference with the spacecraft. It should not require special tank design features and should not degrade system reliability or present any safety hazards. Performance should not be degraded by variations

in propellant temperature, mission duration, or operating duty cycle. Each system was examined in light of these goals, which are summarized in Table 2-1.

### 2.1.2 System Characteristics

The method used to orient the propellants in the tanks will have a major effect on the design and selection of the propellant gauging system. The two most common techniques are 1) use of a positive expulsion device such as a bladder, or diaphragm, and 2) use of an auxiliary engine to settle the propellants in the tanks. Since, in most cases, positive expulsion devices result in heavier systems, they are used when settling is not feasible or the propellant quantity is small. Most bipropellant RCS propulsion systems employ bladders.

Propellant settling without a containment device requires the use of a propulsion system. This technique is normally used for those applications where the weight savings derived through elimination of the bladder are significantly large to justify it. Most main propulsion systems use this technique (i.e., Apollo SPS, LMDE, LMAE). The differences in both the operating environments and in the problem areas associated with the two orientation techniques are sufficiently large that the system which appears best for one may not even be applicable to the other. Thus, while it is recognized that an ideal gauging system should be capable of operating independently of the acceleration field or orientation technique, this often may not be possible. In a study of this type it was necessary to establish a priority of requirements. Gauging systems which can measure the propellant quantity accurately at accelerations above 0.1 g are shown in Table 2-2. At low or zero gravity, developed systems do not exist. Feasibility has been demonstrated for a number of systems for propellant gauging in bladder tanks under low and zero gravity conditions. For unoriented propellant at low gravity no system exists at the present time for propellant gauging. Therefore, emphasis during this study was placed on gauging under low or zero gravity conditions in a bladderless tank.



Table 2-2. Existing High Gravity Gauging Systems

System	Principle of Operation	Major Advantages	Major Disadvantages
<u>Level Gauges</u>			
Capacitance	Measures capacitance of liquid in stillwell. Measured capacitance is then linear function of liquid level	Developed, good accuracy, low power, compensates for propellant density change	Complicated tank installation, high cost, subject to drift
Radioisotope	Measures attenuated gamma radiation between detector and source located in stillwell along length of tank.	Good accuracy Low power Compensates for propellant density change	Requires stillwell, handling of radioisotope
Point Sensors	Determines time when liquid level drops to sensor location (Capacitance hot wire, magnetostrictive and nuclear point sensor can be used)	Developed, highly accurate, simple installation. Excellent for propellant utilization. Can be spaced to provide more accuracy near tank depletion	Does not provide continuous reading Sensors can be skipped during multiple firings
<u>Other Types</u>			
Radio Frequency	Measures tank cavity mode frequency	Easy installation Light, simple	Not developed. Conductivity of fuel
Integrating Flowmeters	Measures propellant flowrate out of tank Integrates to obtain quantity used	Simple installation, light	Does not provide recalibration, cannot be used to check loading, error becomes large with multiple firings

### 2.1.3 Gauging Under Normal Gravity Conditions

A number of systems presently exist to measure propellant quantity under normal and high gravitational conditions. The majority of these systems measure the height of the propellant in a tank as shown in Figure 2-1. This height is then converted to volume, using the tank dimensions, and into mass, using the propellant density. Such systems range in accuracy and complexity from the simple float gauge in an automobile to the redundant capacitor and point sensor propellant utilization system on the Apollo vehicle. All of these height measuring devices, however, depend on the existence of a gravitational or acceleration field to maintain the propellant in a known spatial position in the tank. Usually, the height of propellant is measured at only one location in a tank and thus is sensitive both to random fluctuations in the propellant height, such as sloshing, as well as to systematic variations. The prime criterion which determines whether a level type gauge may be used is the relative size of the acceleration forces and the surface tension forces. At equilibrium, the buoyancy force will balance the surface tension force, causing a rise in liquid height in a tube.

$$F_{\text{ACCELERATION}} = F_{\text{Surface Tension}}$$

$$\pi r^2 h \rho a = 2\pi r \sigma \cos \theta$$

or

$$h = \frac{2\sigma \cos \theta}{r\rho a}$$

where h = height of liquid  
in tube above  
liquid level

$\theta$  = angle of contact

r = radius of tube

$\rho$  = density of liquid

$\sigma$  = surface tension

a = acceleration

If the acceleration force is not sufficiently large, the liquid will crawl up along the sides of the level gauge and invalidate the reading, as shown in Figure 2-1. This occurs when the acceleration force is roughly equal

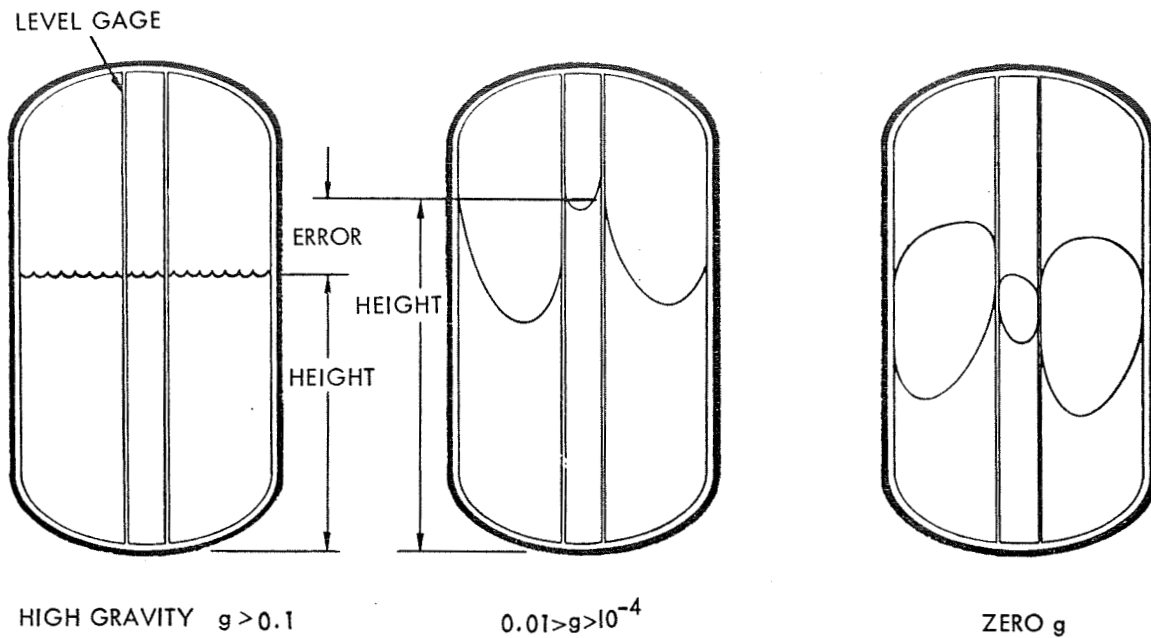


Figure 2-1. Effect of Gravity on a Level Gauge

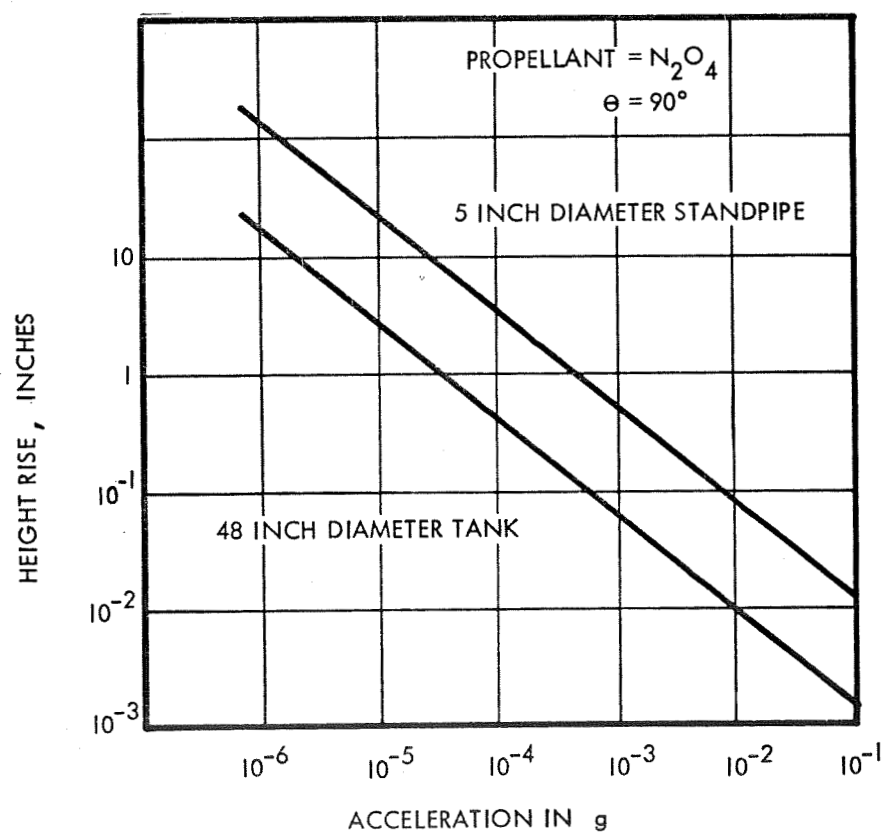


Figure 2-2. Level Increase Versus Acceleration

to the surface force. In Figure 2-2 the variation in height for  $N_2O_4$  in a typical propellant tank is shown as a function of the applied acceleration field.

Other techniques which indirectly depend on having oriented propellants may also be used for gauging propellant during engine firing. Integrating flowmeters can be used in missions where the propellant is used in one large single firing. Since they do not have the capability of independently recalibrating the propellant quantity, they are subject to appreciable errors as a result of either leakage or errors in loading. In addition, they lose accuracy when a large number of individual firings are performed.

In Table 2-2, a summary of the available high gravity gauges is presented, along with a brief summary of these characteristics.

#### 2.1.4 Gauging in a Bladder Tank Under Low Gravity

Feasibility has been demonstrated for a number of different techniques for gauging propellant quantity in a bladder-containing tank. Most of these systems, as shown in Table 2-3, actually measure the ullage gas volume. The primary problem areas for these systems are associated with the diffusion of propellant vapor into the ullage gas and the diffusion of constituents of the ullage gas into the propellant.

Diffusion of tracer gas through the bladder can degrade the accuracy of tracer gas systems, unless the diffusion rates are small and predictable. If appreciable diffusion occurs, the measured concentration of tracer gas will not indicate the true ullage volume.

Diffusion of propellant vapor into the ullage gas causes changes in the gas properties (as well as possibly corroding sensitive detection elements). The density of the vapor is appreciably different from the density of the pressurant. This can cause an error in the infrasonic systems if, due to stratification, the vapor composition in the ullage volume is different from the composition in the reference volume.

The PVT systems are also affected by propellant vapor diffusion. In the PVT system, the ullage volume is determined by a helium mass balance. If the gas in the ullage volume consists of an unknown mixture of helium and propellant vapor, an error is introduced. In the bladderless tank, the vapor concentration at equilibrium can be predicted by the

Table 2-3. Gauging Systems for Bladder Tanks

<u>System</u>	<u>Principle of Operation</u>	<u>Major Advantages</u>	<u>Major Disadvantages</u>
1. Pressurant Gas Balance			
1.1 PVT system	Maintains mass balance on pressurant through pressure and temperature measurements of gas in pressurant and propellant tanks and measurement of propellant temperature	Simple, low weight, low power	Low accuracy, needs separate pressurization system for each propellant tank
1.2 pV system	Maintains mass balance on pressurant through radiation attenuation density measurements of gas in propellant and pressurant tanks and measurement of propellant temperature	Same as above, with higher accuracy	Needs separate pressurization system for each propellant tank
2. Tracer Gas Systems			
2.1 Radioactive Tracer	Relates measurement of tracer gas concentration in ullage to propellant quantity Uses radiation detection measurements	Can be used for pressurant as well as propellant leak detection Digital signal output, high accuracy	Affected by diffusion of trace gas through bladder; cannot be used without bladder
2.2 Stable Tracer	Uses infrared detection measurements	No associated radiation	More complex and less accurate measurement than radioactive tracer
3. Acoustical Systems	Low-frequency pressure wave induced in propellant tank and reference volume. Relates phase shift of pressure signals to propellant quantity.	Rapid response mass readout	Sensitive to spacecraft vibrations and temperature gradients in propellant, and gas
4. Nuclear Attenuation	Relates attenuation of gamma radiation through propellant to propellant quantity	Direct mass measurement, completely external to tank	High external radiation field, tank-to-tank interference, relatively low accuracy

measurement of propellant bulk temperature and the propellant vapor pressure. In the bladder tank, equilibrium may never exist and the vapor concentration is a function of time.

During the past several years TRW has conducted experiments and analytical studies of the permeability of bladder materials in conjunction with several propellant gauging programs. These studies have included the diffusion rate measurements of helium, nitrogen, krypton, and carbon dioxide gases through several bladder materials. Gas diffusion data obtained to date are presented in Table 2-4.

The gas diffusion rates through bladders were determined by establishing a gas pressure gradient across a representative sample of the test material. The bladder sample is held between two gas vessels: a high pressure vessel which is maintained at 200 psig, and a low pressure vessel which is initially at either 1 or 15 psia. The rate at which gas diffuses through the specimen is determined by monitoring the pressure rise in the low pressure gas vessel.

The bladder samples have been found to obey Fick's law:

$$q = P_o A \Delta P$$

$q$  = gas permeation per unit time

$P_o$  = permeability constant

$A$  = sample area

$\Delta P$  = partial pressure differential

Table 2-4. Gas Diffusion Rates (200 psig)

Bladder Material	Gas Diffusion Rate, Standard cc/hr in <sup>2</sup>			
	<u>N<sub>2</sub></u>	<u>He</u>	<u>Kr</u>	<u>CO<sub>2</sub></u>
Teflon Laminate (TFE-FEP)	0.76-0.91	14.7-17.7	0.67	3.85
Aluminum Teflon Laminate	0.0034-0.006	0.0525		
Teflon Codispersion (TFE-FEP)	1.66	22.9		
Ethyl Propylene	0.256	1.144		

The leakage rate of  $N_2O_4$  through several bladder materials has been evaluated at TRW in two independent sets of experiments.  $N_2O_4$  leakage was measured through a Teflon-laminate bladder in a propellant tank at a rocket test stand and for a number of bladder materials in laboratory tests. No difference between the two sets of test data was discernible. The tests show that appreciable  $N_2O_4$  diffusion occurs through both Teflon bladder materials tested. The diffusion rate through the TFE codispersion Teflon material was measured to be  $0.3 \text{ mg/cm}^2/\text{hr}$ . The TFE/FEP Teflon-laminate material was appreciably better, with a diffusion rate of  $0.14 \text{ mg/cm}^2/\text{hr}$ . Tests on aluminized Teflon-laminate bladders indicated that the  $N_2O_4$  diffusion was negligible. Thus, it seems probable that adequate gauging accuracy could be obtained with any of the proposed systems provided the aluminized Teflon bladder is used.

A positive displacement device used to contain the propellant in the tank can also serve as a propellant gauging system if the dimensional changes in the device with outflow of propellant are predictable. Typical of such devices is the volatile liquid expulsion system which uses a bellows tank to contain the propellants. Simple measurement of the bellows extension gives a direct measurement of the propellant volume. Bladders do not readily lend themselves to the direct measurement of the contained volume because of variations in the shape the bladder can assume. However, by mechanically constraining the folding and location of the bladder, it appears feasible to use the measurement of key dimensions to obtain the liquid volume.

#### 2.1.5 Gauging in a Low Gravity Environment

Zero or low gravity imposes a large number of problems on propellant gauging in bladderless tanks which are usually not significant for a high gravity gauge. The first is that the actual propellant location is not usually known. Thus, systems which depend on measuring key dimensions of the propellant volume will be appreciably in error. The ideal measurement system should be sensitive only to propellant mass or volume and independent of the actual propellant location. As will be

shown in Section 3, this is difficult to achieve in practice and poses the single most severe constraint on the feasibility of potential gauging systems under zero gravity. For example, force fields follow an inverse square-of-the-distance law with obvious sensitivity to actual propellant location. Attenuation techniques, in general, follow exponential laws and are applicable primarily for narrow beams. In both of these cases, some improvement in performance can be achieved by using a large number of sensors and statistical weighing of the individual measurements with a resultant increase in weight and complexity.

Another problem in low gravity fields is that the propellant freely migrates under the influence of small accelerations caused by attitude control jets and personnel motion. Unless some effort is made to limit the motion of the liquid, it will tend to be somewhat randomly located. This results in difficulty when there is a requirement for communicating with or sampling the ullage gas. As the dominant force acting on the liquid is surface tension, controlled surface tension devices to partially orient the propellant are investigated in Section 2.1.5.1.

Under the best of conditions, when making an experimental measurement of a fluid property, the question arises as to whether a measurement made at a certain point is truly representative of the average bulk properties. Under zero gravity conditions, the uncertainty is greatly increased. Under conditions of normal gravity, natural convection causes most of the mixing. Under zero gravity conditions, whatever mixing does occur is by the much slower process of diffusion. This imposes an appreciable accuracy limitation on most proposed systems. Those systems which do not directly measure propellant mass require measurements of the propellant temperature to obtain the propellant density. If the measured temperature is appreciably different from the average bulk temperature of the propellant, the reported mass will be in error.

For assurance that the composition of the gas in the ullage space or in a reference volume is truly representative of the average gas composition, some type of gas-sampling technique is often required. This is particularly critical when fresh gas from the pressurant tank is passed into the ullage volume. In Section 2.1.5.2, the results of a brief study of gas and vapor stratification are presented.



In summary, an ideal propellant gauging system for operation at zero or low gravity should not be sensitive to the propellant location within the tank; should not require stratification sensitive measurements; and should be capable of operating whether the sensor is in contact with propellant or pressurant gas.

#### 2.1.5.1 Ullage Gas Orientation by Surface Treatment

A number of different systems examined in the study contained a requirement for a sensor to be located in an ullage bubble. While it is well known that liquid/gas separation can be obtained by the use of screens and other high surface tension devices, simpler techniques also appear possible, i. e., coating of portions of the tank wall with non-wetting materials.

This section describes the liquid behavior in a cylindrical tank under zero g environment. Particular attention is devoted to those applications for which it is desirable to have the ullage located at a definite region inside the tank at all times. Numerical results are carried out for a cylindrical tank of 48-inch diameter, 150-inch height and 89% filled with nitrogen tetroxide,  $N_2O_4$ . It is found that the interface will remain stable if the disturbance accelerations are less  $10^{-3}$  to  $10^{-4}$  g.

#### Static Interface Configuration Under Zero g

For a wetting surface with contact angle  $\theta (0^\circ \leq \theta \leq 90^\circ)$ , the static interface ( $z = y(r)$  in Figure 2-3) under zero g environment is a part of a spherical surface intersecting at an angle  $\theta$  with the tank wall (see, for example, Reference 2-1). The function  $y(r)$  is given by the equation below.

$$\left[ \sec \theta - (y - y_0)/a \right]^2 + (r/a)^2 = \sec^2 \theta \quad (2.1-1)$$

For  $\theta = 0^\circ$  ( $\sec \theta = 1$ ), Equation 2.1-1 shows that  $y(r)$  is a hemispherical surface and

$$y_0 = y(a) - a = h - a \quad (2.1-2)$$

For  $\theta = 90^\circ$  ( $\sec \theta = \infty$ ), Equation 2.1-2 shows that  $y(r)$  is a flat surface and

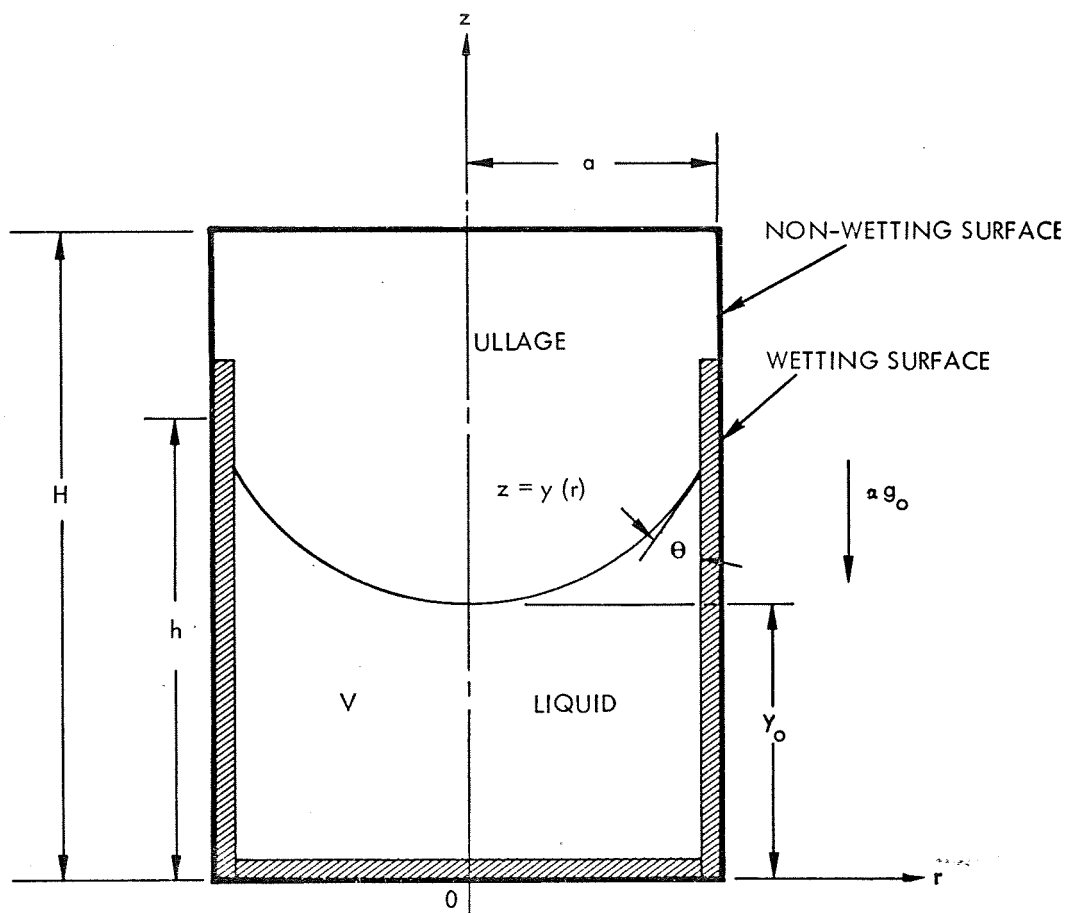


Figure 2-3. Geometry of Tank

$$y_0 = h + y(r) \quad (2.1-3)$$

For  $\theta = 0^\circ$  and a liquid volume  $V$  equal to 80% of the total tank volume.  $(\pi a^2 H)$  we find

$$V = \frac{89}{100} \pi a^2 (150) = \pi a^2 h - \frac{2}{3} \pi a^3 \quad (2.1-4)$$

or

$$h = \frac{2}{3}a + 133.50 = 149.50 \text{ in.} \quad (2.1-5)$$

and for  $\theta = 90^\circ$

$$V = \frac{89}{100} \pi a^2 (150) = \pi a^2 h \quad (2.1-6)$$

or

$$h = \frac{89}{100} (150) = 133.50 \text{ in.} \quad (2.1-7)$$

Thus if the interior surface of the tank is prepared so that the bottom surface and the portion of the cylindrical surface for  $0 \leq z \leq 149.50$  in. are wetting while the top surface and the portion of the cylindrical surface for  $149.5 \geq x \geq 150$  in. are non-wetting (Teflon, etc.), the ullage will always be at the top of the tank. The actual interface shape and the height  $h$  depend on the contact angle ( $\theta$  in Figure 2-3) between the liquid and the solid surface at the liquid-gas-solid intersection on the wall. For larger contact angles the allowable liquid volume is more than for smaller contact angles. Note that for  $\theta = 0^\circ$ , the maximum allowable percentage of liquid volume that can be stabilized for the selected tank configuration is determined from Equation 2.1-4 by letting  $H = h = 150$ .

$$\frac{x}{100} \pi a^2 (150) = \pi a^2 (150) - \frac{2}{3} \pi a^3 \quad (2.1-8)$$

or

$$x = 89.33333 \quad (2.1-9)$$

On the other hand if  $\theta = 90^\circ$ , this technique can be used for liquid volume up to 100% of the tank volume. For some typical values of contact angles for various solid-liquid-gas combinations see, for example, Reference 2-2.

#### Natural Frequencies of the Liquid

For  $\theta = 90^\circ$  (i.e., the case of a flat interface) the natural angular frequencies  $\omega_n$  of the liquid, including the surface tension effects, are given by the following expression (see, for example, Reference 2-3).

$$\omega_n^2 = \frac{\sigma}{\rho a^3} \left( k_{1n}^2 + B \right) k_{1n} \tanh k_{1n} \frac{h}{a} \quad (2.1-10)$$

where

$\sigma$  = surface tension of  $N_2O_4$  = 27.5 dyne/cm

$\rho$  = density of  $N_2O_4$  = 1.45 gm/cm<sup>3</sup>

$B = \frac{\alpha g_o \rho a^2}{\sigma} = 3146 \alpha$  = Bond number for  $N_2O_4$

$g_o$  = gravitational acceleration at sea level = 980.66 cm/sec<sup>2</sup>

$\alpha$  = acceleration level in g (2.1-11)

$k_{1n}$  = characteristic mode numbers

where  $k_{11} = 1.841$

$k_{12} = 5.331$

$k_{13} = 8.536$

$k_{14} = 11.706$

Thus for  $\alpha = 0$  (zero g environments) the fundamental natural frequency ( $n = 1$ ) for the 89% full tank of  $N_2O_4$  ( $h = 133.50$  in) according to Equation 2.1-7 is

$$\omega_1 = \left( \frac{\sigma}{\rho a^3} k_{11}^3 \tanh k_{11} \frac{h}{a} \right)^{1/2}$$

$$\omega_1 = \left[ \frac{27.5/1.45}{24^3} (1.841)^3 \tanh \left( 1.841 \frac{133.50}{24} \right) \right]^{1/2}$$

$$\omega_1 = 0.092520 \text{ rad/sec}$$

$$\text{or } f_1 = 0.014725 \text{ cps} \quad (2.1-12)$$

For contact angles other than 90° Reference 2-2 gives an approximate formula for the fundamental frequency

$$\omega_1^2 = \frac{\sigma}{\rho a^3} (6.255 + 1.841B - 4.755 \cos \theta) \tanh 1.841 \frac{y_0}{a} \quad (2.1-13)$$

Thus for  $\theta = 0^\circ$  in the case of 89% full liquid,  $y_0 = 149.50 - 24.00$  (according to Equations 2.1-2 and 2.1-5) and since at zero  $g$  we have  $B = 0$ .

$$\omega_1 = \left[ \frac{27.5/1.45}{24^3} (6.255 - 4.755) \tanh \left( 1.841 \frac{125.50}{24} \right) \right]^{1/2}$$

$$\omega_1 = 0.045354 \text{ rad/sec}$$

$$\text{or } f_1 = 0.0072183 \text{ cps} \quad (2.1-14)$$

To avoid resonance phenomena, any disturbance at or near these natural frequencies should be avoided.

#### Dynamic Stability Under Adverse Thrust

Equation 2.1-10 shows that if the Bond number,  $B$ , is more negative than  $-3.39$  (in the case of  $\theta = 90^\circ$ ), the frequency will be imaginary, indicating a dynamic instability. This corresponds to

$$\alpha = \frac{-3.39}{3146.37} = -1.08 \times 10^{-3} \quad (2.1-15)$$

Similarly, according to Equation 2.1-13, dynamic instability will occur in the case of  $\theta = 0^\circ$  if  $\alpha$  is more negative than

$$\alpha = \frac{-0.84}{3146.37} = -2.7 \times 10^{-4} \quad (2.1-16)$$

Equations 2.1-15 and 2.1-16 show that under transverse disturbance, an acceleration in excess of  $1.08 \times 10^{-3} g_0$  in  $-z$  direction (Figure 2-3) in the case of  $\theta = 90^\circ$ , or an acceleration in excess of  $2.7 \times 10^{-4} g$  in  $-z$  direction in the case of  $\theta = 0^\circ$ , will render the liquid unstable.

#### 2.1.5.2 Mixing Processes in Vapor-Gas Mixtures

In this section, a brief discussion of the mixing rates of helium and propellant vapor under zero gravity will be presented. Since some of

the systems discussed in Section 3 are dependent upon obtaining good mixing between the helium and propellant vapor, some estimates are required of the time that it will take a vapor/gas mixture to attain equilibrium.

The mixing process between gas and vapor under normal gravity conditions is controlled by three processes: forced convection, free convection, and diffusion. Under zero gravity, free convection under the influence of temperature gradients does not occur. Forced convection can occur as a result of fluid motions either under the influence of small acceleration fields or because of propellant expulsion or pressurant introduction. However, it is quite difficult to predict these effects, particularly under zero gravity. The last process, diffusion, is the slowest mixing process. It is, however, amenable to calculation. Thus, recognizing that the mixing process may be drastically speeded up by forced convection currents in the tank, calculations are presented below for the diffusion-limited case. This condition represents the upper limit in the mixing time.

To examine an idealized diffusion-limited mixing process, consider the tank shown in Figure 2-4. The tank is initially 95% full and pressurized with helium. The engine ignites and pure helium gas enters at the top of the tank. A large gradient in the propellant vapor concentration is established in the tank with almost pure helium near the top and a layer of helium saturated with propellant vapor near the liquid surface. When most of the propellant is depleted, the engine is shut off. The liquid reorients itself to a near spherical shape, thus minimizing the surface tension energy. If during this process no forced mixing of vapor and helium occurs, the situation would be that shown in Figure 2-4. The layer near the propellant surface is saturated with vapor and the center of the bubble consists of pure helium. Calculations showing the rate of diffusion for spherical gas pockets under these highly stratified conditions are shown in Figure 2-5. As can be seen, the mixing time

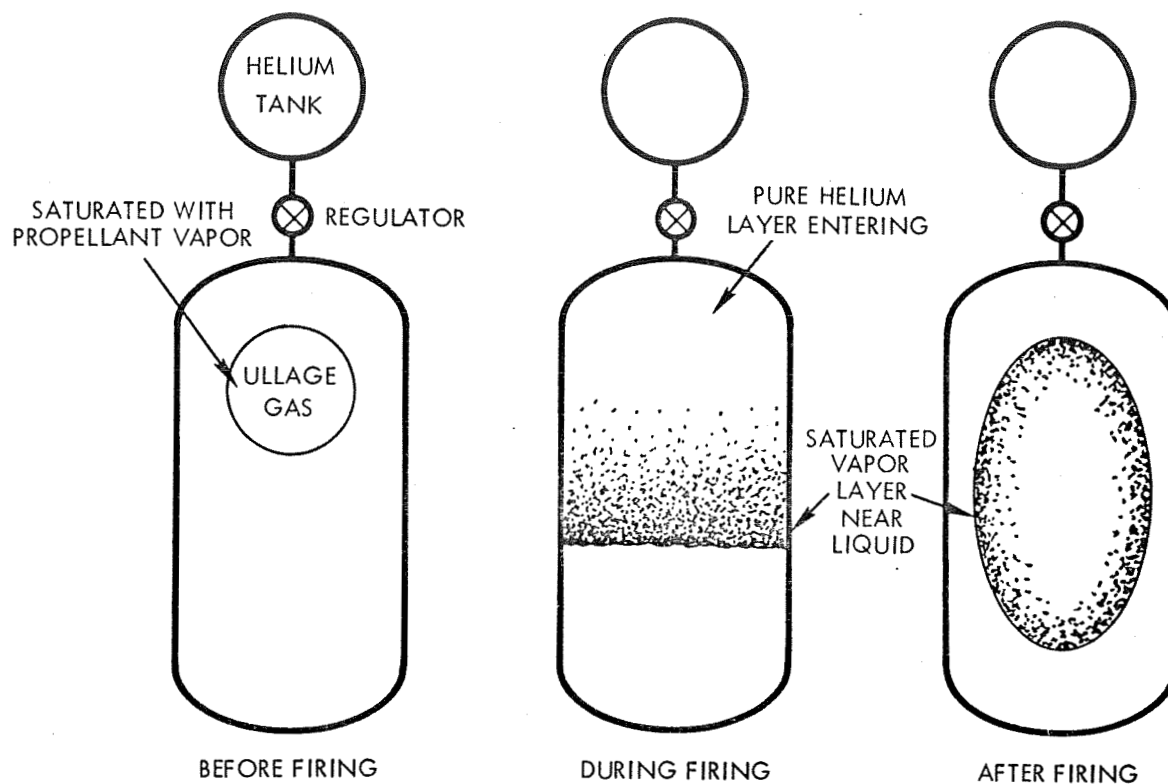


Figure 2-4. Diffusion-Limited Mixing Process

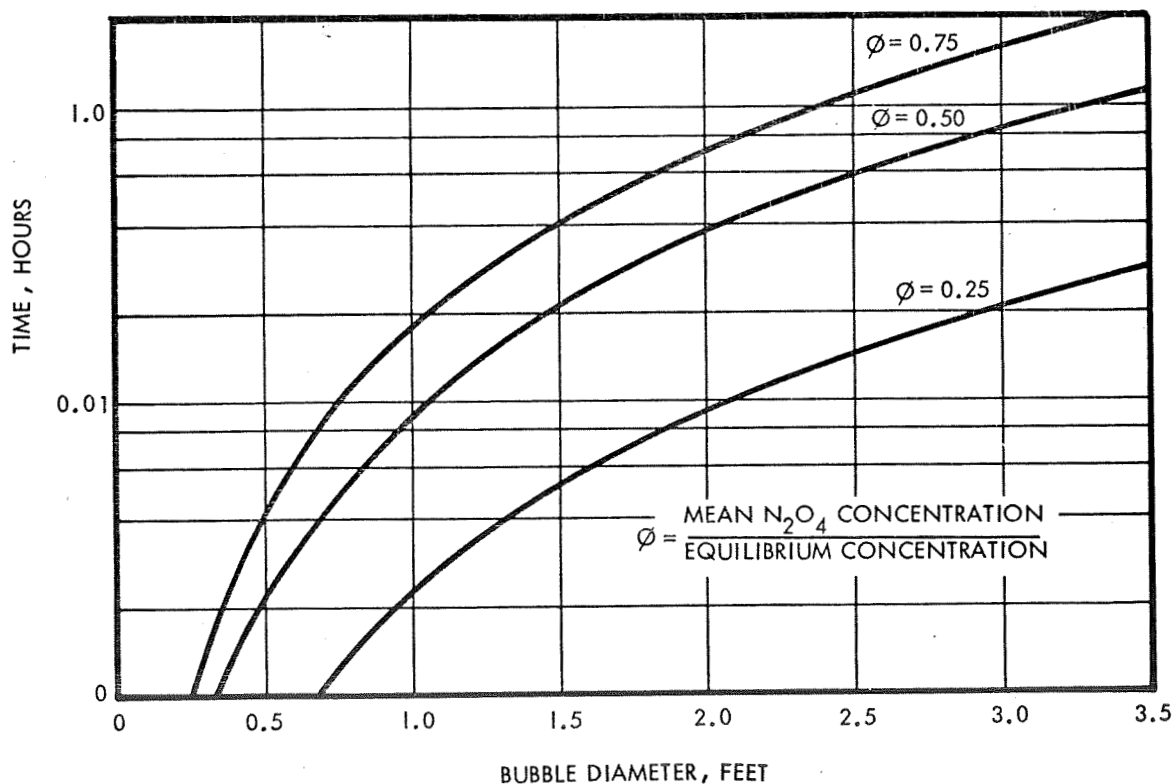


Figure 2-5. Rate of  $\text{N}_2\text{O}_4$  Diffusion into Helium

constant for a typical size gas pocket is about 20 minutes. Thus, even in this severely pessimistic case, complete mixing would be finished in less than one hour. When one includes the effect of convective currents caused by the velocity of the entering helium, sloshing and splashing of propellants during engine shutoff, and movement of the propellant under the influence of surface tension, it becomes apparent that complete mixing will occur quite rapidly, perhaps within 5 to 10 minutes.

## 2.2 PROPELLANT CHARACTERISTICS

A systematic survey of the properties of the two specified propellants ( $\text{N}_2\text{O}_4$ ) and Aerozine-50) was carried out early in the general survey to determine which, if any, of these properties could form the basis of a propellant gauging system. These properties are summarized in this section. Some properties were not available and these were calculated where possible. In one case, some simple experiments were performed to obtain light attenuation properties for infrared, visible, and ultraviolet radiation.

### 2.2.1 Physical Properties of Propellants

NITROGEN TETROXIDE MIL-P-26539 (USAF). Nitrogen tetroxide, also known as dinitrogen tetroxide and NTO, is actually an equilibrium mixture of nitrogen tetroxide ( $\text{N}_2\text{O}_4$ ) and nitrogen dioxide ( $\text{NO}_2$ ); the percentage of  $\text{NO}_2$  increases with increasing temperature. In the solid state,  $\text{N}_2\text{O}_4$  is colorless; in the liquid state the equilibrium mixture is yellow to red-brown, varying with temperature and pressure; in the gaseous state it is red-brown. Nitrogen tetroxide is a highly reactive, toxic oxidizer which is thermally stable and insensitive to all types of mechanical shock and impact. Although nonflammable, it will support combustion, and upon contact with high-energy fuels such as hydrazine, will react hypergolically. It has an irritating, unpleasant, acid-like odor.

AEROZINE-50 (A-50) MIL-P-27402 (USAF). Aerozine-50 is a nominal 50:50 mixture by weight of hydrazine and unsymmetrical dimethylhydrazine (UDMH). It is a clear, colorless, hygroscopic (absorbs moisture readily) liquid, with a characteristic ammoniacal odor. When exposed to the air, a distinct fishy odor is evident in addition



to the ammonia odor, probably due to air oxidation of UDMH. To prevent degradation of performance due to moisture absorption from the air, Aerozine-50 should be stored and handled in closed dry equipment under a blanket of nitrogen. Aerozine-50 is insensitive to mechanical shock but is flammable in both liquid and vapor states. At room temperature the vapor over Aerozine-50 is greater than 90 percent UDMH. Aerozine-50 is considered to be a hazardous propellant due to its toxicity and flammability.

The physical, thermal, and electrical properties of the propellants are presented in Tables 2-5 and 2-6.

### 2.2.2 Transmission Characteristics of Propellants

In Figures 2-6, 2-7, 2-8, and 2-9 the attenuation characteristics of the propellants to light, X-rays, and neutrons are presented. The latter three curves have been calculated from nuclear data while the light characteristics were obtained experimentally.

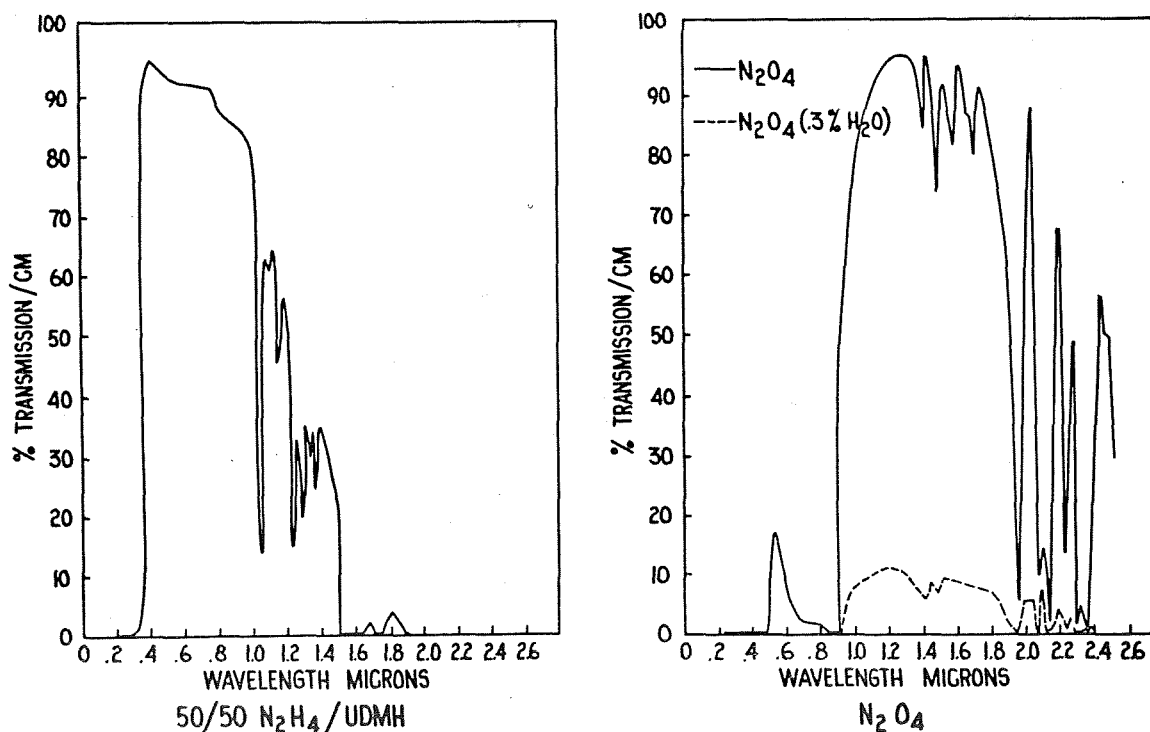


Figure 2-6. Light Attenuation Characteristics

Table 2-5. Properties of Nitrogen Tetroxide, (NTO),  $N_2O_4$

PROPERTY	VALUES							
Molecular Weight	92.02							
Boiling Point, °F	70							
Freezing Point, °F	11.8							
Critical Temperature, °F	317							
Critical Pressure, psia	1496							
Density, lb <sub>m</sub> /ft <sup>3</sup>	at 1000 psi		<u>20°F</u>	<u>60°F</u>	<u>100°F</u>	<u>160°F</u>		
	at vapor pressure		94.5	91.4	88.3	83.7		
			93.9	90.9	87.6	82.1		
Vapor Pressure, psia	<u>14°F</u>	<u>68°F</u>	<u>100°F</u>	<u>200°F</u>				
	2.90	13.92	30.69	235.01				
Heat of Vaporization, Btu/lb <sub>m</sub>	178 (at 70°F)							
Heat of Fusion, Btu/lb <sub>m</sub>	68.4							
	Bubble Point				5000 psi			
Viscosity, Centipoise	<u>40°F</u>	<u>70°F</u>	<u>100°F</u>	<u>200°F</u>	<u>40°F</u>	<u>70°F</u>	<u>100°F</u>	<u>200°F</u>
Viscosity, lb <sub>m</sub> /sec ft(x10 <sup>-4</sup> )	0.50	0.41	0.34	0.16	-	0.48	0.39	0.21
	3.36	2.75	2.28	1.075	-	3.22	2.62	1.41
Specific Heat, Btu/lb <sub>m</sub> °F	<u>20°F</u>	<u>40°F</u>	<u>60°F</u>	<u>130°F</u>				
	0.356	0.359	0.365	0.437				
Surface Tension, lb <sub>f</sub> /ft	<u>34.9°F</u>	<u>67.6°F</u>						
	0.0021	0.0019						
Thermal Conductivity Btu/ft <sup>2</sup> /hr/(°F/ft)	0.0755							
Electrical Conductivity, mho/cm	<u>45°F</u>	<u>68°F</u>						
	1.17 x 10 <sup>-12</sup>		2.24 x 10 <sup>-12</sup>					
Dielectric Constant	2.38 @ 68°F							

Table 2-6. Properties of Aerozine-50 (A-50, 50/50, UDMH/Hydrazine),  
 $(\text{CH}_2)_2\text{N}_2\text{H}_2/\text{N}_2\text{H}_4$

PROPERTY	VALUES							
Molecular Weight	45.0 average							
Boiling Point, °F	146 for UDMH and 235 for N <sub>2</sub> H <sub>4</sub>							
Freezing Point, °F	18.8							
Critical Temperature, °F	634							
Critical Pressure, psia	1696							
Density, lb <sub>m</sub> /ft <sup>3</sup>		<u>20°F</u>	<u>60°F</u>	<u>100°F</u>	<u>160°F</u>			
	at 1 atm	57.9	56.6	55.4	53.4			
	at 1000 psia	-	57.0	55.7	53.9			
Vapor Pressure, psia	<u>20°F</u>	<u>60°F</u>	<u>100°F</u>	<u>120°F</u>	<u>160°F</u>			
	0.60	1.70	4.60	7.00	15.0			
Heat of Vaporization, Btu/lb <sub>m</sub>	425.8 (at B. P.)							
Heat of Fusion, Btu/lb <sub>m</sub>								
	1 atm				1000 psia			
Viscosity, Centipoise	<u>20°F</u>	<u>60°F</u>	<u>100°F</u>	<u>160°F</u>	<u>20°F</u>	<u>60°F</u>	<u>100°F</u>	<u>160°F</u>
	1.505	0.944	0.665	0.453	-	0.949	0.669	0.457
	Viscosity, lb <sub>m</sub> /sec ft(x10 <sup>4</sup> )	10.11	6.35	4.47	3.04	-	6.38	4.50
Specific Heat, Btu/lb <sub>m</sub> °F	<u>40°F</u>	<u>80°F</u>	<u>120°F</u>	<u>160°F</u>				
	0.685	0.694	0.705	0.717				
Surface Tension, lb <sub>f</sub> /ft	2.8 x 10 <sup>-3</sup> @ 68°F							
Thermal Conductivity Btu/ft <sup>2</sup> /hr/(°F/ft)	0.151							
Electrical Conductivity, mho/cm	6.2 x 10 <sup>-3</sup> - 7.04 x 10 <sup>-3</sup>							
Dielectric Constant	33 @ 68°F estimated from data on UDMH & Hydrazine							

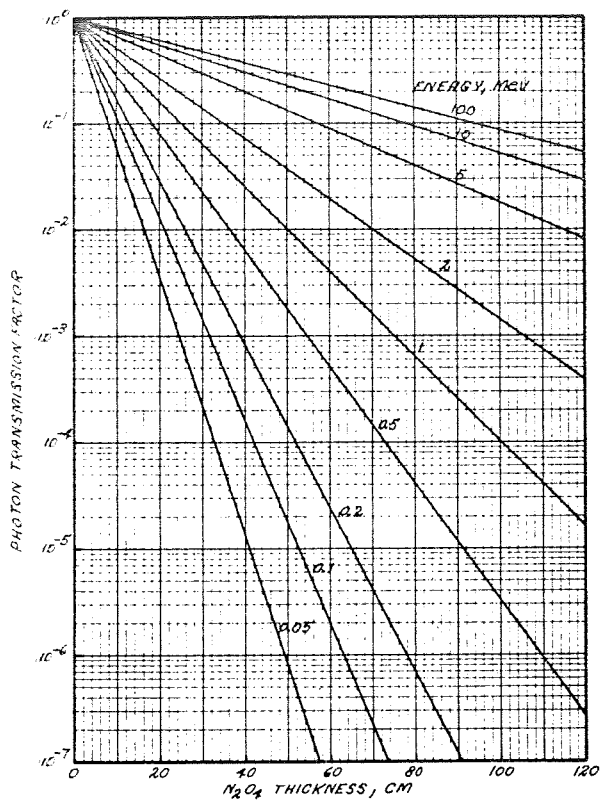


Figure 2-7. Photon Transmission in  $N_2O_4$  Oxidizer

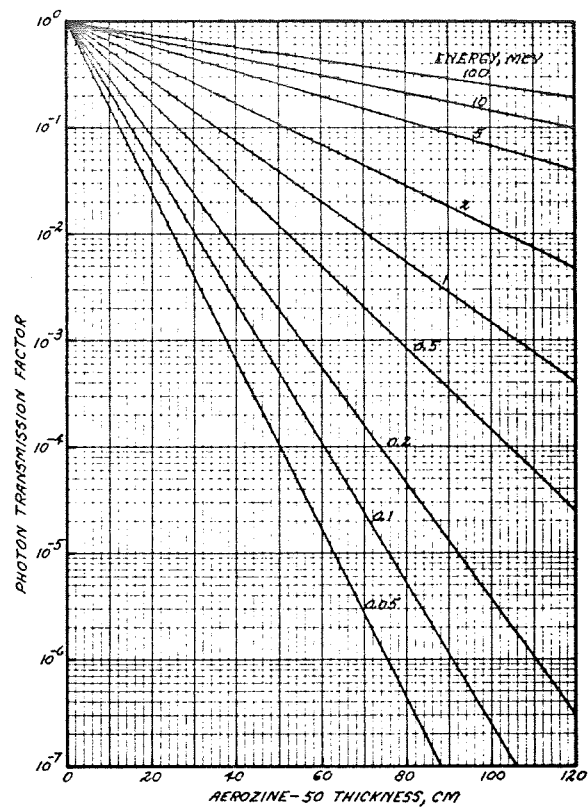


Figure 2-8. Photon Transmission in Aerozine-50 Fuel

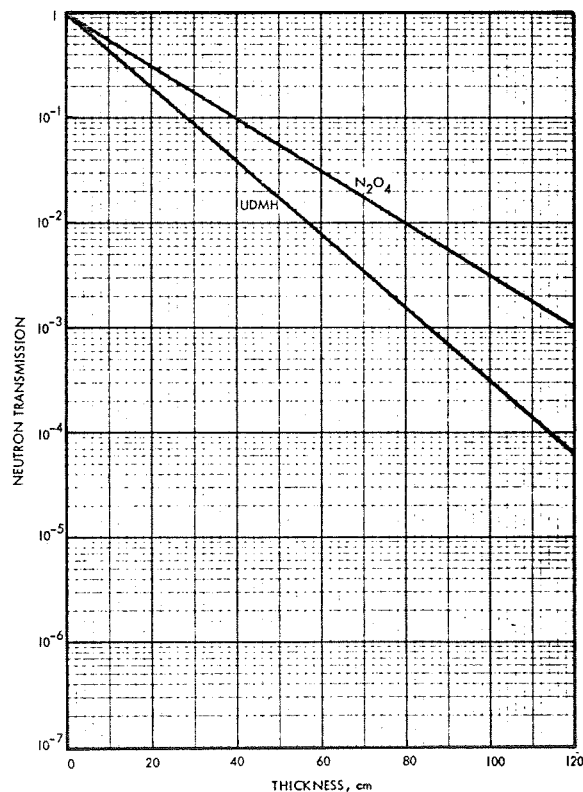


Figure 2-9. Neutron Transmission, 8 Mev "Removal"

### 3. OUTLINE OF POSSIBLE GAUGING TECHNIQUES

This section presents a brief discussion of the various techniques studied during the general survey which might be applicable to propellant gauging. In addition to presenting the systems, a brief discussion of their predominant problem areas is included. For this effort the systems were evaluated on the basis of their capability to adequately gauge the specified propellants under zero and low gravity conditions in a bladderless tank. Some of the rejected systems might, therefore, be quite adequate for gauging when the propellant orientation is known or when the propellants are different.

None of the systems studied appeared capable of meeting the overall requirements stated in Section 2. Two systems, the RIGS (Resonant Infrasonic Gauging System) and the RHO gauge, appear capable of gauging the propellant under zero gravity to an accuracy of  $\pm 1.5\%$  ( $3\sigma$ ). However, both of these systems can be appreciably in error during and immediately after a long engine firing. One system, employing a phase shift measurement from a laser appears to be promising for propellants which are highly transparent.

#### 3.1 ACOUSTICAL TECHNIQUES

Among the most attractive approaches to the measurement of propellant quantity under zero gravity are the acoustical techniques. While this attractiveness arises from the apparent simplicity of the ideas and methods involved, the systems are not as simple as they initially appear. There are, however, real advantages to the acoustical methods which justify careful study.

The primary advantage of these systems lies in the fact that low frequency acoustical techniques measure the gas volume directly and are not sensitive to the actual dimensions of that volume. This is a result of the large difference in compressibility between the gas and the liquid. Major problems are encountered in the actual design of a system, primarily related to the variations in  $\gamma$ , the ratio of specific heats, and liquid entry into the acoustical elements. In addition, as pointed out in Section 3.1.1.4, the frequency selected must be low enough to insure

effective communication between all of the gas cavity. However, the potential of a direct measurement of the ullage volume is so attractive that appreciable effort to overcome these problems is worthwhile.

The acoustical systems considered in this section can be classified as infrasonic and acoustic mode systems. The infrasonic systems may be further categorized as either amplitude sensitive, phase sensitive, or resonant systems.

### 3.1.1 Infrasonic Systems

#### 3.1.1.1 General Analysis

Infrasonic systems measure the compliance or springiness of a gas. For example, consider the system shown in Figure 3-1. At the start the gas pressure in the tank is  $P_o$ . The tank volume is then changed by a known quantity,  $\Delta V$ . The increase in pressure in the tank, using the perfect gas law is

$$PV^K = \text{CONSTANT} \quad (3.1-1)$$

$$\frac{dP}{P_o} = -K \frac{dV}{V_o} \quad (3.1-2)$$

where

$P$ = pressure	sub $_o$ = refers to initial condition
$V$ = volume	sub $_R$ = refers to reference volume
$\gamma$ = ratio of specific heats	sub $_1$ = refers to volume No. 1
$\phi$ = volumetric flourate	sub $_2$ = refers to volume No. 2
$A$ = area	
$M$ = inertance	
$m$ = mass	
$C$ = capacitance	
$c_a$ = acoustic velocity	
$l$ = length	
$\omega$ = angular velocity = $2\pi f$	
$f$ = frequency	
$R$ = flow resistance	

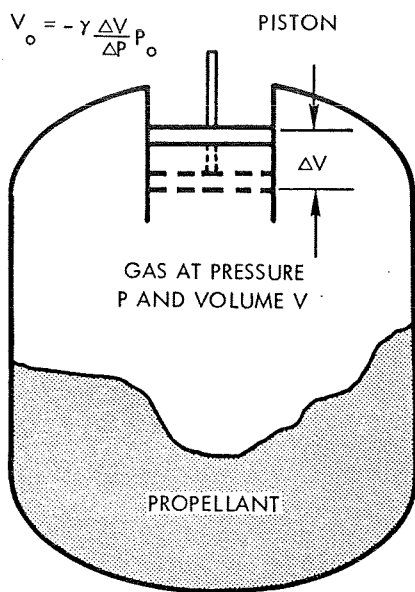


Figure 3-1. Simple Piston System

or for small V

$$\frac{\Delta P}{P_o} = -K \frac{\Delta V}{V_o} \quad (3.1-3)$$

or

$$V_o = -K \frac{\Delta V}{\Delta P} P_o \quad (3.1-4)$$

where K = polytropic expansion coefficient.

If the process is done rapidly, the system is adiabatic and K is equal to the ratio of specific heats,  $\gamma$ .

$$V_o = -\gamma \frac{\Delta V}{\Delta P} P_o \text{ (adiabatic)} \quad (3.1-5)$$

Thus, if  $\gamma$  and  $P_o$  are known, the tank volume can be calculated. Because measurement of  $\gamma$  and  $P_o$  complicate the system, it has been proposed to automatically compensate for these quantities by use of a reference volume as shown in Figure 3-2. As the same small volume change is applied to both volumes  $V_o$  and  $V_R$ , the ratio of the two volumes is

$$\frac{V_o}{V_R} = \frac{\gamma_o}{\gamma_R} \frac{P_o}{P_R} \frac{\Delta P_R}{\Delta P_o} \quad (3.1-6)$$

If the two pressures are equalized by a low frequency acoustical filter, then  $P_o = P_R$ . Also, if the composition of the gases in both volumes are the same,  $\gamma_o = \gamma_R$ . Thus,

$$\frac{V_o}{V_R} = \frac{\Delta P_R}{\Delta P_o} \quad (3.1-7)$$

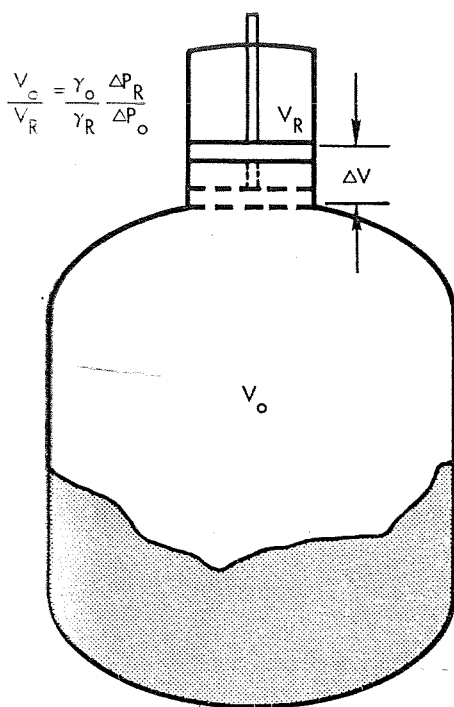


Figure 3-2. Piston System with Reference Volume

This is the basis of the system proposed by Simmonds Precision Products in Reference 3-1. As can be seen from the above equations, it is necessary in this system to insure that  $\gamma$  in the reference volume is the same as that in the tank. Under conditions of zero gravity this is difficult. In Figure 3-3, the variation in  $\gamma$  with temperature is shown for helium pressurant at 200 psi saturated with nitrogen tetroxide vapor. The lack of convection currents under zero gravity, together with the poor communication between the two volumes through the low

frequency acoustical filter, almost insures that the gas composition in the two volumes will be different for appreciable periods after any firing. The magnitude of the error will be directly proportional to the variation in the  $\gamma$  between the two volumes.

A second, and perhaps more difficult problem is the accurate measurement of the pressure change in the ullage gas, since this pressure change can vary over a 40:1 range. With the propellant nearly depleted, an accuracy of 0.0125% of the full tank measurement is required to maintain the error from this source below 0.5% of the full tank weight. Recognizing the difficulty of the problem, Simmonds (Reference 3-1) proposed a force balance technique similar to that used in high grade seismic accelerometers. These devices have achieved accuracies of 0.005% of full scale. However, such accuracies have been experienced only for slowly varying accelerations while using pulse torquing digital techniques with appreciable smoothing, not sinusoidal inputs. In addition, small random vibrations, accelerations, and pressure fluctuations during engine firing will add appreciable noise to the system.



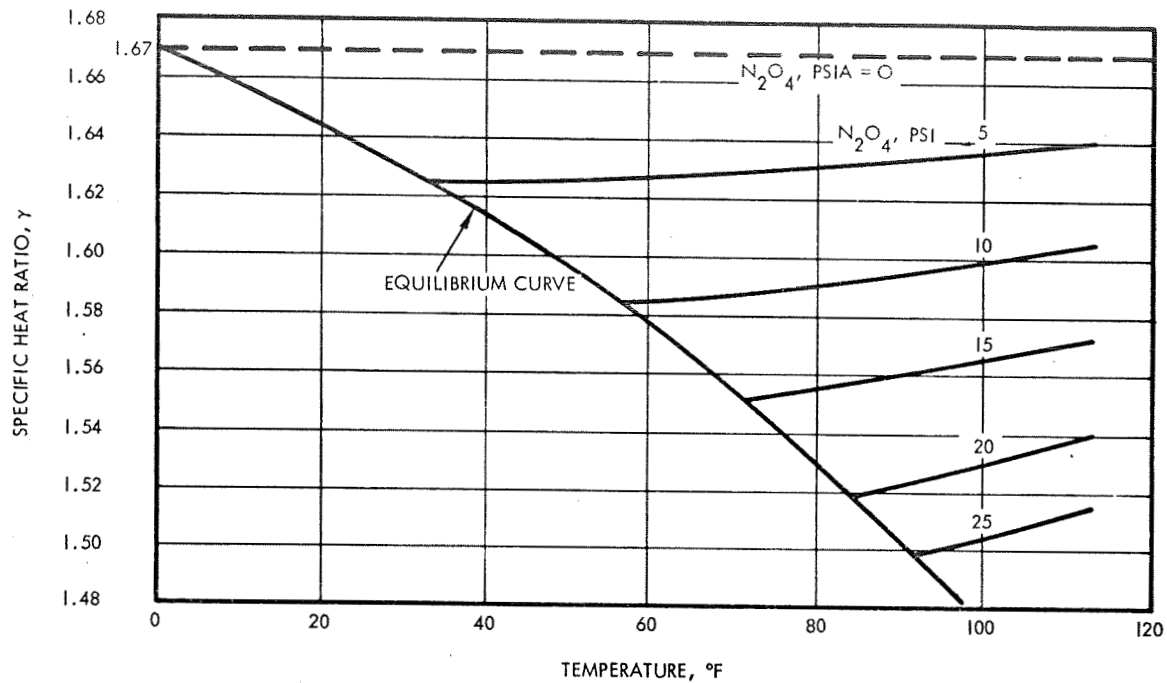


Figure 3-3. Variation of Gamma with  $N_2O_4$  Concentration and Temperature

Because of the difficulty of achieving accurate wide range amplitude measurement, phase sensitive systems appear to be more desirable.

### 3.1.1.2 Phase Sensitive Systems

The phase sensitive systems are based on the fact that at low frequencies (wavelengths appreciably greater than tank dimensions) the various acoustical elements act as lumped impedances and can be treated as analogues of normal electrical networks. In Figure 3-4, the equivalent analogues are shown for acoustical, electrical, and mechanical systems.

The acoustical resistance is defined by the pressure drop required to cause a unit volume flowrate through the resistance element. In general, the resistance is designed to operate in the laminar flow region by providing many small openings and the flowrate is directly proportional to the pressure drop. Thus, the acoustical resistance  $R_A$  is

$$R_A = \frac{Q}{\Delta P} \left[ \text{units of } \frac{\text{ft}^5}{\text{lb}_f \text{sec}} \right] \quad (3.1-8)$$

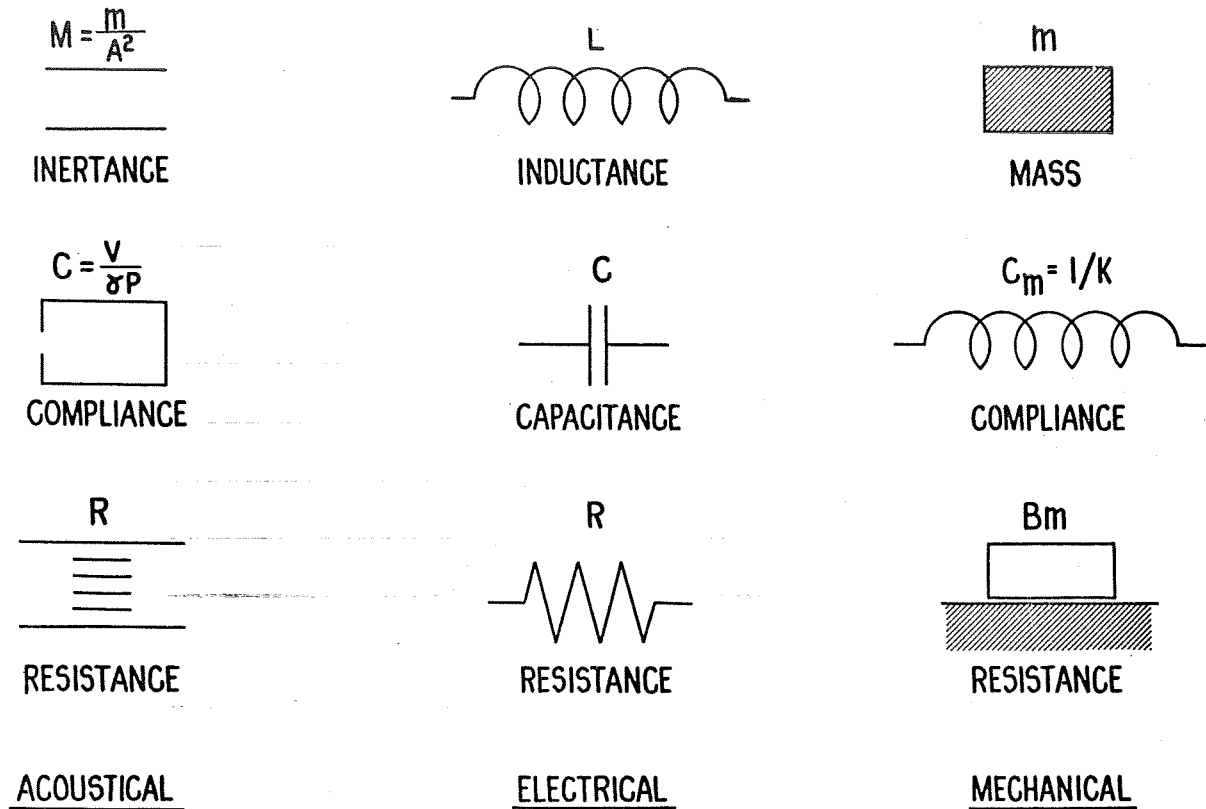


Figure 3-4. Acoustical, Electrical and Mechanical Analogues

The acoustical inertance,  $M$ , is analogous to electrical inductance. The acoustical inertance,  $M$ , of an element is defined as

$$M = m/A^2 \quad (3.1-9)$$

where  $A$  is the effective radiation area of the mass,  $m$ .

The acoustical compliance  $C$  of an element is defined as the volume displacement produced by application of a unit pressure change. It is the analogue of electrical capacitance, which is similarly defined as the change per unit of applied voltage. For an enclosed volume  $V_o$ , Equation 3.1-5 leads to

$$C = \frac{V_o}{\gamma P_o} \quad (3.1-10)$$

As long as the acoustical wavelength is large compared to any tank dimensions and the pressure wave is small in amplitude, these lumped parameters will adequately represent the acoustical system. The driving pressure,  $P$ , is analogous to voltage and the acoustical flowrate,  $Q$ , analogous to current. Consider the following simple example.

Everyone is familiar with the tone generated by blowing across the top of a narrow-neck bottle. The effect (a Helmholtz resonator) can be simply analyzed by using the analogs developed previously. The equivalent circuit for a Helmholtz resonator is shown in Figure 3-5 where the resistance, compliance, and inductance are as shown below

$$R = \frac{Q}{\Delta P} = \frac{\rho_o \omega^2}{2\pi c_a}$$

$$M = \frac{m}{A^2} = \frac{\rho_o \ell}{A} \quad (\text{assuming a uniform cross-sectional area long length, } \ell)$$

$$C = \frac{V}{\gamma P} = \frac{V}{\rho_o c_a^2}$$

Resonance occurs when  $\omega M = 1/\omega C$  or

$$\omega_o = c_a \sqrt{\frac{A}{\ell V}}$$

where  $c_a$  = acoustic velocity

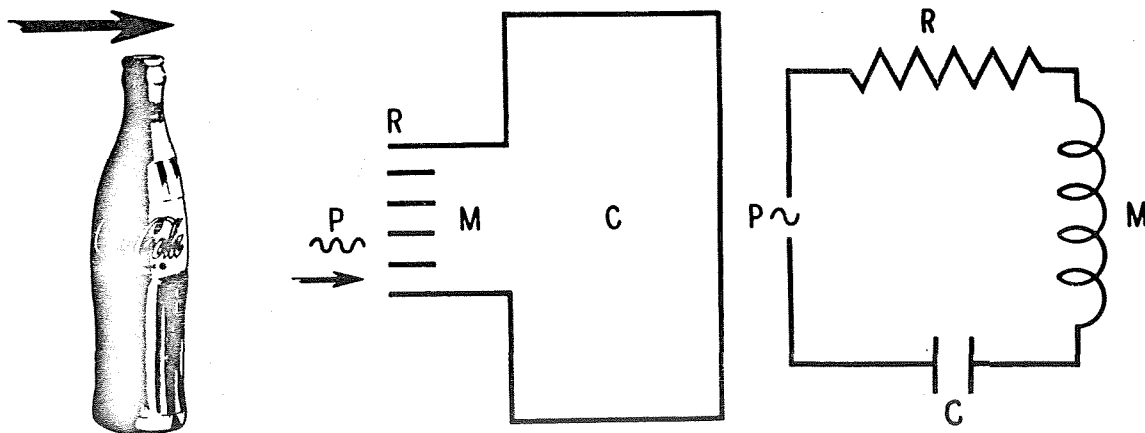


Figure 3-5. Helmholtz Resonator

The sharpness or  $Q$  at resonance is definitely

$$Q = \frac{\omega_o M}{R} = 2\pi \sqrt{\frac{\ell^3 V}{A^3}}$$

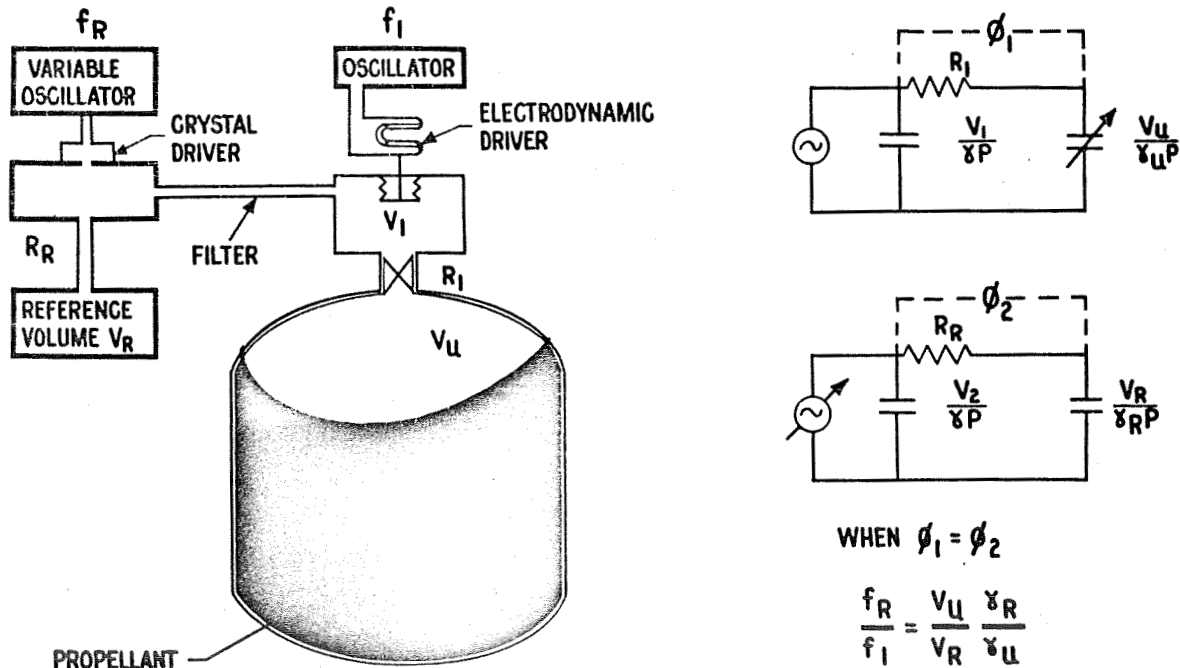
Now consider an actual system. The system shown in Figure 3-6 consists of a sinusoidal driver and two volumes separated by an acoustical resistance. This can be represented by an equivalent circuit shown in Figure 3-6.

where

$$C_1 = \frac{V_R}{\gamma P_o} \text{ and } C_2 = \frac{V_u}{\gamma P_o}$$

The amplitude change across the resistor  $R$  is

$$\frac{P_2}{P_1} = \frac{R}{\sqrt{R^2 + \left(\frac{1}{\omega C}\right)^2}} \quad (3.1-11)$$



The phase shift across the resistor R is

$$\phi = \arctan \frac{1}{\omega C_a R_a} = \arctan \frac{\gamma P_o}{2\pi f V_u R_a} \quad (3.1-12)$$

where  $\omega = 2\pi \times \text{frequency}$ .

The system above is the main element of the gauging system developed by Acoustica Associates under contract to the Air Force (References 3-2 and 3-3). In order to measure the phase shift, Acoustica utilized a phase lock system in which the phase shift in a reference volume (see Figure 3-6) was maintained the same as that in the ullage system by driving with a variable frequency source. When the two phase angles are equal

$$\frac{\gamma_u P_u}{2\pi f_u V_u R_{a_u}} = \frac{\gamma_R P_R}{2\pi f_R V_R R_{a_R}} \quad (3.1-13)$$

If the pressure and specific heat ratios are the same in both volumes then

$$V_u = \frac{f_R V_R R_{a_R}}{f_u R_{a_u}} = \frac{f_R}{f_u} K \quad (3.1-14)$$

The value of the constant can be determined by calibration.

This system has certain basic difficulties. First, as constituted, liquid entering the reference volume and acoustical resistance can completely void the system. Any attempt to use heaters, surface tension devices, etc., to eliminate liquid entry, serve only to isolate the reference volume and insure that the composition and thus  $\gamma$  will be different from that in the tanks. In addition, the value of the acoustical resistance is temperature sensitive.

A better approach for zero gravity gauging appears to be to completely isolate the driver and reference volumes and to correct for the  $\gamma$  variation by external transducers. Such a system appears in Figure 3-7. Provided the isolating diaphragm has sufficiently low mass and the spring rate, the basic equation is still the same except that the  $\gamma$

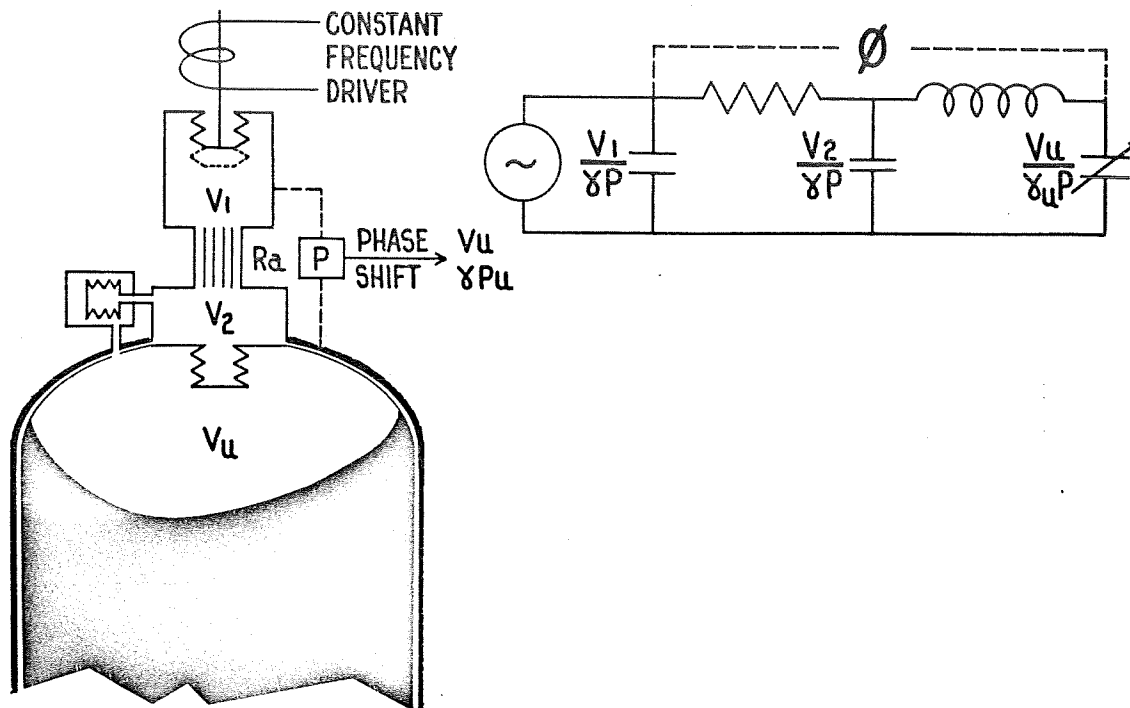


Figure 3-7. Phase Sensitive Infrasonic System

correction is not handled automatically. The system is further analyzed in Section 4.1 and has certain major shortcomings, namely: the system becomes non-operative if liquid is directly on the diaphragm; the acoustic resistances are quite temperature sensitive; and slight nonlinearities in the system can lead to appreciable shifts in the phase angle and reduce the accuracy of the system.

### 3.1.1.3 Resonant Mass Systems

In order to minimize some of these effects an additional infrasonic system was devised. This system, the resonant infrasonic gauging system (RIGS), utilizes a resonance between a supported weight and the compliance of the gas volume. The RIGS system, with its equivalent circuit is shown in Figure 3-8. A complete preliminary analysis of the system is found in Section 4.1. The system operates by using a variable frequency driver to seek a null pressure in the driving volume. At this point, the mass of the diaphragm is in resonance with the tank ullage volume, as shown in Figure 3-9. Thus,

$$\omega^2 = \frac{1}{M} = \frac{\gamma P A^2}{m V_u} \quad (3.1-15)$$

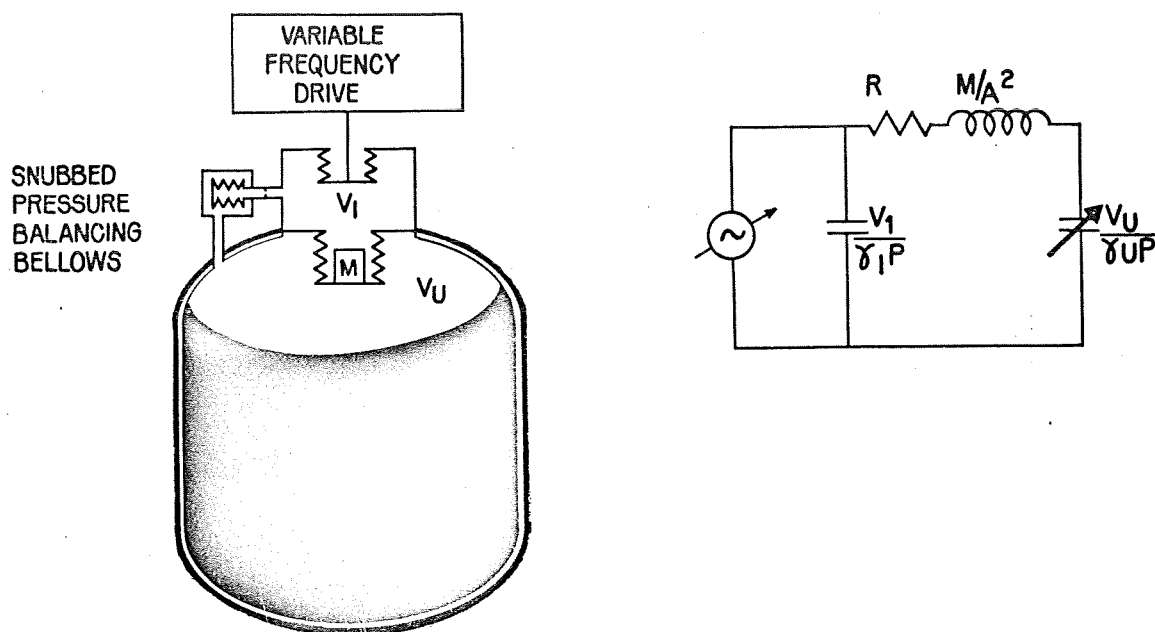


Figure 3-8. Resonant Infrasonic Gauging System, RIGS

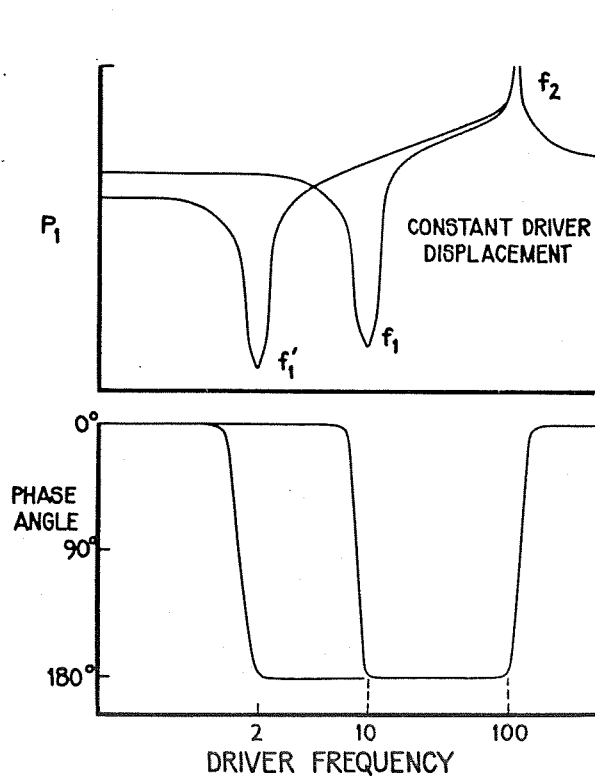


Figure 3-9. RIGS Response

or

$$V_u = \frac{\gamma P}{4\pi^2 f_R^2} \frac{A^2}{M} = \text{Constant} \times \frac{\gamma P}{f_R^2} \quad (3.1-16)$$

Since the system does not depend on an acoustical resistance, the sensitivity to temperature is reduced. The resonant technique is also insensitive to nonlinearities in the system. Major disadvantages include the sensitivity to  $\gamma$  and the affect of liquid against the mass diaphragm.

### 3.1.1.4 Transmission of Infrasonic Waves Through Liquid

One of the major problem areas associated with all of the infrasonic systems is the detection of gas pockets submerged in the liquid, as shown in Figure 3-10. In order for the submerged gas pocket to respond to the input driver the mass of propellant between the ullage gas and the gas pocket must be accelerated. In this situation there is an additional impedance due to the liquid mass, as shown in Figure 3-10. The effective compliance of the gas pocket is

$$\frac{1}{C_{gp}} = \frac{1}{C_{gp}} - \frac{\omega^2 M_p}{A^2} = \frac{1}{C_{gp}} \left( 1 - \frac{\omega^2 M_p C_{gp}}{A^2} \right) \quad (3.1-17)$$

SUBMERGED GAS POCKETS

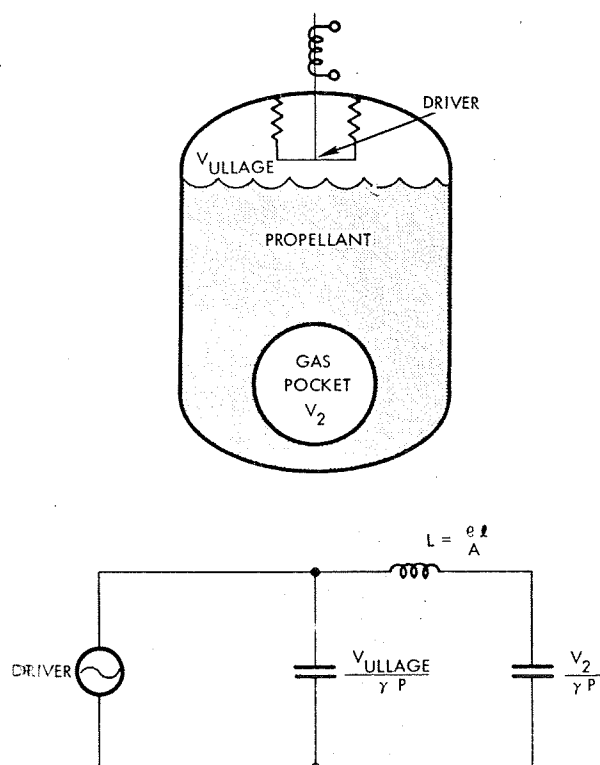


Figure 3-10. Submerged Gas Pocket Analogues

In Figure 3-11, the error in measuring a 1 cubic foot volume of submerged gas is shown as a function of both the submerged distance and frequency. As can be seen from the figure, frequencies above 10 cps will lead to appreciable error in detection of submerged gas for the Apollo-size tanks. This limits the allowable frequency range for all of the infrasonic systems.

### 3.1.2 Acoustical Resonance Counting

The existence of normal modes (or standing waves) in an acoustical cavity, is a well known phenomenon, which has been extensively studied because of its importance in architectural acoustics (See References 3-4 and 3-5).



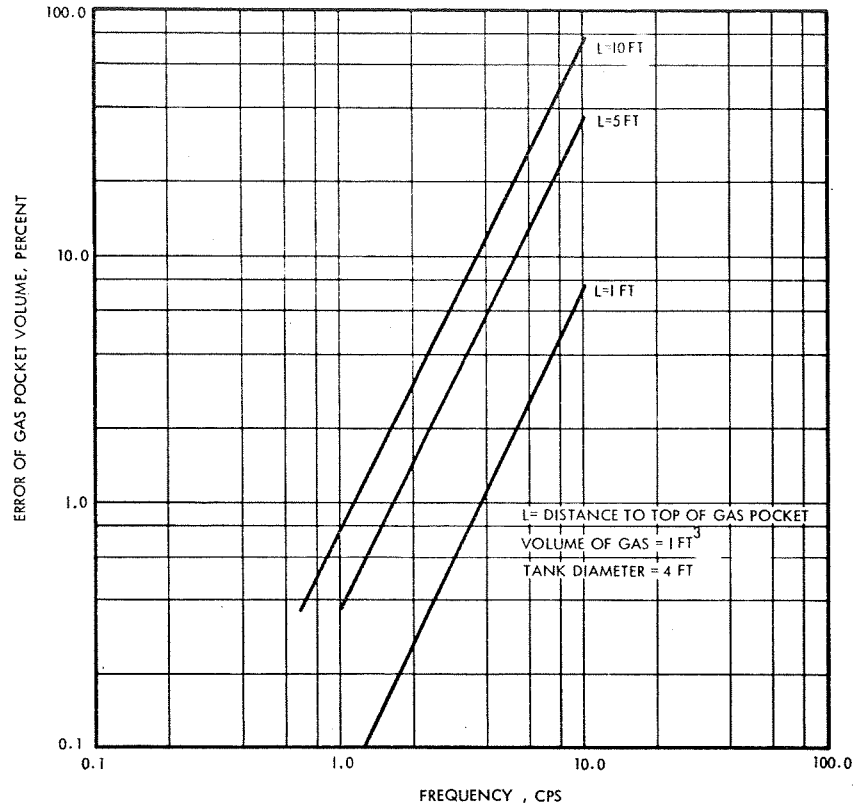


Figure 3-11. Effect of Frequency of Gas Pocket Attenuation

It can be shown that for a rigid rectangular enclosure standing waves will exist at frequencies satisfying Equation 3.1-18 below.

$$f = \frac{c}{2} \left[ \left( \frac{n_x}{l_x} \right)^2 + \left( \frac{n_y}{l_y} \right)^2 + \left( \frac{n_z}{l_z} \right)^2 \right]^{\frac{1}{2}} \quad (3.1-18)$$

when

$l_x, l_y, l_z$  = length in indicated direction

$c$  = velocity of sound

$n_x, n_y, n_z$  = characteristic integer

= 0, 1, 2, 3, .....

An infinite number of such modes exists, and can be characterized by the three characteristic integers,  $n_x$ ,  $n_y$ , and  $n_z$  as it varies between 0 and infinity. It should be apparent from the equation that the frequency of each single mode is strongly dependent on physical dimensions of the cavity and will change as the shape of the cavity (ullage space) varies. Thus, the measurement of a single resonant frequency will not adequately measure the ullage volume under zero gravity.

A somewhat different approach is suggested in Reference 3-6, based on the distribution of the normal modes. The total number of modes below a given frequency in a rectangular cavity is expressed in Equation 3.1-19

$$N = \frac{4\pi V}{3} \left(\frac{f}{c}\right)^3 + \frac{\pi S}{4} \left(\frac{f}{c}\right)^2 + \frac{L}{8} \left(\frac{f}{c}\right) \quad (3.1-19)$$

where

$V$  = total volume of the cavity

$S$  = total surface area of cavity

$L$  = sum of the length of the sides of the cavity

$f$  = frequency

$N$  = total number of resonant modes below frequency  $f$ .

The number of normal modes having frequencies in a bandwidth,  $\Delta f$ , centered around frequency,  $f$ , can be obtained by differentiating Equation 3.1-19

$$\frac{\Delta N}{\Delta f} \cong \frac{dN}{df} = \frac{1}{C} \left[ 4\pi V \left(\frac{f}{c}\right)^2 + \frac{\pi}{2} S \left(\frac{f}{c}\right) + \frac{L}{8} \right] \quad (3.1-20)$$

where

$\Delta N$  = number of modes in band  $\Delta f$ ,

$\Delta f$  = frequency band centered around  $f$ .

It is apparent from Equation 3.1-20 that as the frequency increases, the effect of the surface area and length-dependent terms become negligible and the approximation shown in Equation 3.1-21 becomes valid.

$$\Delta N = \frac{1}{C} 4\pi V \left(\frac{f}{c}\right)^2 \Delta f \quad (3.1-21)$$

as  $f$  grows large

Under these conditions, the number of normal modes is independent of the dimensions or shape of the cavity and becomes a direct function of the ullage volume. Therefore, if the number of normal modes can be measured, the ullage volume and then the propellant volume and mass can be obtained.

The simplest method of counting modes is to excite the cavity with a sine wave of changing frequency. When the driver frequency matches that of each mode in succession, a resonance is noted and automatically counted.

Unfortunately this method, simple as it seems, has certain fundamental difficulties. Primary among these difficulties is the large number of degenerate normal modes usually present. Degenerate modes are standing waves having different characteristic integers but the same characteristic frequency, i. e., only a single mode will be detected at the characteristic frequency even though multiple modes are actually present. The number of degeneracies increases as the degree of symmetry of the cavity increases. In the case of cubes and spheres sixfold degeneracies are quite common. For gauging under zero gravity where propellant orientation is somewhat random, it will be impossible to distinguish between a change in the ullage volume and a change of shape or characteristic dimension and symmetry of the ullage space.

While the above appears sufficient to eliminate the system from further consideration, analyses indicated the following additional shortcomings of the system:

- Since the technique requires high frequencies, any submerged gases would not be detected (see Section 3.1.1.4).

- The large number of maxima to be counted ( $>10^4$ ) over narrow band would be difficult to implement. As shown in Figure 3-12, the modes are not evenly spaced, but occur at random frequencies. Thus, the transducer must be able to detect the equivalent of  $10^5$  to  $10^6$  evenly spaced modes in order to not count closely spaced multiple modes as a single mode.
- Viscous damping in the gas would tend to smear out the individual modes.

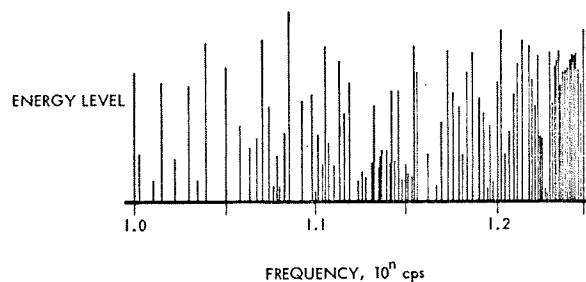


Figure 3-12. Typical Mode Pattern in Propellant Tank

For an infinitely slowly changing frequency, the interaction between the cavity and the transducer will have approximately the shape of a normal resonance curve. In order to distinguish clearly between two such interaction curves, the two curves should intersect at something less than half their maximum values. To get  $10^5$  different modes equally spaced in wavelength ratio into an octave, the wavelength ratio between each two must be 1.000007.

In order to have two modes, spaced by this wavelength ratio, separately countable, the  $Q$  for the two modes must be greater than  $1/(\text{wavelength ratio} - 1)$ . This quantity,  $Q$ , is simply  $2\pi/\text{frictional dissipation}$ , (Reference 3-7), where the frictional dissipation is the fraction of energy stored in the standing sound waves of the excited mode which is dissipated in air friction and similar losses, each cycle. Thus the frictional dissipation must be less than  $4.4 \times 10^{-5}$  of the input power.

Since the frictional dissipation is likely to be approximately 1% due to thermodynamic losses in the fluid, and losses through the boundaries of the cavity to the air, the supports, and the piping, it is plain that the individual normal modes will be so smeared out that several thousand would be excited by any given wavelength of excitation. The simple method of mode counting then fails by a factor of something like a thousand of being realizable in a practical situation.

### 3.2 INTERACTION WITH AN ELECTROMAGNETIC FIELD

When propellant is placed in an electromagnetic field, it interacts with the field to alter it in a predictable manner. In this section we will investigate the use of these interactions to gauge the propellant quantity.

Electromagnetic radiation covers a wide variety of phenomena, ranging from radio frequency waves to gamma radiation. However, all electromagnetic radiation may be characterized by any of three parameters; the wavelength, the frequency, or the energy of the photon waves. All three are interrelated as follows:

$$c = \lambda \nu \quad (3.2-1)$$

and

$$E = h\nu = \frac{hc}{\lambda} \quad (3.2-2)$$

where

$\nu$  = frequency

$c$  = speed of propagation

$\lambda$  = wavelength

$h$  = Planck's Constant

$E$  = Energy

For a better understanding of the possible interactions between the field and the propellant, a brief description of dominant effects over the entire range of electromagnetic spectrum follows. Figure 3-13 shows the primary regions of propellant and field interaction. At radio frequencies, the wavelength of the radiation is long compared with

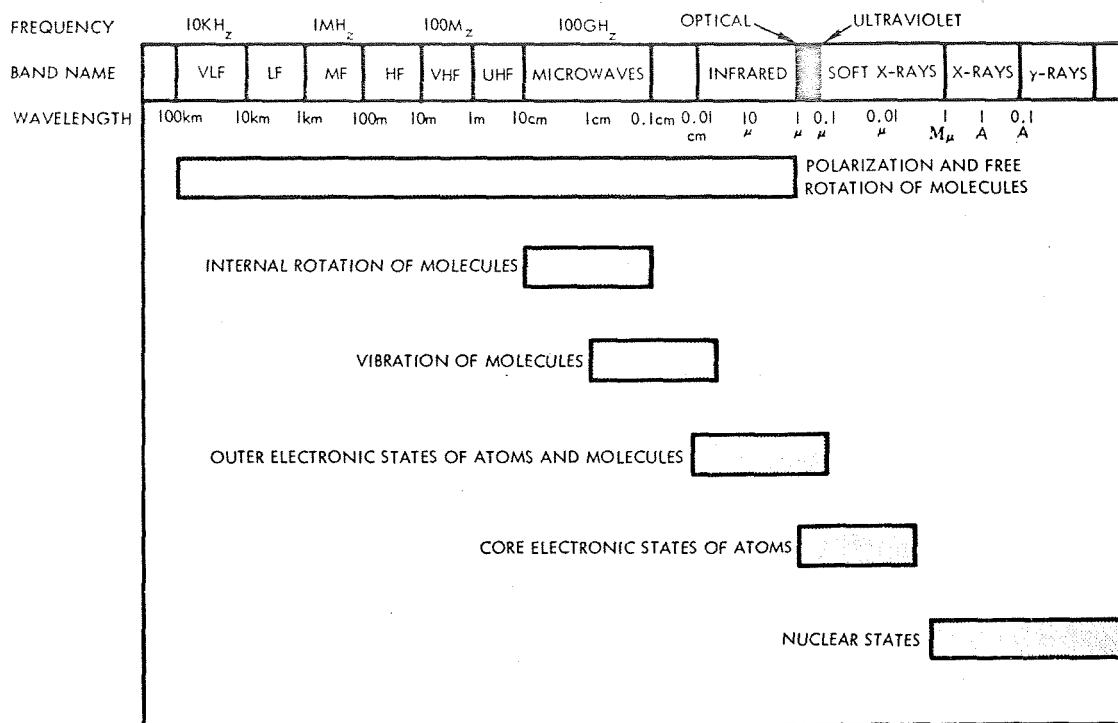


Figure 3-13. Electromagnetic Radiation Spectrum

dimensions of the propellant molecules, and the primary interaction is polarization of the molecules. Since the propellants are non-magnetic, the effects of the magnetic dipole are negligible and the electric dipole properties are dominant. A dielectric material increases the storage capacity of a capacitor by neutralizing charges at the electrode surface which otherwise would contribute to the field. We may visualize this effect, dielectric polarization, as the action of dipole chains which form under the influence of an applied field and bind countercharges with their free ends at the conductive surface as shown in Figure 3-14. The net effect of the dipole charge is to increase the ability of the conducting surface to retain the charge. The ratio of the charge-containing capability of a material to that of a vacuum is called its dielectric constant,  $\epsilon$ .

In the radio frequency region, one additional property of great importance is the electric conductivity of the propellant. The conductivity determines the rate of dissipation in the propellant. The loss factor is the ratio of the loss (due to the conductivity of the material)

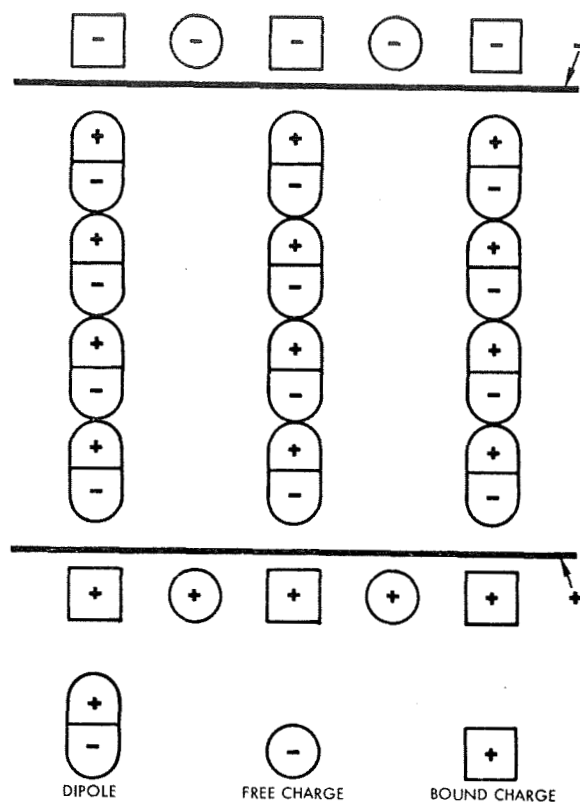


Figure 3-14. Dielectric Effect of a Polar Molecule

divided by its reactive component (due to the dielectric effect). For a given material, as the frequency increases the loss factor due to conductivity decreases, and finally becomes negligible in the high energy microwave region for any liquids that we will consider. Typical curves of loss factors versus frequency for Aerozine-50 are shown in Figure 3-15.

At higher frequencies, the next region of interest consists of infrared radiation visible light, and ultraviolet radiation. In this region, as shown in Figures 3-13, the wavelengths are comparable to that of the atoms and molecules of the propellant. Thus, in this region the primary interaction is absorption of an electromagnetic wave resulting in an increased rotational and vibrational energy state of the propellant molecules. This energy can be eventually dissipated either in heat, or in the

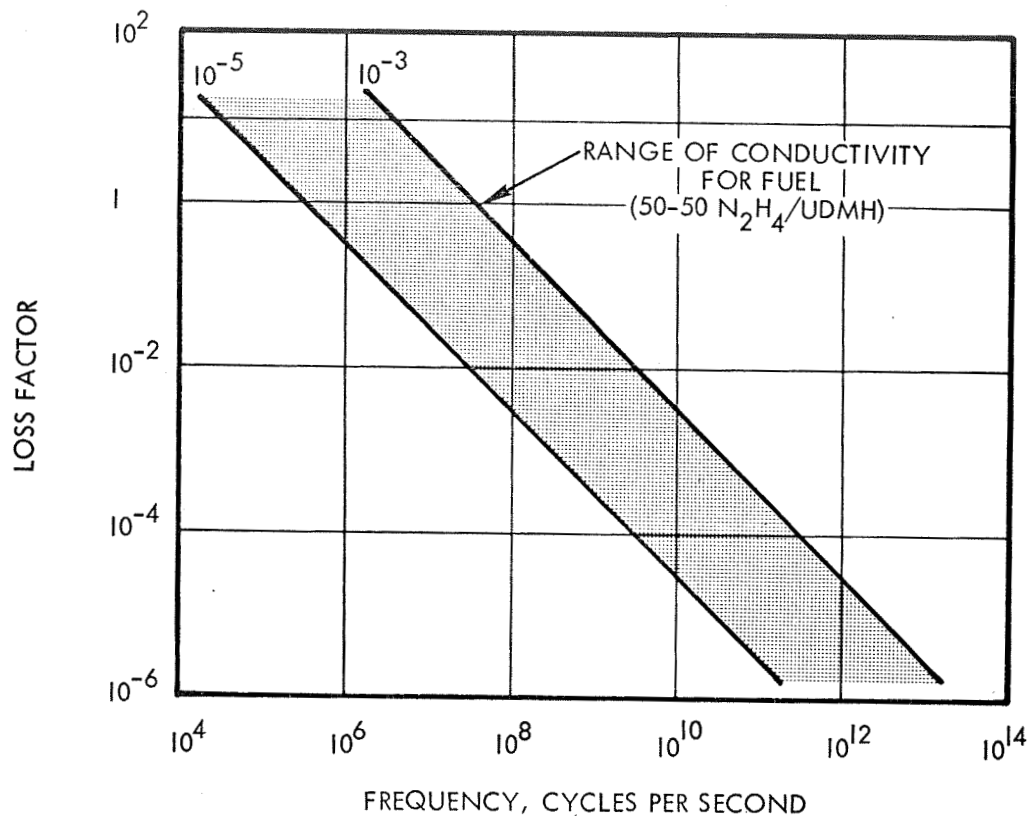


Figure 3-15. Loss Factor for Fuel Versus Frequency

case of energetic waves, as secondary radiation at different wavelengths. Dielectric polarization continues to be important in this region, resulting in a reduced velocity of light through the propellant compared to that of a vacuum.

Further increases in the energy of the electromagnetic radiation leads to the region of X-rays and gamma rays. In this region the interactions are with nuclear and core electronic states of the atom. The speed of the electromagnetic wave is that of free space and polarization is no longer of any importance. The energy of the electromagnetic radiation is quite high in this region and secondary photon emission, resulting from the interactions of the propellant and the primary photon, is quite common. Most propellants are rather transparent in this range;



thus, each region of the electromagnetic spectrum may be characterized by certain basic interactions. These are summarized below and form the basis of a number of possible gauging systems.

**Radio Frequency**

Wavelength is long compared to atoms, can be the same magnitude as that of the tankage.

Dielectric properties dominate.

Primary loss mode conduction up until microwave region.

**Light (IR, Visible, UV)**

Wave length is comparable to the size of atoms and molecules, thus waves act primarily as beams.

Speed of light affected by dielectric properties.

Primary loss mode is photon absorption by interaction with atomic and molecular energy modes.

Refraction at interfaces is important.

**X-Ray, Gamma Ray**

Wavelength is small compared to atoms, waves act as sharp beams.

Speed of propagation close to that of vacuum, unaffected by dielectric properties.

Primary loss mode is photon absorption by nuclear interactions, usually resulting in secondary photons being emitted.

**3.2.1 Radio Frequency Techniques**

The statement of work for the study specifically eliminated radio frequency systems from the study. However, during the brainstorming sessions a number of RF systems were suggested and critiqued. In the interest of completeness, a brief summary of these systems is presented in this section.

### 3.2.1.1 Single Resonant Mode

Appreciable industrial effort has been expended upon the single resonant mode technique (References 3-8, 3-9, and 3-10). In this system electromagnetic energy is pumped into a cavity partially filled with propellant and a number of resonant modes are excited. Selecting a single mode, the frequency of the standing wave will be a function of the dimension of the cavity, the speed of propagation, and a series of characteristic numbers as shown below for a rectangular cavity (Reference 3-11).

$$f_{\text{mode}} = \frac{c}{2\pi} \left[ \left( \frac{m\pi}{x} \right)^2 + \left( \frac{n\pi}{y} \right)^2 + \left( \frac{p\pi}{z} \right)^2 \right]^{1/2} \quad (3.2-3)$$

where

$f$  = frequency of mode

$c$  = velocity of wave in media

$x, y, z$  = dimensions of cavity

$m, n, p$  = characteristic integers = 0, 1, 2, 3 .....

Since the velocity of propagation for a non-magnetic material is uniquely related to the dielectric constant of the media and speed of light in a vacuum by Equation 3.2-4, the frequency of resonance can be related to the average dielectric constant of the cavity as shown in Equation 3.2-5.

$$\frac{c}{c_0} = (\epsilon)^{-1/2} \quad (3.2-4)$$

where

$\epsilon$  = dielectric constant of material relative to free space

$c_0$  = speed of light in free space

combining Equations 3.2-3 and 3.2-4 one obtains,

$$f = \frac{c_o \epsilon^{-1/2}}{2\pi} \left[ \left( \frac{m\pi}{x} \right)^2 + \left( \frac{n\pi}{y} \right)^2 + \left( \frac{p\pi}{z} \right)^2 \right]^{1/2} \quad (3.2-5)$$

Unfortunately, the value of the average dielectric constant in a mixed media (gas and propellant) is dependent on the actual location of the propellant, not just on the relative quantities of the two media. Material located near antinodes of the standing wave will have a negligible effect on the frequency, while material located near nodal points will have large effects. Thus under zero gravity, when the propellant location is not accurately known, the quantity of propellant cannot be accurately determined.

#### 3.2.1.2 Resonant Mode Counting

As the frequency of a single mode cannot be used to determine the propellant quantity it was thought that perhaps the mode counting technique discussed under the acoustical systems in Section 3.1 could be applied. As shown in Equation 3.2-6, the total number of modes in a given radio frequency band is double the number for the equivalent acoustical system since both transverse magnetic (TM) and transverse electrical (TE) waves must be considered.

$$N = \frac{8\pi f^2 \epsilon}{3 c_o} \Delta f \quad (3.2-6)$$

Thus, by using a mode-counting technique similar to that presented for the acoustical system in Section 3.1, it would appear, at first, possible to measure the average dielectric constant and hence the propellant quantities. However, the problem of degenerate modes discussed in Section 3.1 can lead to appreciable difficulties. If the dielectric constant of the two media are close together, the shift in frequency of the individual modes will be small and in all likelihood, will not greatly affect the

number of degenerate modes. However, for materials having substantially different dielectric constants, such as helium and the fuel, the concept of an average dielectric constant is appreciably in error and both the number and degeneracies of the modes will be quite drastically affected by the actual distribution of the fuel.

A secondary problem with this type of system is the conductivity of the fuel. Though the loss factor decreases linearly with increasing frequency as shown in Figure 3-15 the required Q for mode detection increases at higher frequency. The effect of the fuel conductivity in smearing out some of the significant modes can then be appreciable. The equivalent acoustical case was discussed in Section 3.1.2.

#### 3.2.1.3 Low Frequency Measurement

Low frequency measurements with RF waves which are appreciably larger than any tank dimension, are analogous to the acoustical infrasonic techniques discussed in Section 3.1. It can be shown that at these frequencies the basic quantity measured is the capacitance between the driving coil and the tank wall. As discussed in Section 3.3.2, the capacitance is sensitive to propellant orientation.

#### 3.2.1.4 Loss Factor Measurement

It was proposed to measure the effective loss factor in the propellant tank which could then be related to the quantity of propellant. This technique appeared to also be quite sensitive to the propellant location.

#### 3.2.2 Interaction with Light Beams

As pointed out earlier, the wavelength of light (visible, IR or UV) is appreciably less than any pathlength within the tank. Thus the interactions between the field and propellant are quite localized and the light waves may be characterized as beams. This presents one of the main problems to gauging with light; namely, the narrowness of typical beams results in essentially local sampling of the system which may not be adequately representative of the larger volume. While good accuracy

can be obtained in situations where the propellant orientation is known, this can lead to appreciable errors, with a more random configuration. One way out of this problem is to use more and more beams until in the limit an infinite number are used and the error from this source is negligible. Under these conditions, both a large beam area and a large detector area are required.

In this wavelength region, the energy loss is largely by photon absorption which follows Beer's Law namely,

$$\frac{dI}{dx} = -\mu\rho I \quad (3.2-7)$$

When integrated over a given beam length, this becomes Equation 3.2-8 which assumes no scattering.

$$I = I_0 e^{-\mu\rho L} \quad (3.2-8)$$

where

$I$  = Beam intensity

$I_0$  = Initial intensity

$\mu$  = Mass attenuation coefficient

$L$  = Beam length

This is the basis of the attenuation techniques presented in Section 3.2.2.1.

The velocity of propagation of light through the propellant is also affected by the dielectric constant of the propellant

$$c = c_0 (\epsilon)^{-1/2} \quad (3.2-4)$$

Thus, the transit time of a light beam through a length of propellant and pressurant is directly related to the relative lengths of the two media:

$$t = \frac{L_p}{c_p} + \frac{(L_T - L_p)}{c_o} \quad (3.2-9)$$

as from Equation 3.2-4  $c_p = c_o \epsilon^{-1/2}$

$$t - t_g = \frac{L_p}{c_o} (\epsilon^{1/2} - 1) \quad (3.2-10)$$

where

$t$  = transit time through gas/propellant mixture

$t_g$  = transit time through same length filled only with gas

$L_p, L_T$  = path length for propellant and total respectively

This linear relationship is the basis of the phase techniques presented in Section 3.2.2.2. In order to determine the power requirements for such systems it is necessary to know the attenuation or transmission characteristics of the propellant. These were determined experimentally by TRW and reported in Section 2. Unfortunately, the lack of sufficiently transparent windows in the  $N_2O_4$  makes the use of light interaction techniques impractical.

### 3.2.2.1 Attenuation Techniques

These techniques employ the attenuation of multiple light sources as measured by multiple detectors to determine the quantity of propellant. They are similar in character to the nuclear or X-ray attenuation technique found in References 3-11, 3-12, and 3-13, except that higher power levels are required and no external radiation is present. As shown previously, the quantity of propellant in a given pathlength can be determined by Equation 3.2-8. In actuality, this equation is not sufficient to describe the situation as scattering of light becomes important. More precisely then

$$I = I_o B e^{-\mu \rho L} \quad (3.2-11)$$

where  $B$  is the buildup factor due to scattering of light into the detectors outside the idealized source/detector line-of-sight. The buildup factor

depends on the liquid gas interfaces, the refractive index of the propellant, photon energy, and actual source/detector geometry. In some cases, namely at high energies, it can be used to advantage by helping to linearize the relationship between attenuation and beam length. However, with random variations in propellant orientation, large variations in B due to refractions of the beam will occur with resulting inaccuracies.

The exponential form of the attenuation equation leads to problems of correctly correlating the results of multiple source/detector schemes. A number of possible single source/multiple detector techniques were examined, but none seemed satisfactory. By using individual source/detector combinations the exponential factor can be removed by having each detector output proportional to the log of the intensity. However, this is assuming that refractions will be negligible, which is not realistic. The basic tradeoff appears to be between the number of individual source/detectors which can be tolerated and the required accuracy. This problem has been studied in some depth in Reference 3-13, for relatively well behaved propellant under zero gravity. It appears that a minimum of 15 detectors would be required to meet a 5% ( $3\sigma$ ) accuracy, with the number of detectors increasing rapidly with increasing accuracy requirements.

Other major problems with this system are the variability in light absorption properties of the propellant caused by contaminants, availability of transparent windows, and the high power requirements.

#### 3.2.2.2 Phase Shift (Transmission Time) Systems

Another possible technique using light sources is the measurement of the transmission time of the beam through the propellant. As shown in Equations 3.2-9 and 3.2-10, the difference in the velocity of light in the pressurant and the propellant results in a linear relationship between the propellant quantity in the path and the transmission time. Recent developments in the field of high intensity light sources (Xenon tubes), coherent light sources (lasers), and high response detectors (gallium arsenide cells) make it possible to accurately determine the transmission time of light in mixed media.

For example, consider the system shown in Figure 3-16. Light from a modulated laser passes through the propellant and is detected by a gallium arsenide cell. The phase of the light is compared to that received from the same source through a length of calibrated light pipe. The difference in phase between the two beams is directly related to quantity of propellant in the beam length by Equation 3.2-10. This type of system can serve as a simple high gravity level gauge.

A second system which might be more attractive for zero g gauging is shown in Figure 3-17. A single laser source is used to scan a large number of individual detectors using a rotating mirror. As in the case of the attenuation system, a large number of detectors is required in order to achieve any reasonable degree of accuracy. However, because of the linear pathlength relationship, the system is less sensitive to the actual geometry of the propellant. As attenuation is unimportant the system is not sensitive to small quantities of contaminants.

Refraction of the beam poses a major problem here, as it can result in an appreciable lengthening of the pathlength. This is particularly a problem with the fuel, which has a very high refractive index. Statistical analysis would be required in order to determine the optimum location and number of detectors required. Although this analysis was not undertaken because of the high attenuation of light in the oxidizer, the technique appears to be promising for relatively transparent propellants.

#### 3.2.2.3 Phosphorescence

The basic purpose of the phosphorescent approach is to reduce the sensitivity of the attenuation technique discussed in Section 3.2.2.1. A phosphorescent material is one which absorbs photons at one energy and re-emits the energy at a different specific energy level. Let us first consider the case where a known quantity of tracer is dissolved in the propellant and uniformly illuminated with a light source. If the propellant is completely transparent to both the activating and phosphorescing light waves, then the total flux at the phosphorescent frequency is a direct measure of the amount of tracer present. This in turn gives a measure of the propellant quantity.



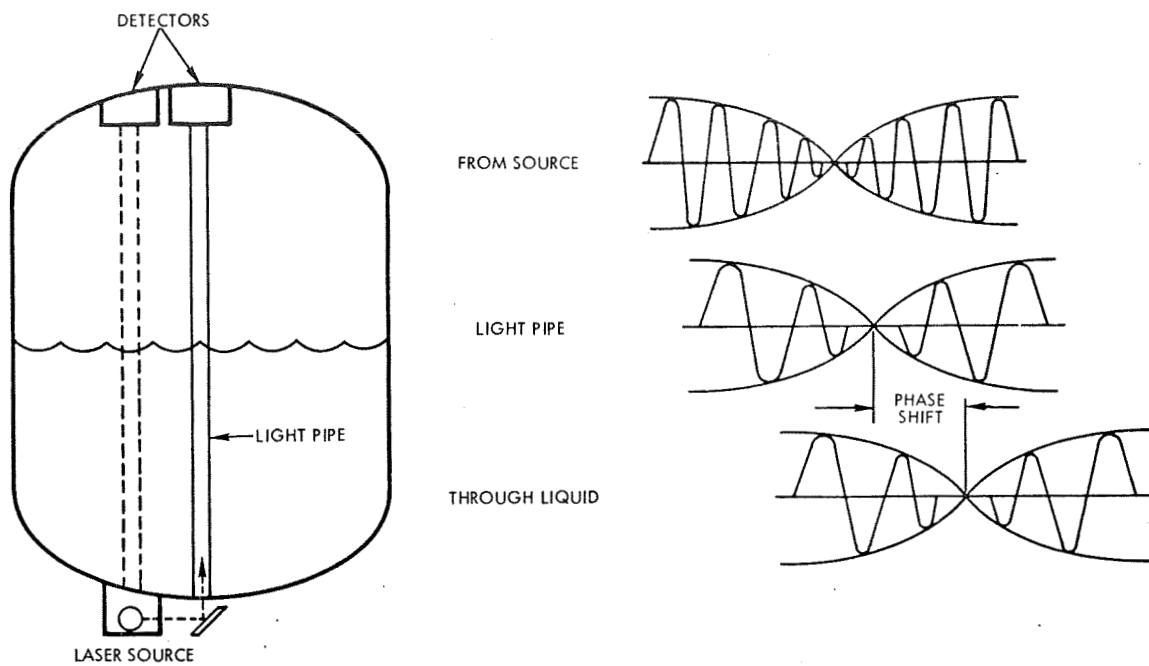


Figure 3-16. Laser Phase Technique

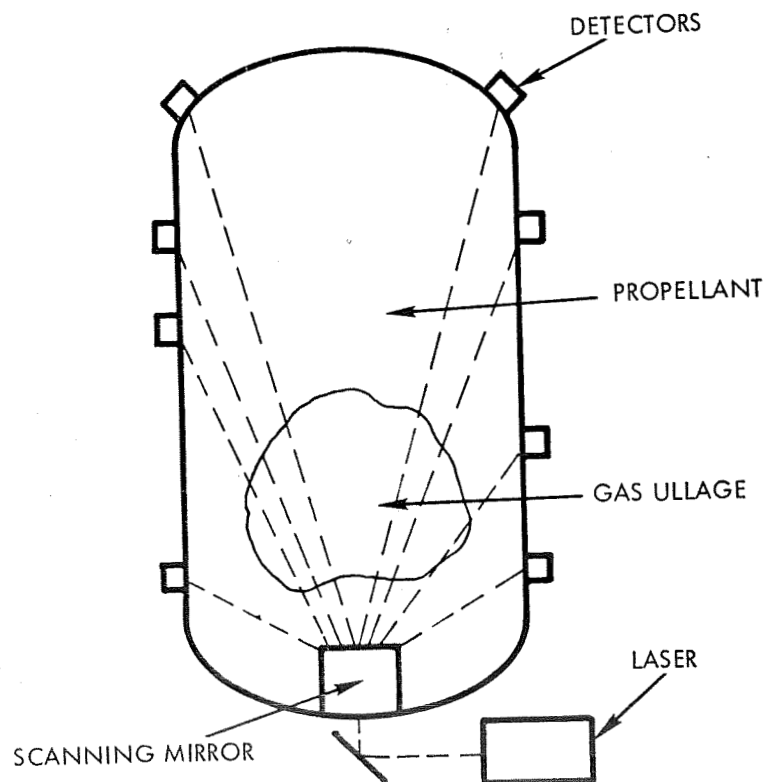


Figure 3-17. Scanning Laser Schematic

Obviously this is an unrealistic case. The propellant will not be completely transparent to either frequency, but will attenuate the radiation both from phosphorescence and the primary source, as shown below for a one-dimensional beam.

$$I_F = AI_o \frac{e^{-\mu_F \rho x} - e^{-\mu_F \rho x}}{\mu_\rho - \mu_F} \quad (3.2-12)$$

For the special case of  $\mu_\rho = \mu_F = \mu$

$$I_F = AI_o X e^{-\mu \rho x} \quad (3.2-12a)$$

where

$\mu_F$  = mass absorption coefficient of phosphorescent radiation

$\mu_\rho$  = mass absorption coefficient of primary radiation

$I_F$  = intensity of phosphorescent radiation at distance  $x$

Actually, as the emitted radiation is isentropic, the 3-dimensional effects must be included. However, since no sufficiently transparent windows exist in  $N_2O_4$ , no further work was performed.

#### 3.2.2.4 Other Light Interaction Systems

A number of other techniques were briefly examined in the course of the study. All required highly transparent windows which are not present in the  $N_2O_4$ .

In one proposed technique, the Raman effect is used to essentially provide a self-phosphorescence of the propellant. In the Raman effect, light is scattered by interaction of the beam with the molecules. The frequency of

the scattered light is different from the input frequency by an amount equivalent to a fundamental vibrational or rotational frequency of the molecule. As the propellant would strongly absorb at its fundamental frequency, the Raman effect allows self-phosphorescent measurements at frequencies at which windows might exist.

Another technique briefly examined was the measurement of the decay time of a high intensity light pulse. For a relatively transparent propellant, located in a tank with highly reflective walls, a light pulse will be reflected through the propellant numerous times before being completely absorbed. The decay rate of the light can then be related to the quantity of absorbing material (propellant) in the tank. Unfortunately, the reflectivity and transparency required are not attainable in this case.

### 3.2.3 Gamma and X-Ray Techniques

The statement of work specifically eliminated nuclear attenuation systems from this study. However, in the interest of completeness, a brief summary of these systems is presented in this section.

#### 3.2.3.1 Attenuation Techniques

The discussion of the light attenuation system (Section 3.2.2.1) is in general applicable to the gamma and X-ray attenuation techniques. The primary differences result from the availability of transparent windows. At the high energies, a propellant refractive index of unity, and the possibility of using external sources because the tank walls are comparatively transparent. Since the refractive index of the propellant is close to unity, refraction of the beam is negligible. Any scattering that does occur is a result of photon interaction with the atomic electrons. The buildup factors are, therefore, somewhat more predictable. As multiple isotope sources are available a broader beam can be used and power requirements are lowered. However, accuracies of  $\pm 5\%$  ( $3\sigma$ ) or better are still difficult to achieve with a limited number of detectors.

One of the major problems other than accuracy is crosstalk between adjacent tanks. This can be eliminated by using pulsed X-ray sources timed to be non-interfering rather than isotopes which emit continuously. This, however, results in higher electrical power demands. One additional problem is the quantity of external radiation generated.

### 3.3 INTERACTION WITH OTHER FIELDS AND BEAMS

In this section, a number of different techniques using field and/or beams to measure propellant quantity under zero gravity are discussed. None of the techniques presented appear to have sufficient promise to warrant further examination in this study.

#### 3.3.1 Gravitational Field Measurement

One of the basic properties of all matter is the presence of gravitational attraction to other masses. The basic law governing the attraction between point source is

$$F = \frac{Gm_1 m_2}{r^2} \quad (3.3-1)$$

where

$G$  = gravitational constant

$F_1$  = attractive force between  $m_1$  and  $m_2$

$r$  = distance between masses of  $m_1$  and  $m_2$

$m_1$  = mass of accelerometer pendulum

$m_2$  = mass of propellant bodies

Applying Newton's first law:

$$a = \frac{F}{m_2} = \frac{m_1 G}{r^2} \quad (3.3-2)$$

where

$a$  = acceleration exerted on  $m_1$  by  $m_2$ .

The acceleration sensed by an accelerometer placed near surface of a typical propellant tank, as shown in Figure 3-18, will vary from  $10^5$  to  $10^{-10}$  g which is partially within the range of existing high accuracy digital accelerometers. Ignoring for the moment the question of how to accurately measure these low accelerations, let us examine the potential of a propellant gauging system under zero gravity using perfect accelerometers.

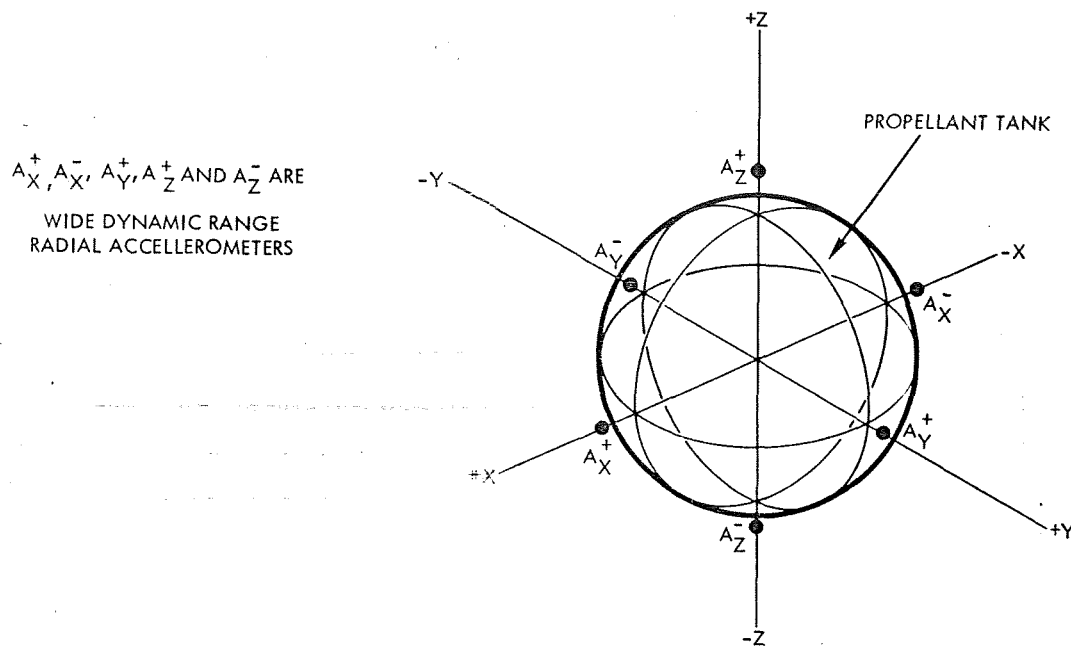


Figure 3-18. Propellant Gauging by Gravitational Attraction

Numerous problems became immediately apparent:

- 1) Equation 3.3-2 is only an approximation for well behaved propellant masses such as point sources, spheres, etc. Appreciable errors will be experienced with bodies having long thin shapes such as slabs, etc.
- 2) The accelerometers will not only detect the mass in the particular tank being gauged, but also all the mass in the other tanks as well as that of the vehicle itself. While it may be possible to calibrate or cancel out the effect of the fixed vehicle weight, it does not appear possible to eliminate the "cross talk" between tanks.
- 3) The field is basically an  $R^2$  field, not a linear one. The measurement will thus be quite sensitive to propellant position and simple averaging of opposing accelerometers cannot be used to cancel such effects.
- 4) The accelerometers will detect small perturbations such as roll and yaw rates and consider them as changes in mass.

### 3.3.2 Electric Field Interaction

Three possible gauging techniques were examined which utilized the interaction of the propellant with an electrical field. Because of the conductivity of the fuel, the first two techniques, capacitance and dielectrophoresis, were eliminated. The third technique utilized the conductivity, but was found to be highly sensitive to the location of the propellant.

### 3.3.2.1 Capacitance Systems

The statement of work for this study specifically deleted capacitance-type systems from the study. However, in the interest of completeness this small section is included on capacitance systems reflecting discussions which occurred prior to the study and during the brainstorming sessions.

Capacitance systems have been used successfully for many years in measuring propellant quantities under normal gravity conditions. Basically, the measurement is of the dielectrical strength between two conductors. As the propellant dielectric constant is appreciably different from that of the pressurant gas the measured capacitance is directly related to the propellant mass. A number of systems has been proposed utilizing this principle under zero gravity, including the use of numbers of multiple wires within the tankage and the use of shaped plate capacitors. The problem when using a capacitance system under zero-gravity conditions is that the measured capacity is a function not only of the dielectric constant of the propellant, but is actually a function of the propellant position relative to the plates and wires.

Figure 3-19 shows a simple square tank with two plates located at opposite faces of the tank. It is apparent that the maximum capacitance will occur when the propellant is located as a vertical slab (Figure 3-19b) and the minimum capacitance will occur when the propellant is a horizontal slab (Figure 3-19a). All other distributions will have capacitance values between these limits. If the average difference between these limits is calculated, it is found to be expressed by the following equation:

$$\Delta = \pm 1/2 \left[ \frac{C_M - C_a}{K - 1} \right] \left[ \frac{1}{C_a} - \frac{K}{C_M} \right] \times 100 \quad (3.3-3)$$

where

$K$  = dielectric constant of propellant

$C_M$  = measured capacitance      Tank empty  $C_M = C_a$

Tank full  $C_M = KC_a$

$C_a$  = capacitance of plates in gas

$\Delta$  = ambiguity error, percent of full tank

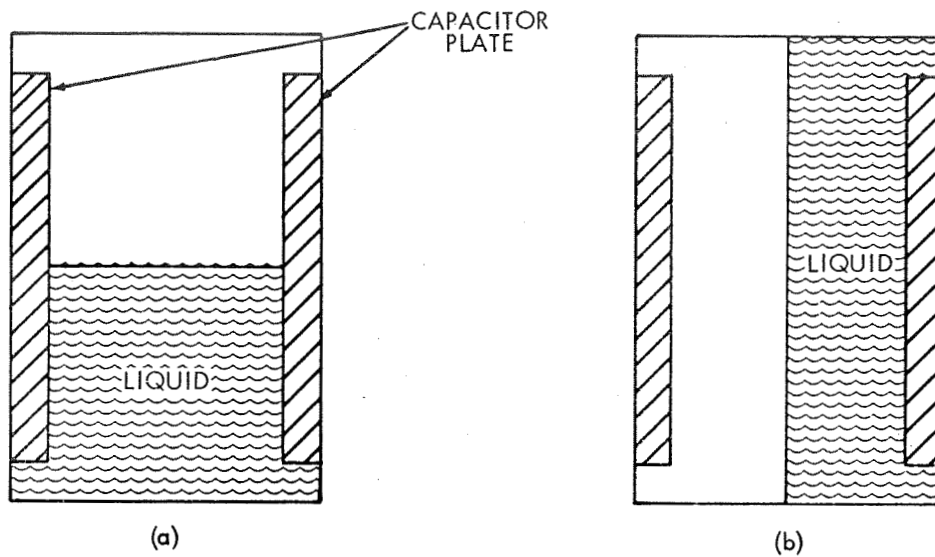
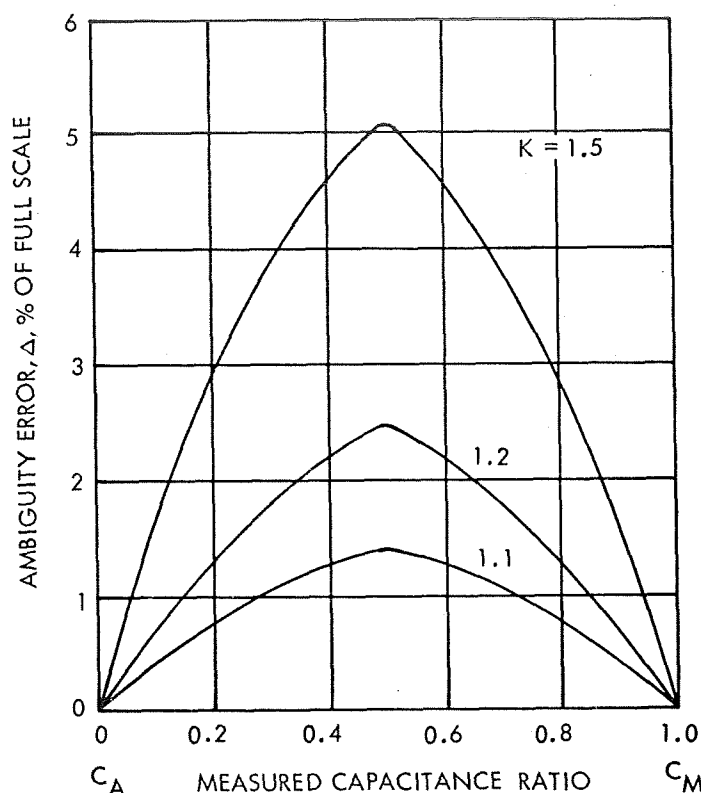


Figure 3-19. Effect of Propellant Orientation

A plot of this error is shown in Figure 3-20 for capacitances between  $C_a$  (empty tank) and  $KC_a$  (full tank) for a number of values of  $K$ . It can be seen that the ambiguity error,  $\Delta$ , decreases as the dielectric constant  $K$  approaches unity, and actually becomes zero at  $K = 1$ . However, the accuracy of the gauging system itself diverges in the opposite direction. At  $K = 1$ , the system cannot distinguish between propellant and pressurant (assuming that  $K = 1$  for the pressurant) and the overall measurement accuracy becomes zero. Obviously, the overall system accuracy must be evaluated.

The configuration presented above assumes that the electric field is uniform between the plates. Other configurations were briefly examined to determine whether they could provide decreased sensitivity to propellant position. It soon became apparent that any other plate configuration would not provide a uniform field and only serve to make the gauge more sensitive to propellant position. With a non-uniform propellant, located in a high field strength, location would have a larger effect than the same propellant located in a low field strength area.

In addition, it became apparent that for the case of conducting tank walls the field would not be uniform and propellant near the ends of the plate would have greater effect than propellant between the plates.



$C_A$  = PLATE CAPACITANCE  
IN AIR  
 $C_M$  = MEASURED  
PLATE CAPACITANCE  
 $K$  = DIELECTRIC  
CONSTANT  
OF FLUID

Figure 3-20. Variation of Error with Dielectric Constant

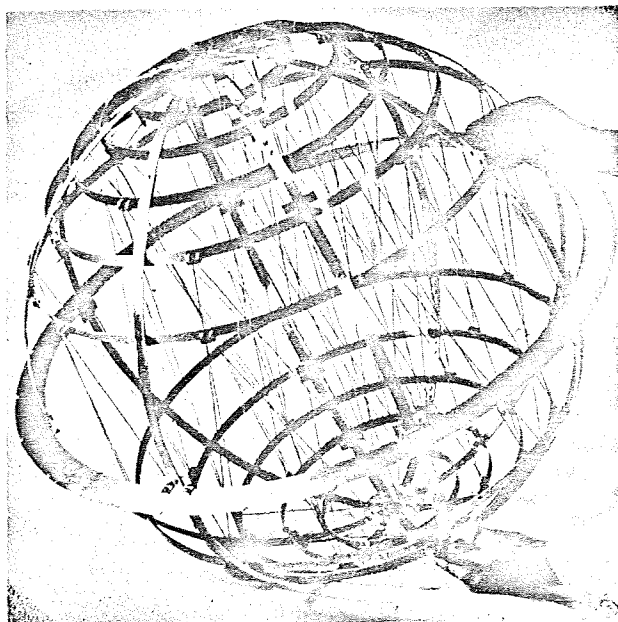


Figure 3-21. Simmonds Grid Capacitance Gauge

Another type of capacitance system utilizes a matrix of wires within the propellant tank, thus essentially subdividing the tank into a large number of individual cells. Figure 3-21 shows a typical tank presently under development by Simmonds. If the propellant is randomly distributed throughout the tank, the net effect will be to cancel out the sensitivity to propellant location. Unfortunately, under zero or low gravity the presence of the large number of wires will perturb the propellant to be preferentially located

close to the wire. This is true for both wetting and nonwetting wires. As the field strength is appreciably higher near the wires than in the space between the wires, the resulting measurement will be sensitive to propellant location.



### 3.3.2.2 Dielectrophoresis

The technique of dielectrophoresis is not a gauging system in the conventional sense of the term, but rather a propellant orientation device which may be used as a gauging system. The process involves the motion of a dielectric under the influence of a non-uniform electric field. Motion of the dielectric fluid results from the field-induced pressure which directs the fluid toward the region of highest field strength. The actual force exerted on the fluid is a function of the field strength and the dielectric constant of the liquid. The non-uniform field is created by shaping the electrodes as shown in Figure 3-22 thus forcing the fluid to flow to and remain in a specified location. For more detail on the technique the reader is referred to Reference 3-14, 3-15, and 3-16.

With the propellant oriented, any of a large number of high gravity techniques can be used to measure the propellant volume. The simplest technique would appear to be to measure the change in voltage gradient along the plates caused by the dielectric propellant. While this technique seems feasible for the oxidizer, the high conductivity of the fuel results in excessive power requirements. The system was therefore not studied further.

### 3.3.3 Magnetic Field Interactions

Three possible gauging techniques were examined which utilized magnetic fields. None of the approaches appeared promising.

#### 3.3.3.1 Ferromagnetic Doping of the Propellants

A small concentration of ferromagnetic material could be added as a colloid to the propellant, thus giving the propellant diamagnetic properties. The perturbation in an electromagnetic field induced by coils submerged within the tank (see Figure 3-23) would then be a measure of the quantity of a diamagnetic material, and hence of the propellant. Simple analysis showed that this system has the same problems discussed for the capacitance system in Section 3.3.2, namely, the measurement is sensitive to the location of the propellant. As the differences in diamagnetic constants of the propellant and the ullage gas would be large, the errors were correspondingly larger than for the capacitance system.

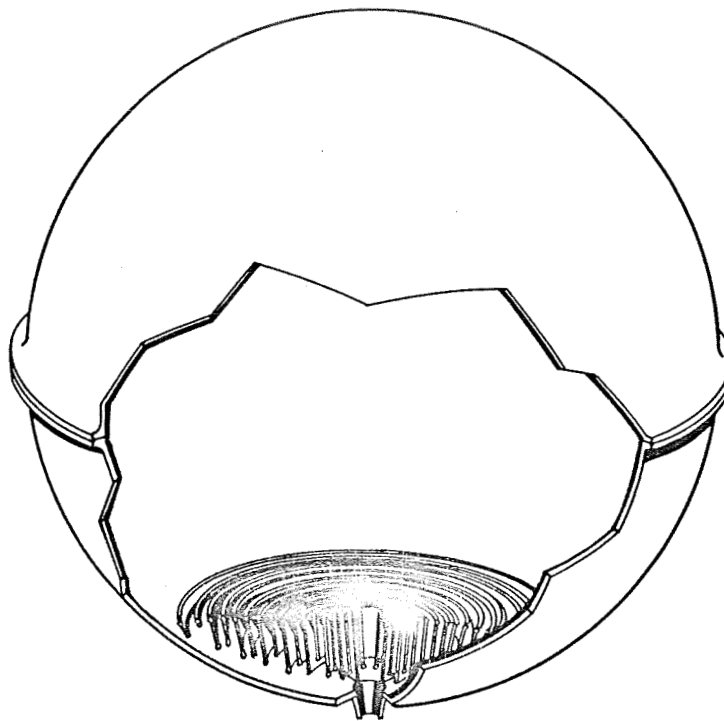


Figure 3-22. Typical Localized Dielectrophoreses Device

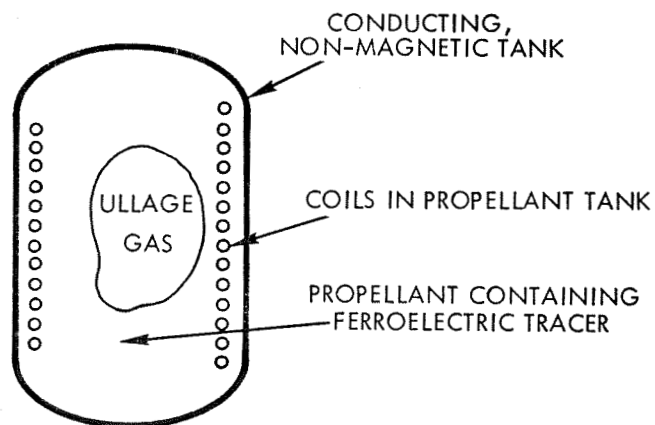


Figure 3-23. Perturbation in an Electromagnetic Field Induced by Submerged Coils

### 3.3.3.2 Magnetic Doping of the Propellants

A small amount of magnetic material could be dispersed as a colloid in the propellant. The induced magnetic field could then be measured with magnetometers. The system is highly sensitive to propellant position because of the variation of the field strength with  $R^2$ .

### 3.3.3.3 Nuclear Magnetic Resonance

Most atomic nuclei possess both angular momentum and a magnetic moment and, therefore, precess in the presence of a magnetic field at a predictable frequency

$$f = \mu H_o / I \quad (3.3-4)$$

$\mu$  = nuclear angular momentum

$H_o$  = external magnetic strength

$I$  = magnetic moment

$f$  = frequency of precession

Such a precessing nucleus will interchange energy perpendicular to the primary field with a secondary magnetic field of different frequency. As a result, there will be a net power absorption from the secondary field which is proportional to the number of atoms in the field. This effect has been used for chemical analysis of trace materials and was proposed as a possible means of propellant gauging.

Preliminary examination showed that this technique would require huge magnets and large power consumptions. Field strengths on the order of several thousands of gauss/cm were required before the measurement could be made. The concept was dropped as impractical.

### 3.3.4 Interaction with Neutron Beams

The systems discussed in this section all utilize neutron beams to attempt to measure the quantity of propellant in the tank. All of these

systems were eliminated from further consideration because of the high level of external radiation associated with the neutron beam. They are included only for completeness.

#### 3.3.4.1 (n, $\gamma$ ) Activation (Doped)

This concept requires that the propellant be doped with an element that has a high (n,  $\gamma$ ) reaction cross-section and then activated with a neutron source. The number of ensuing gammas that are counted by multiple detectors are related to the quantity of propellant. This concept has the advantage that the propellant is only radioactive during the period of measurement. This is ensured by employing high (n,  $\gamma$ ) cross-section elements with short half-lives. The neutron source can remain shielded except during the periods when measurements are desired.

Difficulties with the system include the high energy gamma ray required if the gamma ray is not to be appreciably attenuated by the propellant, the weight and size of the shielded neutron source, and the external radiation level.

#### 3.3.4.2 Pulse Analysis

The pulse analysis technique is based on the thermalization of the neutrons as they are transported through the propellant. For example, a monoenergetic pulse of neutrons will be slowed down to form a continuous spectrum, as shown in Figure 3-24.

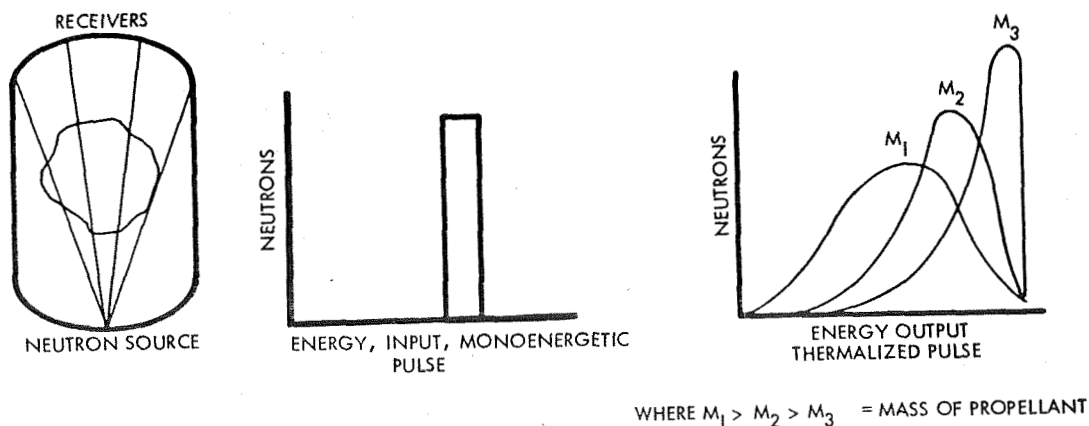


Figure 3-24. Monoenergetic Pulse of Neutrons Slowed Down to Form a Continuous Spectrum

The quantity of propellant between the source and detector will thus be related to the shape of the detected spectrum; the more propellant, the lower in energy will be the peak of the spectrum. The gauge could be calibrated to give a direct relation between the spectrum energy peak and the quantity of propellant between the source and detector.

#### 3.3.4.3 Ionization Gauge - (Electroscope)

The principle of this method is based upon the ionizing effect of neutrons as they pass through material. A burst of neutrons impinging on the propellant causes ionization of a small quantity of propellant. The magnitude of the total ionization will depend upon the amount of propellant present in the tanks. The ionization could be measured with a type of electroscope or by electric field measurement techniques. The technique will not work, however, because of the conductivity of the propellants.

#### 3.3.4.4 Tank Wall Activation

The principle of this method is based on the propellant shielding the tank walls from neutrons emitted from a centrally located neutron source. Thus, the more propellant in the tank, the more attenuation between the source and the tank wall. The neutrons captured in the tank wall will produce a certain degree of activation (the tank wall material may be doped with a high activation cross-section element). This activation can be detected by detectors placed around the outside of the tank wall. An average activation will yield an indication of the quantity of propellant in the tank (high activation, less propellant present). A short half-life activation element is desirable for short response times. A pulsed neutron source, as opposed to a continuous neutron source, would be better suited for this application. This system is sensitive to propellant location. Propellant located near the source would be exposed, by the geometry, to higher concentrations of neutrons and thus attenuate the beam more strongly.

### 3.4 OTHER DIRECT MEASURING TECHNIQUES

#### 3.4.1 Inertial Measuring Techniques

A number of techniques for the direct measurement of the propellant mass will be discussed in this section. The suggestions represent only a few of the more promising techniques discussed in various brainstorming sessions.

Under the influence of known acceleration fields the measurement of the propellant mass can be accomplished by direct weighing or force measurement and application of Newton's first law.

$$F = m \frac{a}{g_c} \quad (3.4-1)$$

where

$F$  = measured force,  $\text{lb}_f$

$m$  = mass,  $\text{lb}_m$

$a$  = acceleration,  $\text{ft/sec}^2$

$g_c$  = conversion factor,  $32.179 \text{ lb}_m / \text{lb}_f \text{ ft/sec}^2$

All of the propellant must be accelerating uniformly at the input acceleration to make such a measurement. If, for example, a pocket of propellant is separated from the main propellant mass and therefore, is not accelerating it will not be measured. Errors can also be introduced by geysering or surface tension.

From this it is apparent that to actually weigh the propellant, a high  $g$  field that is applied for a relatively long time period is required. In order to measure the propellant mass under low or zero gravity conditions, other techniques must be used.

One technique which seemed to hold some promise for gauging under zero or low gravity was the paddle wheel shown in Figure 3-25. The paddle wheel is made of a light mesh screen and rotates about the centerline of the tank at constant angular velocity. Initially the propellant in the tank is somewhat randomly located but as the paddle continues to rotate the propellant ultimately moves with the velocity of the paddle. The force required to rotate the propellant is largely a function of the frictional loss at the wall. By superimposing a small amplitude sinusoidal change in velocity on the constant angular motion, it is possible to cancel out the effects of the frictional loss. The force required to impose the sinusoidal input on the propellant is primarily a function of the rotational moment of inertia of the propellant and hence, related to the propellant mass. Further analysis showed that the inertia was dependent on the radial distribution of the propellant which in turn was dependent on the viscosity and surface tension of the propellant.

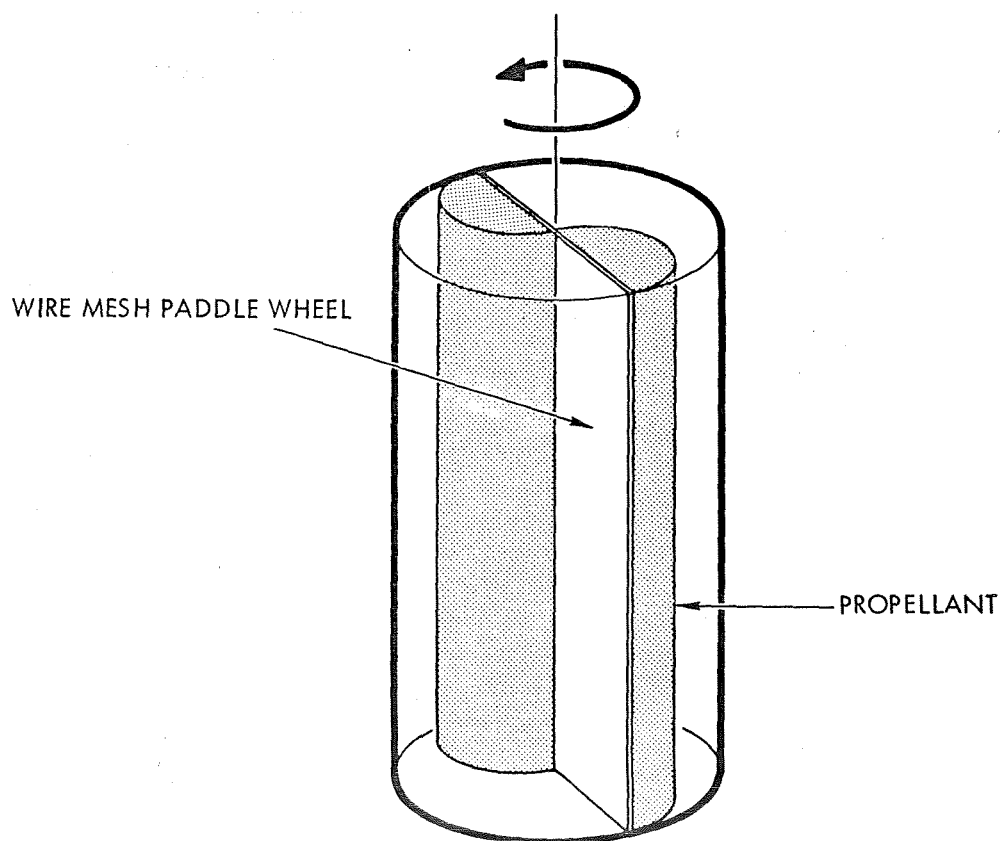


Figure 3-25. Schematic of Paddlewheel Gauging System

Since it appeared quite difficult to predict the radial distribution, this concept was dropped. However, one interesting aspect of this system was that it induced roll torques on the vehicle and thus if desired, could have served as an inertial wheel in an attitude control system. It was, of course, a high mass, low velocity, inertial wheel rather than the more normal low mass, high velocity devices presently used.

#### 3.4.2 Titration Techniques

The use of titration techniques to measure the quantity of propellant has been previously proposed (Reference 3-6) and briefly investigated during this study. The basic idea of this approach is simple. If a known quantity of a tracer is added to an unknown quantity of propellant and thoroughly mixed, the concentration of the tracer in the propellant will give a direct measure of the propellant quantity, as follows:

$$\text{weight of propellant} = \frac{\text{weight of tracer}}{\text{concentration of tracer}}$$

(3.4-2)

Proposed quantities to be used for titration included dyes, radio-isotopes, gas, and heat. This relationship is obviously truly independent of any external factors. The major difficulty, particularly under low or zero gravity, is attaining uniform mixing. Under high gravity conditions, convection currents can be counted on to help with the mixing under zero gravity. The difficulties of achieving uniform distribution of the titrating quantity eliminated this technique.



### 3.5 ULLAGE VOLUME MEASURING SYSTEMS

#### 3.5.1 Pressurant Gas Balance Systems

In this type of system, the mass of propellant remaining in the propellant tank is determined by performing a material balance on the pressurant gas. The pressurant gas mass remaining in the pressurant tank is calculated from the gas density and tank volume. The pressurant gas mass in the propellant tanks is then calculated by the difference between the initial mass and present mass in the pressurant tank. The gas mass in the propellant tank is combined with the gas density in the propellant tank to give the ullage volume. By difference, the propellant volume is determined. This volume is converted into a propellant mass through the propellant density, which is determined from propellant temperature measurement. The equation relating the propellant mass to the measured quantities is shown below:

$$M_P = M_{P_o} \frac{\rho_P}{\rho_{P_o}} \left[ 1 - \frac{V_g \rho_{P_o} \rho_{g_o}}{M_{P_o} \rho_g^*} \left( 1 - \frac{\rho_g}{\rho_{g_o}} \right) - \frac{V_{u_o} \rho_{P_o}}{M_{P_o}} \left( \frac{\rho_{g_o}^* - \rho_g}{\rho_g^*} \right) \right] \quad (3.5-1)$$

where

$M_P$  = mass of propellant

$\rho_g$  = density of gas in pressurant tank

$\rho_g^*$  = density of pressurant gas in propellant tank

$\rho_P$  = density of propellant

$V_g$  = volume of pressurant tank

$V_u$  = volume of ullage

sub o = initial conditions

To maintain an accuracy of  $\pm 0.25\%$  of full scale near tank-empty conditions, the error in measurement of the tank volumes, the initial and final propellant and pressurant densities, and the loaded propellant mass must be less than  $\pm 0.1\%$  of full scale for each parameter. If the gas densities are determined from pressure and temperature measurements the problem is increased.

Three system concepts are presented. The first and simplest (PVT) obtains the gas densities from pressure and temperature measurements. The second concept ( $\rho V$ ) measures the pressurant tank gas density directly. The third concept (RHO) measures the change in pressurant density in the propellant tank.

#### 3.5.1.1 PVT Propellant Quantity Gauging System

This system is currently being utilized on the Gemini and Apollo spacecraft where it measures the propellant quantity in the RCS. A schematic of the system is shown in Figure 3-26. This system determines pressurant gas density by sensing the initial temperature and pressure in the helium gas storage container. These values correspond to the baseline full propellant tank condition. The reduction of this pressure (corrected for temperature) as the propellants are consumed is the technique used for determining the residual propellants at any given time. The pressurant temperature and pressure data are sent to the signal processing data computer which, through the use of the spacecraft telemetry system, relays this information to a ground-based computer. Additional data transmitted to the ground to correct for initial and varying propellant tank conditions are initial propellant level (determined by a propellant tank-mounted capacitance probe), propellant

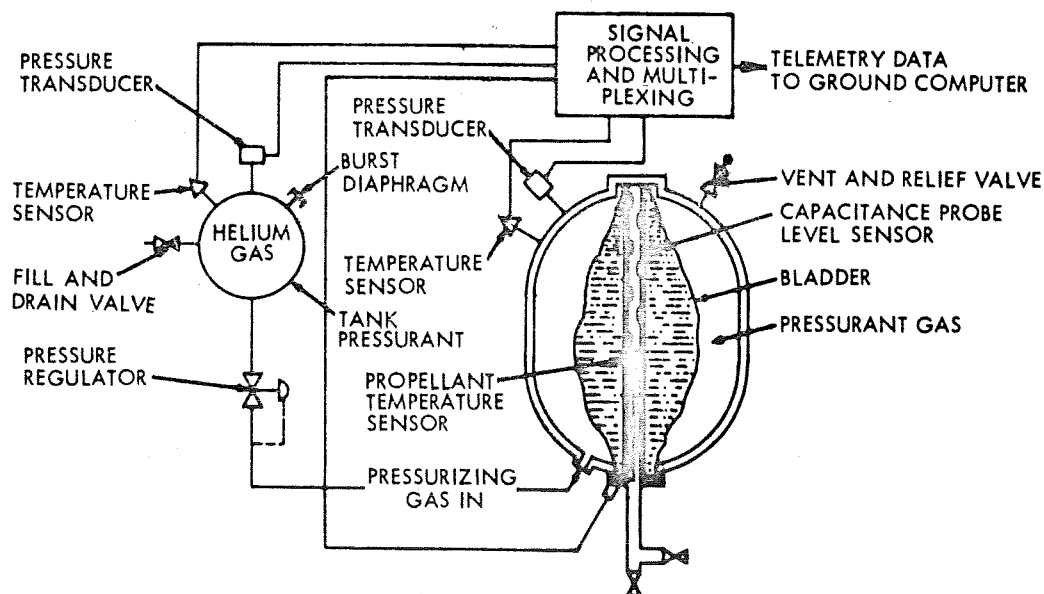


Figure 3-26. PVT Propellant Gauging System Schematic

tank ullage gas temperature and pressure (needed to determine ullage gas density), and propellant density. With this information, the ground based computer is able to compute the total amount of propellant remaining in the propellant tanks fed by each pressure reservoir. When more than one propellant tank is fed by a single pressure reservoir this system cannot indicate the proportion of propellant between the tanks.

The system is lightweight, simple, and does not require much power. Its primary disadvantages are poor overall accuracy, sensitivity to overboard venting and pressurant leakage, and the requirement for individual pressurant bottles for each tank if individual propellant tank quantities are desired.

#### 3.5.1.2 Density-Volume Propellant Gauging Concept

The density-volume ( $\rho V$ ) propellant gauging concept is similar to the PVT concept, except that the gas density in the pressurant tank is measured directly, rather than indirectly, through temperature and pressure measurements. This, coupled with a highly precise means of density measurement, greatly improves the accuracy of the PVT system.

A radioisotope beta-emitter is used in the  $\rho V$  gauge to determine the quantity of pressurant gas expelled into the propellant tank ullage volume. Experiments at TRW Systems have demonstrated the pressure dependence of the count rate from beta radiation transmitted through the gas from a fixed, solid beta source. The data reveal that, as the helium pressurant pressure decreases from 3000 to 150 psia, the count rate increases by a factor of about 2000 for a 1-mC thallium-204 source and a 3-inch source/detector separation distance. Thus, small changes in pressurant tank pressure will cause relatively large changes in the count rate and a system with high accuracy can be obtained.

As the beta attenuation is proportional to the number of atoms per unit volume, density rather than pressure is being measured, and no temperature correction is required. This density (or density ratio) can be used directly in the helium balance (Equation 3.5-1) for the calculation of propellant mass.

The highly accurate pressurant tank density measurement eliminates this as a source of error. The remaining large error source is the actual density of the helium in the propellant tank. For propellants with a low vapor pressure or for tanks containing low impermeable bladders this error source is small. However, for the high vapor pressure  $N_2O_4$ , appreciable error can occur because of the partial pressure of the propellant vapor.

### 3.5.1.3 RHO Gauge

The single largest error source remaining in the  $pV$  system was the uncertainty in the helium density in the propellant tank, therefore, techniques for determining the ullage helium density were investigated. The ullage gas bulk density may be accurately determined by the beta ray attenuation technique used in the pressurant tank. Basically, for the oxidizer tank

$$\eta_{\beta} = 1 - \exp - \left[ \mu_{\rho} (\rho_{He} + \rho_{N_2O_4}) t_{\beta} \right] \quad (3.5-2)$$

After consideration of a number of techniques, it was found that attenuation of soft X-rays (2-20 Kev) was highly dependent on the concentration of heavy atoms and almost transparent to helium as shown below

$$\eta_{\gamma} = 1 - \exp - \left[ \mu_{\gamma He} (\rho_{He} + A \rho_{N_2O_4}) t_{\gamma} \right] \quad (3.5-3)$$

where

$\eta$  = attenuation

$\mu$  = mass attenuation coefficient

$\rho$  = density

$t$  = effective beam length

$$A = \frac{\mu_{\gamma N_2O_4}}{\mu_{\gamma He}} \cong 62 \text{ (proportional to fifth power of atomic number)}$$

sub  $\beta$  = pertaining to beta ray attenuation

$\gamma$  = pertaining to X-ray attenuation

Thus, given the measurement of the average density by the beta attenuation and the  $N_2O_4$  concentration from the X-ray attenuation, the true helium density in the ullage tank can be determined.

In addition to improving the accuracy potential of the  $\rho V$  system, this technique lends itself to serving as a separate gauging system in conjunction with a high gravity gauge. Assume that each individual propellant tank is isolated from the pressurant tank during the coast period. Provided there is no leakage, the quantity of helium and the volume occupied by the helium remains constant. Despite changes in vapor pressure and temperature in the tank, the average helium density remains constant. Any decrease in helium density will be a result of leakage of either helium or propellant. Thus, knowing the quantity of propellant at the termination of engine firing from a high gravity gauge, a limit can be placed on the quantity if any, of propellant leakage out of the tank.

The RHO gauge system is further discussed in Section 4.2.1. Among the major shortcomings of the system are the inability to distinguish between a pressurant and propellant leak, and sensitivity to stratification in the propellant tank. The RHO gauge when used by itself in the propellant tank cannot provide an independent determination of the propellant quantity. However, in conjunction with a high-gravity gauging system it provides a zero-gravity gauging capability. It can also improve the overall accuracy of the  $\rho V$  system when separate pressurant tanks are used for each propellant.

### 3.5.2 Tracer Gas Dilution Systems

The basic concept of a tracer gas dilution gauging system depends on relating the concentration of a tracer gas in the ullage volume of a propellant tank to the quantity of propellant in the tank. The principle of operation is as follows. When the tank is full of propellant, a small quantity of tracer gas is injected into the ullage space. As the propellant

is consumed from the tank, the ullage volume increases, therefore the volume concentration of the tracer is decreased. This dilution effect within the pressurization gas is continuously measured. The measured tracer concentration is related to the propellant remaining by means of a simple algebraic equation. To ensure homogeneity, the gases can be mixed by a gas circulation unit.

A number of basic measurement approaches can be applied to the tracer dilution technique. In one configuration of the system a radioactive trace gas can be used in conjunction with nuclear measurement techniques. In another configuration, an inert trace gas can be used with infrared or other measurement techniques. The radiotracer technique possesses advantages over infrared techniques in the degree of accuracy that may be obtained, primarily because of the digital counting technique. This type of system has demonstrated quite satisfactory performance in tanks containing nonporous bladders. In tanks without bladders, Section 4.3 shows that the majority of the tracer will be dissolved in the propellant, resulting in appreciable errors in the measurement.

#### 4. PRELIMINARY ANALYSIS OF GAUGING SYSTEMS

This section of the report contains detailed analysis of the more promising systems reviewed in Section 3. These include the infrasonic, helium balance, attenuation, and gas tracer systems. As a result of these analyses, two systems—the Resonant Infrasonic Gauging System (RIGS) and the RHO Gauging System have proven the most promising for gauging under the zero-gravity environment.

##### 4.1 INFRASONIC SYSTEMS

The analyses of two types of Infrasonic Systems—the phase-sensitive infrasonic gauge and the resonant infrasonic gauge—are presented in Sections 4.1.1 and 4.1.2. An error analysis and discussion of the RIGS problem areas is presented in Section 4.1.3.

###### 4.1.1 Phase Sensitive Infrasonic System

A preliminary evaluation has been made of the feasibility of a zero g propellant gauging system that measures the compressibility of the pressurizing gas to determine the volume of storable propellant. This is achieved indirectly by measuring the phase shift between the dynamic gas pressure in the propellant tank and that of a small isolated cavity driven by a constant velocity, low frequency acoustic driver.

The system is similar to one developed by Acoustica Associates (Reference 3-2). The Acoustica System ran into the problem of liquid entry into the resistance separating the main tank and the driver cavity which caused the system to malfunction under zero g (Reference 3-3). The proposed solution utilizes a flexible rubber diaphragm to isolate the resistance and driver cavity regions from the main tank (Figure 4-1) thus avoiding this problem. A detailed analysis of the gauging technique is found in Appendix B.

###### 4.1.1.1 Description of Phase-Sensitive Infrasonic System

The proposed Phase-Sensitive Infrasonic System is illustrated schematically in Figure 4-1. It consists of a low-frequency constant-velocity driver which sets up a sinusoidal pressure perturbation in the directly coupled driver cavity Region No. 1. A resistance  $R$  separates

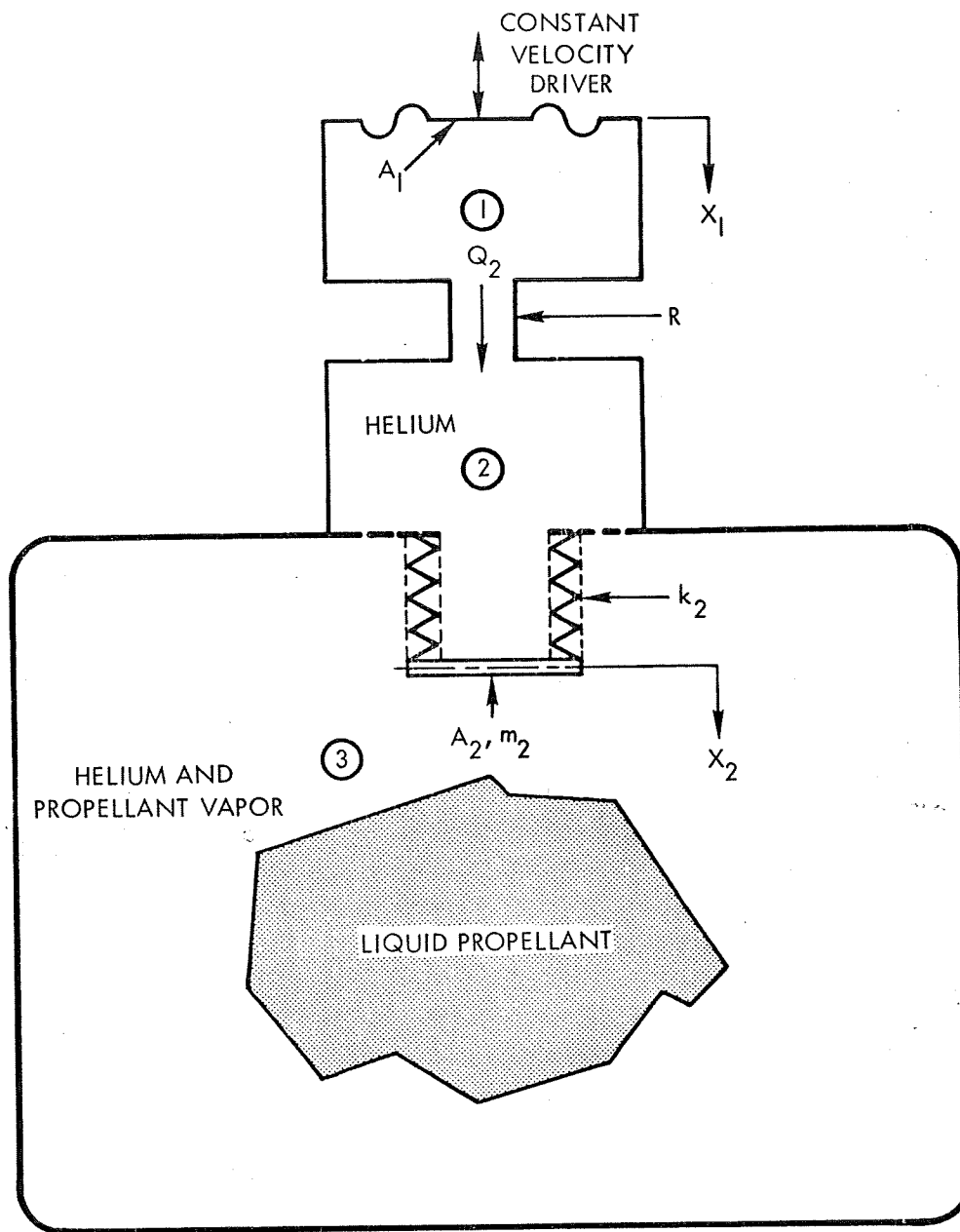


Figure 4-1. Schematic of Infrasonic Propellant Gauge



Regions No. 1 and No. 2 and provides the resistive component needed to produce a measurable phase shift between the pressure in the driver cavity,  $P_1$  and the ullage volume,  $P_3$ . The volume in the driver cavities is selected to be small relative to the gas volume in the main tank. The pressure perturbation and corresponding phase shift between  $P_3$  and  $P_1$  follows, as a first approximation, a first order lag whose time constant is  $RC_3$ , where  $C_3 = (\bar{V}_3/\gamma_3\bar{P}_3)$  is the capacitance of the ullage volume in the main tank undergoing measurement. Thus by measuring the phase shift, the effective capacitance,  $C_3$  of the ullage volume can be determined. Since  $C_3$  is sensitive both to  $\gamma_3$  (the effective specific heat ratio in the void volume of the propellant tank) and  $\bar{P}_3$  (the steady state pressure), these two properties must be measured to ensure proper compensation when they vary from some nominal level. The specific heat ratio can be determined by either: 1) an acoustic velocity measurement in the gas vapor of the propellant tank or 2) a temperature measurement, as the specific heat ratio of the two-component pressurization gas/propellant vapor is related to the temperature of the mixture, for slowly varying (quasi-steady state) conditions. The pressure ( $\bar{P}_3$ ) can be directly measured by a suitable transducer. Thus, measurement of phase shift between  $P_3$  and  $P_1$  permits the determination of gas volume, and indirectly the propellant volume, in the main tank. Refinements in the system consist of an elastic device (denoted by a spring constant  $k_2$ ) separating Regions No. 2 and No. 3. Physically, this is a rubber diaphragm (compatible with the propellants) that allows us to obtain a desirably small spring constant ( $k_2 \approx 0$ ). This is needed to make the measured phase shift sensitive to the ullage volume,  $V_3$ , without interference from  $k_2$ , because the mechanical spring and the equivalent gas spring ( $V_3$ ) work in series. The mass  $m_2$  and the working area of the diaphragm ( $A_2$ ) are also adjusted to make the  $P_1/P_2$  phase shift more sensitive to  $V_3$ . This is especially important as the remaining propellant approaches zero and the system takes on second-order characteristics which give larger phase shifts than the basic first-order system.

#### Nomenclature - Section 4.1.1

<u>Symbol</u>	<u>Description</u>
$\beta$	Bulk modulus
$P$	Pressure
$V$	Volume
$C$	Fluid capacitance

Q	Volumetric flowrate
Q <sub>o</sub>	Ratio of stored to dissipated energy
γ	Specific heat ratio
A	Area
x	Displacement
$\dot{x}$	Velocity
$\bar{x}$	Nominal value of x
R	Gas flow resistance
m	Mass
k	Spring rate
k'	k/A <sup>2</sup>
m'	m/A <sup>2</sup>

#### Subscripts

1	Related to Volume No. 1
2	Related to Volume No. 2
3	Related to Volume No. 3

#### 4.1.1.2 Parametric Studies

The derivation of the transfer function relating the pressure (P<sub>1</sub>) in the driver cavity to the pressure response in the ullage cavity (P<sub>3</sub>) is found in Appendix B, Equation B-38:

$$\frac{P_3}{P_1} = \frac{1}{S^3 m_2' R C_2 C_3 + S^2 M_2' C_3 + S R \left[ \frac{C_2 C_3}{C_{K_2}} + C_2 + C_3 \right] + \frac{C_3}{C_{K_2}} + 1}$$

where the symbols are as defined in Appendix B.

The solution to this equation was implemented on the G. E. time sharing computer utilizing an available frequency response program. This was done to determine suitable design parameters required to obtain a feasible system.

### Selection of Parameters

The results of these solutions for various combinations of parameters are plotted in Figures 4-2 through 4-6. The input parameters which were varied were, frequency, diaphragm mass, resistance, and driving cavity volume. The phase shifts were calculated for an ullage volume variation of 0.3 to 12 ft<sup>3</sup>. A flexible diaphragm with negligible spring rate ( $k_2 \approx 0$ ) was assumed to separate the driver and ullage cavities. On the basis of the analysis, the following combination of input parameters appears best.

Driver Volume ( $V_2$ )	=	5.2 in <sup>3</sup>
Diaphragm Mass	=	0.1 lb for a 1 in <sup>2</sup> driver area
Driver Frequency	=	2 cps
Resistance	=	$2.93 \times 10^{-3}$ lb-sec/in <sup>5</sup>

The effects of varying the diaphragm mass,  $w_2$ , are shown in Figure 4-7. Liquid impinging on the driver diaphragm can cause a change in the effective mass and result in errors. The diaphragm mass of 0.1 lb for a 1 in<sup>2</sup> area is quite sensitive to the addition of mass to the diaphragm while still providing good phase sensitivity to volume change. In order to insure that a change in volume can be distinguished from liquid impinging on the diaphragm, this mass was selected.

The sensitivity of the resulting phase shift measurement to shifts in  $\gamma_3$ , due to the mixture of propellant vapor with the pressurization helium gas, is given in Figure 4-8.

### Sizing Driving Cavity Volume ( $V_1$ )

Figure 4-9 presents the requirements for the volumetric displacement per unit time of the driver, as a function of the driving cavity volume, assuming a measurable perturbation of 0.005 psia in  $P_3$  for the corresponding least sensitive situation; i. e., the empty tank. It can be seen from Figure 4-10 that for  $V_1 \leq 0.03$  ft<sup>3</sup>, the ratio of  $Q_3/Q_1$  is unity when the tank is full (the full tank).

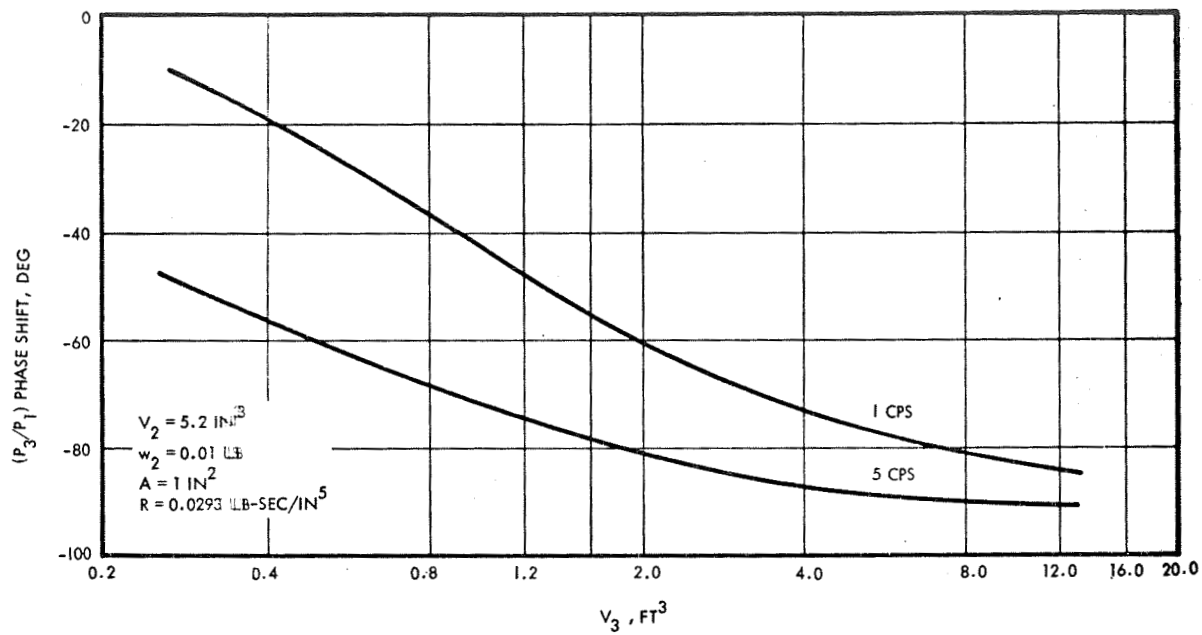


Figure 4-2. Phase Shift vs. Volume and Frequency

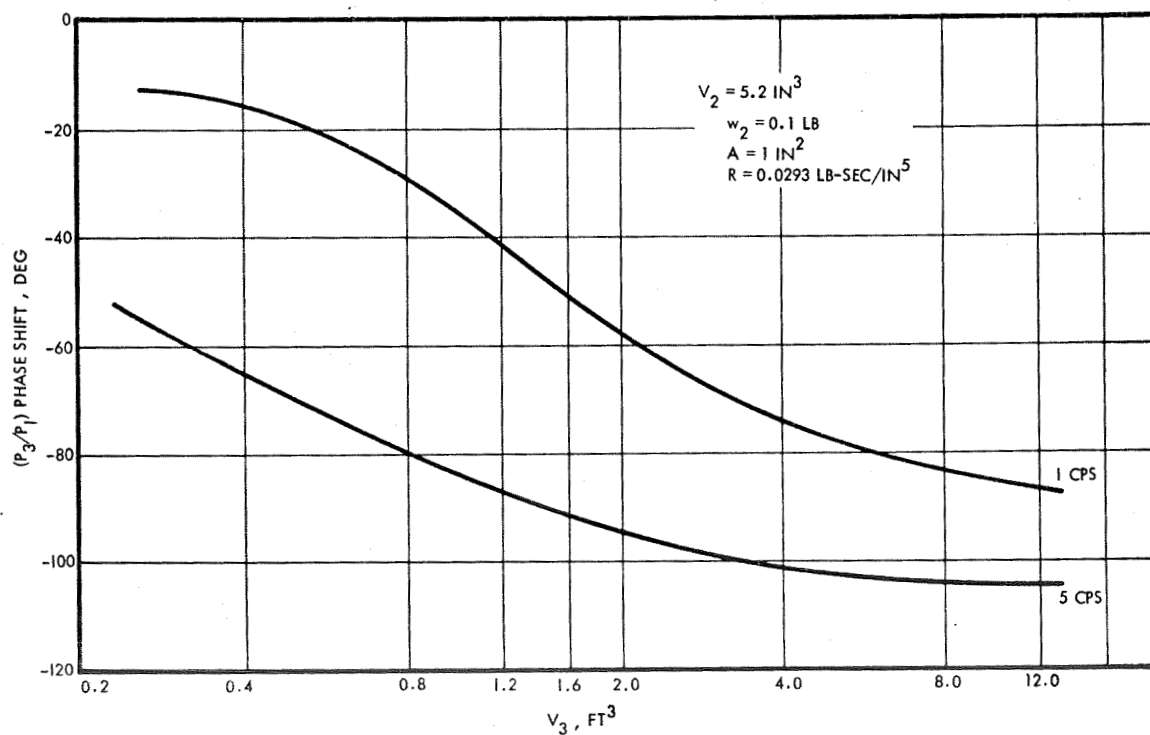


Figure 4-3. Phase Shift vs. Volume and Frequency

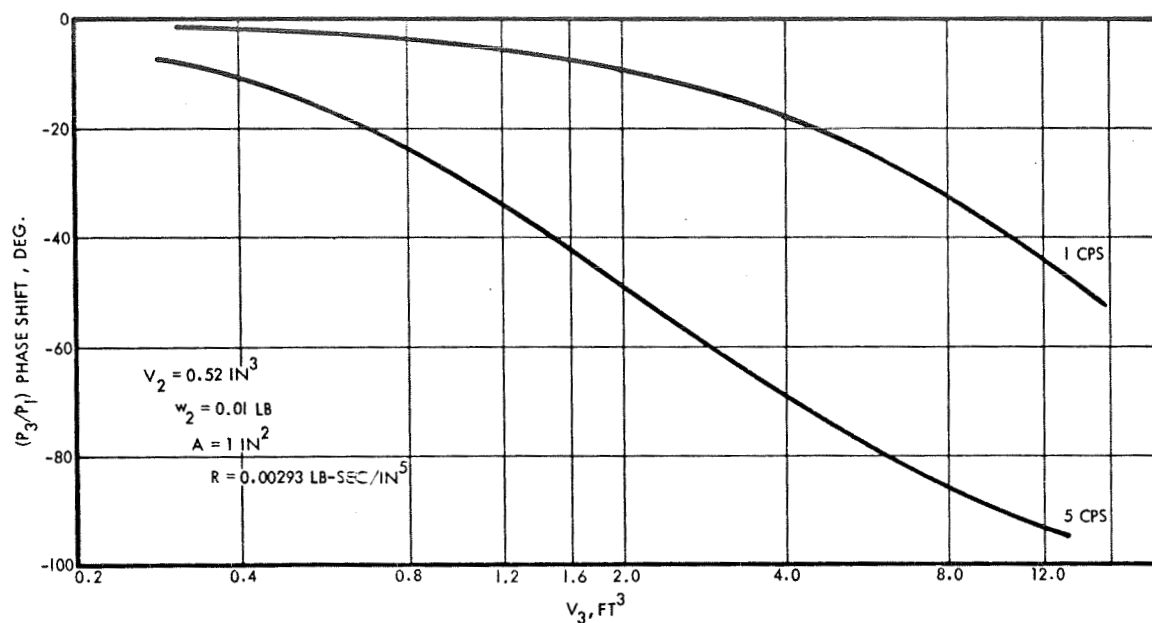


Figure 4-4. Phase Shift vs. Volume and Frequency

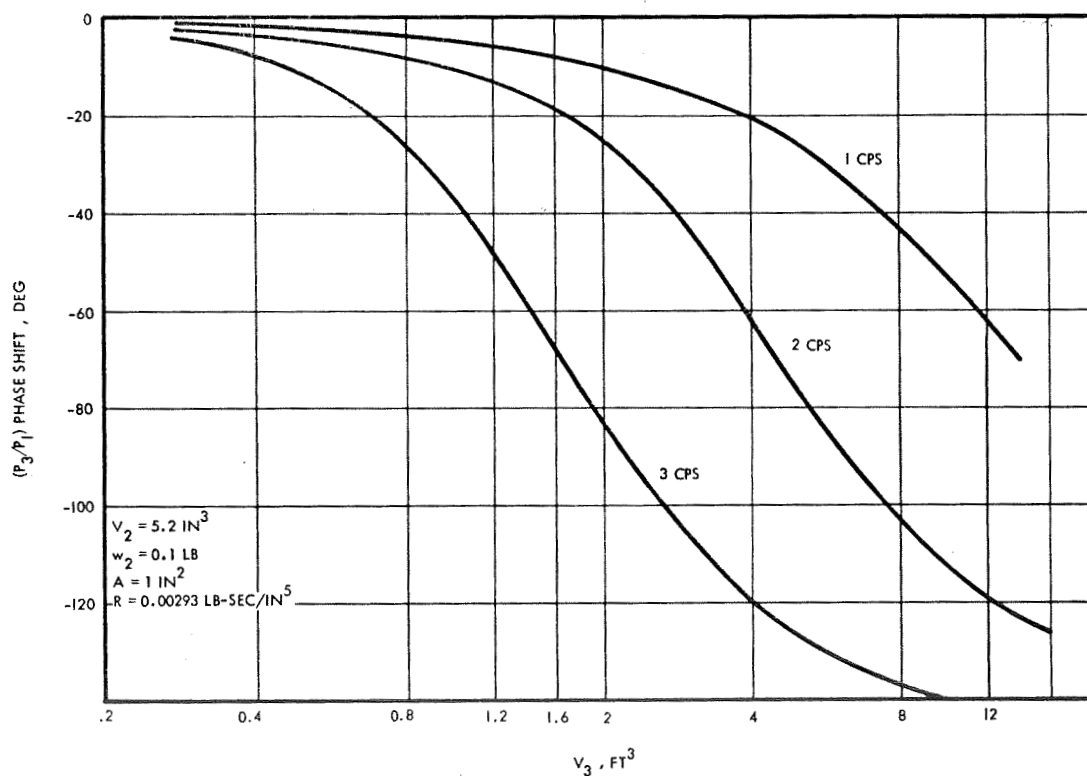


Figure 4-5. Phase Shift vs. Volume and Frequency

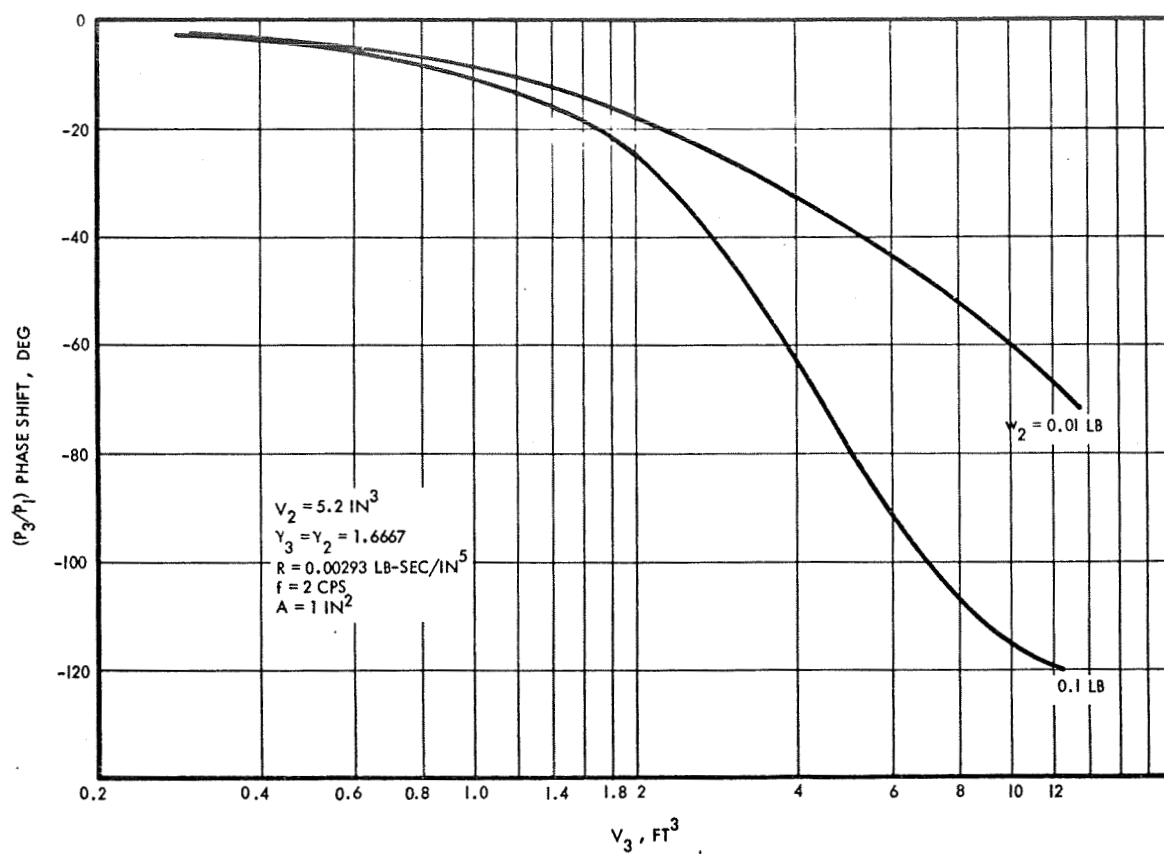


Figure 4-6. Phase Shift vs. Volume for Different Masses

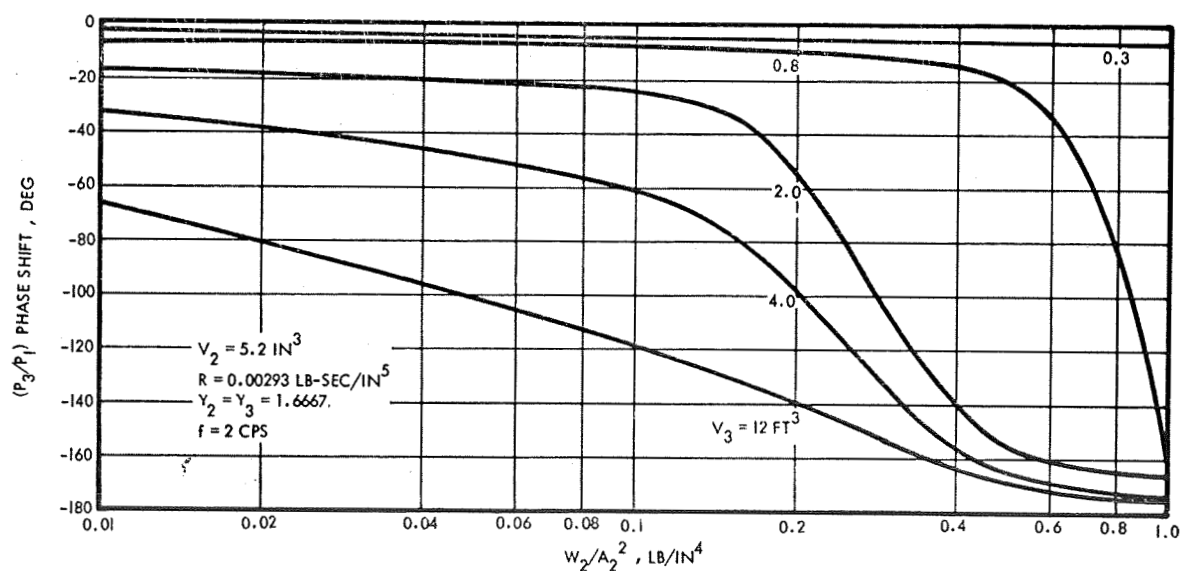


Figure 4-7. Effect of Diaphragm Mass on Phase Shift

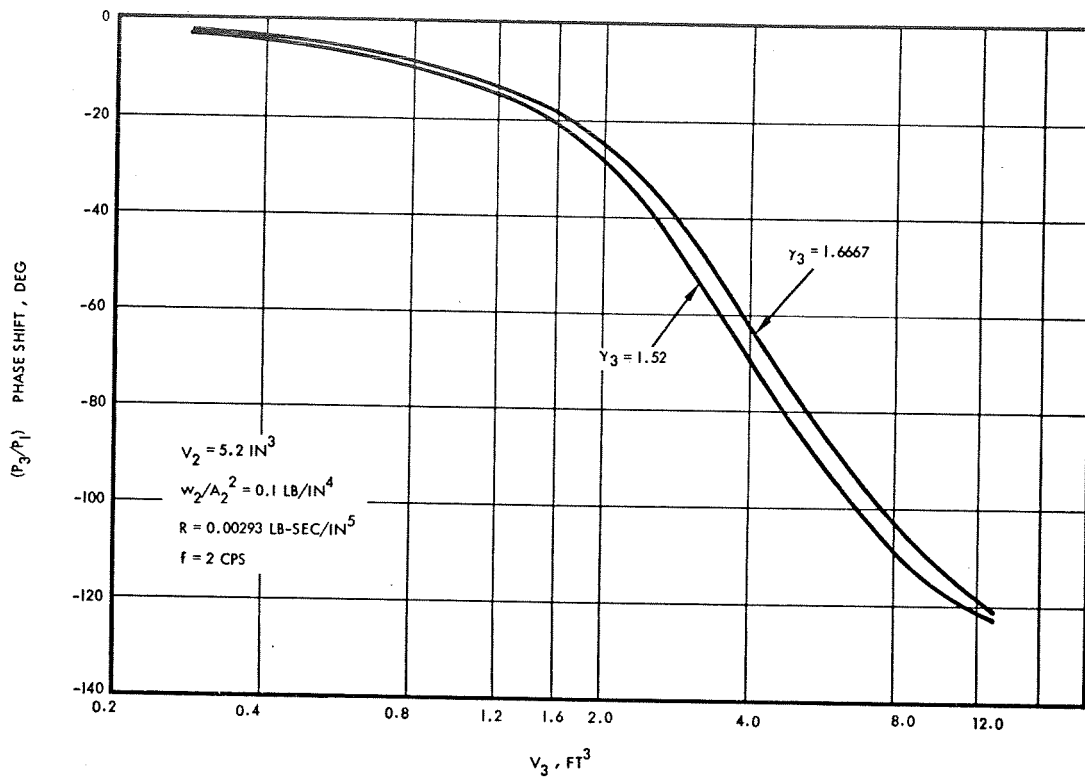


Figure 4-8. Effect of  $\gamma$  on Phase Shift

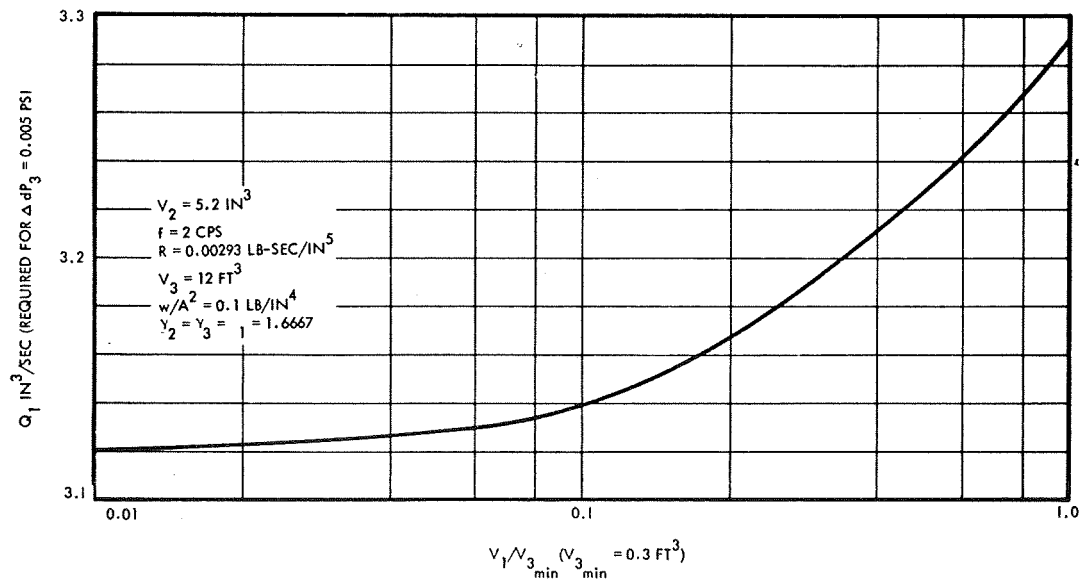


Figure 4-9. Effect of Gas Volume on Driver Displacement

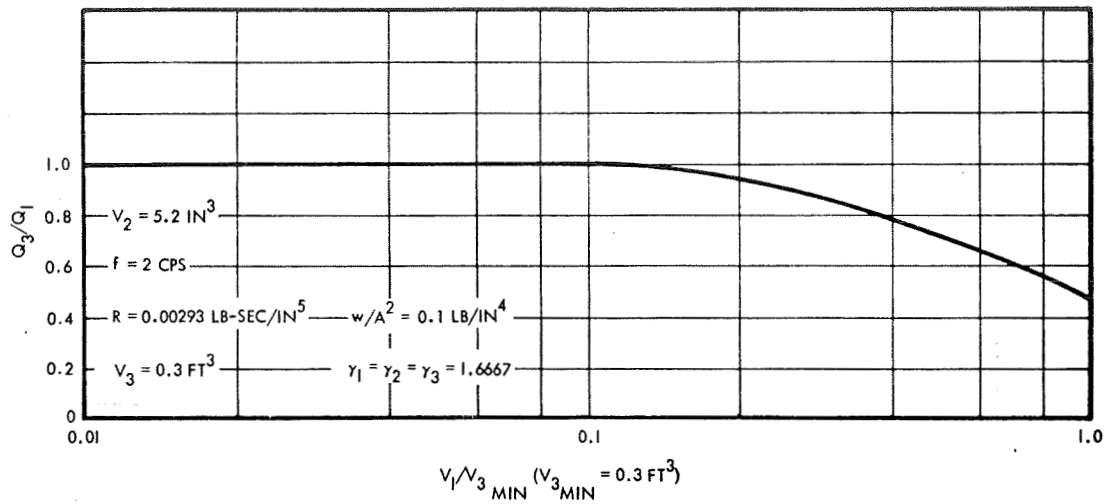


Figure 4-10. Amplitude Ratio vs. Gas Volume

#### Sizing Driver and Flexible Diaphragm Displacement Volumes

For phase resolution, a minimum  $P_3$  of about 0.005 psi has to be sensed. Suitable substitution for a sinusoidal driving function and algebraic reduction of Equation B-47 leads to

$$\left| P_3/Q_1(j\omega) \right| = \frac{1}{\sqrt{\mathcal{R}^2 + \mathcal{I}^2}}$$

where

$$\mathcal{R} = \omega^4 m_2' R C_1 C_2 C_3 - \omega^2 R C_1 (C_2 + C_3)$$

$$\mathcal{I} = -\omega^3 m_2' C_3 (C_1 + C_2) + \omega (C_1 + C_2 + C_3)$$

For

$$V_2 = 0.01 \times 0.3 = 0.003 \text{ ft}^3$$

$$V_3 = 12 \text{ ft}^3 \text{ (worst case)}$$

$$\gamma_2 = \gamma_3 = 1.6667$$



$$P_2 = P_3 = 250 \text{ psia}$$

$$f = 2 \text{ cps}$$

$$R = 0.00293 \text{ lb-sec/in}^5$$

$$w_2/A_2^2 = 0.1 \text{ lb/in}^4$$

we get

$$C_2 = 0.01242 \text{ in}^5/\text{lb}$$

$$C_3 = 49.8 \text{ in}^5/\text{lb}$$

and thus,

$$\mathcal{R} = 0.01173 C_1 - 23 C_1 = -23 C_1$$

$$\mathcal{I} = -25.6 C_1 + 625.7 \text{ for } C_1 \ll 49.8$$

which leads to

$$\frac{P_3}{Q_1} (j\omega)^2 = \frac{1}{1186 C_1^2 + 32000 C_1 + 3.91 \times 10^4}$$

For  $P_3 = 0.005 \text{ psia}$ ,

$$Q_1^2 = (1186 C_1^2 + 32000 C_1 + 3.91 \times 10^4) (0.005)^2$$

$$= 0.0296 C_1^2 + 0.80 C_1 + 9.77$$

$$\text{for } C_1 \ll 1$$

Letting

$$V_1 = 0.003 \text{ ft}^3$$

then

$$C_1 = 0.01245 \text{ in}^5/\text{lb}$$

Thus,

$$Q_1 = \sqrt{9.77} = 3.12 \text{ in}^3/\text{sec}$$

$$Q_1 = A_1 \dot{x}_1 = A_1 \omega x_1 \text{ or } A_1 x_1 = Q_1/\omega$$

for

$$f = 2 \text{ cps}$$

$$A_1 x_1 = \frac{3.12}{2\pi \times 2} = 0.25 \text{ in}^3$$

where

$$x_1 = \text{maximum amplitude of acoustic driver}$$

For the design parameters selected, the ratio of  $Q_3/Q_1 = 1$ , as previously, was used. Thus,

$$A_2 x_2 = A_1 x_1 = 0.25 \text{ in}^3$$

The proposed scheme can be achieved with the following system design parameters (see Figure 4-1):

$$\text{Driver frequency} = 2 \text{ cps}$$

$$V_2 = 0.01 V_3 \text{ minimum}$$

$$0.3 \leq V_3 \leq 12 \text{ ft}^3$$

$$V_1 = 0.1 V_3 \text{ minimum}$$

$$\text{Resistance, } R = 0.00293 \text{ lb-sec/in}^5$$

$$\gamma = 1.67$$

$$P = 250 \text{ psia}$$

$$w_2/A_2^2 = 0.1 \text{ lb/in}^4$$

$$k_2 \approx 0$$

$$A_1 x_1 \text{ max} \approx 0.25 \text{ in}^3$$

#### 4.1.1.3 Conclusions

Preliminary evaluation of the Phase Sensitive Infrasonic System indicates that it is potentially feasible under the assumptions made in the analysis. A system resulting in components of feasible size can be designed. However, the system has a number of major problems. The variation in the specific heat ratio,  $\gamma$ , could cause appreciable errors under transient conditions (see Section 4.1.3.1). The system is sensitive to liquid which may contact the separating diaphragm, and render it inoperative. The acoustical resistance varies over a  $\pm 4$  percent range as the temperature varies. Finally, the phase lock is sensitive to nonlinearities and harmonics in the system. In order to minimize the effect of the latter two items, the Resonant Infrasonic Gauging System (RIGS) was investigated (see Section 4.1.2).

#### 4.1.2 Resonant Infrasonic Gauging System

This section covers the preliminary feasibility evaluation of a zero-g propellant gauging system that utilizes infrasonic measurement of the propellant pressurizing gas compressibility to determine the

volumes of stored propellants. This can be achieved indirectly by determining the anti-resonant system frequency. The anti-resonant frequency can be found by means of either minimum amplitude or 90-degree phase shift measurements of the dynamic gas pressure in a small cavity attached to, but isolated from the main propellant tank. No measurements are required in the propellant tank. The small cavity is driven by a fixed displacement-variable frequency driver.

Preliminary evaluation of the proposed RIGS indicates that it is physically feasible to use this technique for propellant measurement under the requirements of zero-g operation. A comparison of this system with other infrasonic systems can be found in Section 5.

The proposed scheme can be achieved with the following system design parameters (see Figure 4-11):

Driver frequency = 1 to 10 cps

$$w_2/A_2^2 = 0.1 \text{ lb/in}^4$$

$$A_1 x_{1\text{max}} \approx 0.25 \text{ in}^3/\text{cycle}$$

$$V_1 = 0.01 V_2 \text{ minimum}$$

$$0.3 \leq V_2 \leq 12 \text{ ft}^3$$

$$\text{Resistance, } R_2'' \leq 9 \times 10^{-5} \text{ lb-sec/in}^5$$

$$\gamma_2 = 1.67$$

$$\bar{P}_2 = 250 \text{ psi}$$

#### Nomenclature - Section 4.1.2

<u>Symbol</u>	<u>Description</u>	<u>Unit</u>
P	Pressure	psi
V	Volume	in <sup>3</sup>
C	Fluid capacitance	in <sup>5</sup> /lb
Q	Volumetric flowrate	in <sup>3</sup> /sec
Q <sub>o</sub>	Figure of merit for tuned resonant systems	dimensionless

<u>Symbol</u>	<u>Description</u>	<u>Unit</u>
$\gamma$	Specific heat ratio	dimensionless
A	Area	$\text{in}^2$
x	Displacement	in.
$\dot{x}$	Velocity	in/sec
R	Gas flow resistance	$\text{lb-sec/in}^5$
m	Mass	$\text{lb-sec}^2/\text{in}$
$m'$	$m/A^2$	$\text{lb-sec}^2/\text{in}^5$
K	Spring rate	lb/in
$K^1$	$K/A^2$	$\text{lb/in}^5$
w	Weight	lb
s	Laplace notation $\left(= \frac{d}{dt}\right)$	$\text{sec}^{-1}$
$\omega$	Angular velocity	radian/sec
f	Frequency	cycles/sec
$\rho$	Density	$\text{lb/in}^3$
g	Gravitational constant	$\text{in/sec}^2$
c	Acoustic velocity	in/sec
MW	Molecular weight	lb/mol
T	Absolute temperature	$^{\circ}\text{R}$

#### Subscripts

- 0 - low frequency anti-resonant condition
- 1 - related to Volume No. 1
- 2 - related to Volume No. 2
- 3 - high frequency resonant condition or Volume No. 3

#### Superscripts

- $\bar{x}$  - nominal quasi-steady-state value of x
- ' - due to acoustic radiation
- " - due to linear damping

#### 4.1.2.1 Description of RIGS System

The RIGS system studied is shown schematically in Figure 4-11. It consists of a fixed amplitude-variable frequency driver, e. g., servo-electric motor-driven, sinusoidal cam-actuated piston which sets up a pressure perturbation in the directly coupled driver cavity Region No. 1.

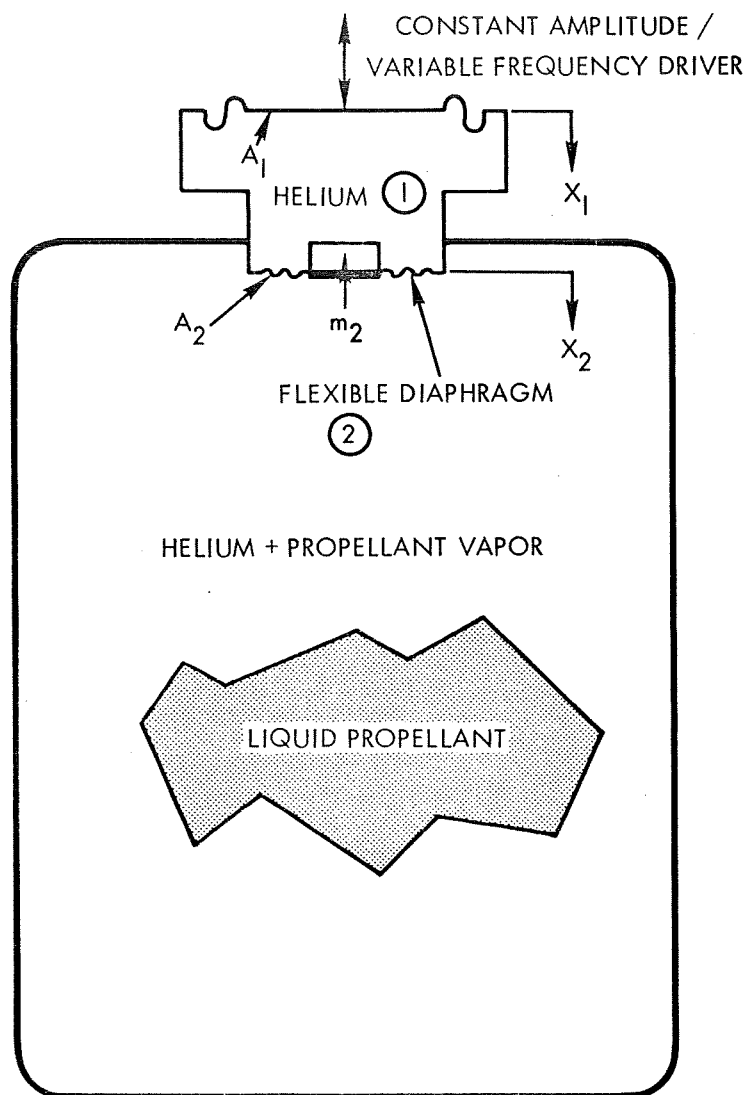


Figure 4-11. Schematic of RIGS

The driver cavity is physically isolated from the gas volume in the main tank (to be measured) by a very low compliance elastomer diaphragm which is compatible with the propellants. The volume of the driver cavity is also very small relative to the main tank ullage gas volume, Region No. 2. The diaphragm is weighted with a mass ( $m_2$ ) which is selected so as to tune the corresponding spring (ullage compressibility)/mass system to a relatively low anti-resonant frequency over the entire operating regime, compared to the resonant frequency of the spring (driver volume 1 compressibility)/mass system. As the propellant is used up, the upper resonant frequency will remain relatively constant as the equivalent gas spring in the driver cavity predominates due to the relatively large volume ratio of  $V_2$  to  $V_1$ . However, the low anti-resonant frequency decreases as the propellant is consumed and is essentially proportional to  $\sqrt{(\gamma_2 \bar{P}_2)/\bar{V}_2}$ , giving a measure of the gas volume and in turn, the propellant volume in the main tank. This anti-resonant frequency can be detected by means of suitable closed loop frequency tracking in either of two ways:

- a. Minimum amplitude sensing technique — system designed to continually adjust the frequency as needed, so that at the anti-resonant point, it locks onto the corresponding minimum pressure amplitude in Region No. 1.
- b. Ninety-degree phase shift sensing technique — at the anti-resonant point, the pressure in Region No. 1 will lead the fixed displacement of the driver by 90-degrees since this is characteristic of the second order spring/mass (finite amount of damping) system that is involved, independent of the amount of damping. Thus, to sense the anti-resonant frequency, the driver frequency is continuously tuned so as to lock onto the corresponding 90-degree phase shift between  $P_1$  and  $x_1$ .

Since the anti-resonant frequency is sensitive to  $\gamma_2$  (the effective specific heat ratio in the void volume of the propellant tank) and  $\bar{P}_2$  (the average tank pressure), these two properties must be measured to ensure proper compensation when they vary from some nominal level. The specific heat ratio can be determined by either (a) an acoustic velocity measurement in the gas/propellant vapor phase of the propellant tank, or (b) a temperature measurement of the quasi-equilibrium gas/propellant vapor mixture. This topic is discussed in Section 4.1.1.3. The steady-state pressure ( $\bar{P}_2$ ) can be directly measured by a suitable transducer.

An elastomer flexible diaphragm is employed which has a negligible spring constant. Suitable quasi-steady-state pressure balancing across this diaphragm is achieved with a low pass band isolation bellows and snubber between the main tank.

#### 4.1.2.2 Parametric Studies

The derivation of the mathematical model of the RIGS system is presented in Section 2 of Appendix B. In this section the effect of the various design parameters will be determined and selection of typical parameters suitable for an actual system will be made.

#### Damping and Frequency Response

In order to evaluate a reasonable magnitude for the built-in damping ( $R_2''$ ), it was assumed that at the anti-resonant frequency, the equivalent  $Q_o$  (a figure of merit used for tuned resonant circuits which measures the ratio of stored to dissipated energy per cycle and in turn is a measure of the tuned circuit bandwidth or tuning sharpness) should be at least 25. By analogy to electrical circuits we get

$$Q_o = \frac{\omega_o \frac{m_2}{A_2^2}}{R_2} \quad (4.1-1)$$

where

$$R_2 = R_2' + R_2'' \text{ (as defined before)}$$

$$\omega_o = 2\pi f_o \text{ (} f_o = \text{anti-resonant tuned low frequency)}$$

In general,  $R_2' \ll R_2''$  thus neglecting  $R_2'$

$$R_2'' = \frac{2\pi f_o \frac{m_2}{A_2^2}}{Q_o} \quad (4.1-2)$$



where

$$f_o = \frac{1}{2\pi} \sqrt{\frac{1}{\frac{m_2}{A_2^2} C_2}} \sqrt{\frac{Q_o^2}{1 + Q_o^2}} \quad (4.1-3)$$

This reduces to essentially the following expression for  $Q_o^2 \gg 1$ ,

$$f_o = \frac{1}{2\pi} \sqrt{\frac{1}{\frac{m_2}{A_2^2} C_2}} \quad (4.1-4)$$

Substituting the value of  $C_2 = \bar{V}_2 / (\gamma_2 \bar{P}_2)$  into Equation (4.1-4) and solving for  $V_2$  we get

$$\bar{V}_2 = \frac{\gamma_2 \bar{P}_2}{4\pi^2 \frac{m_2}{A_2^2}} \left( \frac{1}{f_o^2} \right) \quad (4.1-5)$$

This expression is plotted in Figure 4-12 for the system design parameters selected, over the working range of  $V_2$  (0.3 to 12 ft<sup>3</sup>) that is to be measured. Since the desired  $Q_o$  varies proportionally with frequency (see Equation 4.1-1), we must size  $R_2''$  for the minimum anti-resonant frequency corresponding to a maximum  $V_2 = 12 \text{ ft}^3$  ( $f_o = 1.41 \text{ cps}$  from Figure 4-11) and for a  $w_2/A_2^2 = 0.1 \text{ lb/in}^4$ , thus

$$R_2'' \leq \frac{2\pi \times 1.41 \times 0.1/386}{25} = 9.16 \times 10^{-5} \text{ lb-sec/in}^5$$

from Equation (4.1-2). If we use this value of  $R_2''$ , the corresponding value of  $Q$  will vary from 158 with the initial propellant loading corresponding to a  $V_3 = 0.3 \text{ ft}^3$  ( $f_o = 8.85 \text{ cps}$ ) to a  $Q_o$  of 25 corresponding to a  $V_3 = 12 \text{ ft}^3$  ( $f_o = 1.41 \text{ cps}$ ).

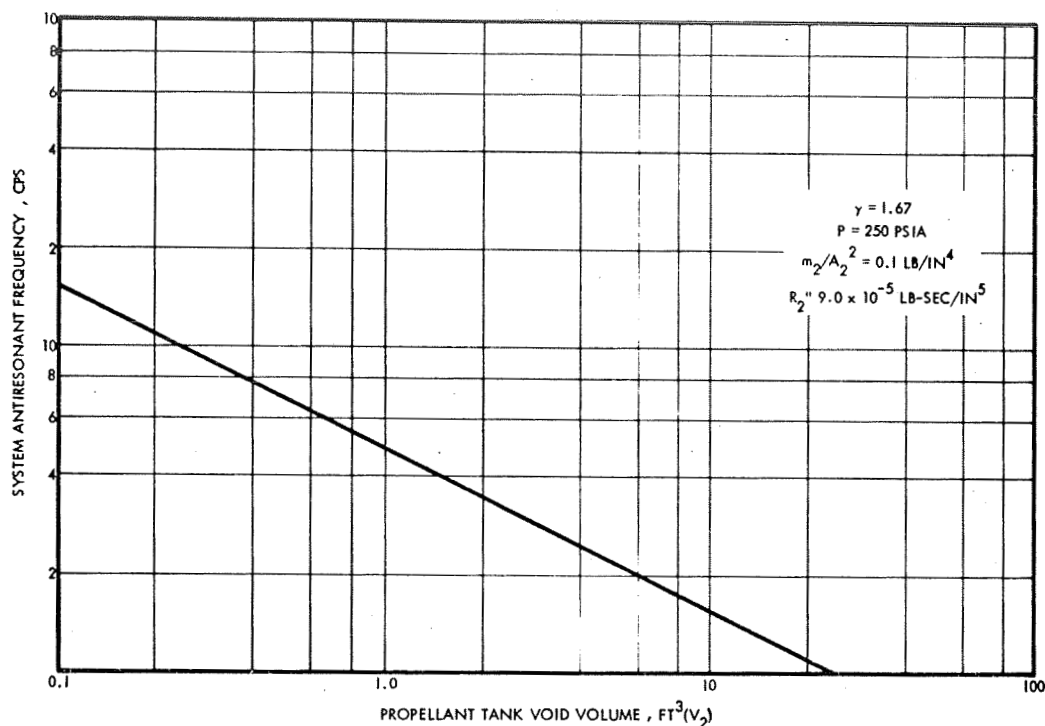


Figure 4-12. System Anti-Resonant Frequency Versus Volume

At the low frequencies involved, the assumption of one continuous void volume in the propellant tank is not needed. Accurate answers can be still obtained, as has been shown previously in Section 3.1.1.4 for a void volume consisting of several bubbles, as the effect of the intervening liquid impedance will be negligible compared to that of the gas/vapor volume compressibility.

At the high frequency resonant condition, the corresponding resonant frequency will be given by:

$$f_3 = \frac{1}{2\pi} \sqrt{\frac{1}{\frac{m_2}{A_2^2} \frac{C_1 C_2}{C_1 + C_2}}} \sqrt{\frac{Q_{o3}^2}{1 + Q_{o3}^2}} \quad (4.1-6)$$

where

$$Q_{o3} = \frac{\omega_3 \frac{m_2}{A_2^2}}{R_2} \quad (4.1-7)$$

Since  $\omega_3 > \omega_0$ , then  $Q_{o_3} > Q_0 > 1$  and Equation 4.1-6 simplifies to

$$f_3 \approx \frac{1}{2\pi} \sqrt{\frac{1}{\frac{m_2}{A_2^2} \frac{C_1 C_2}{C_1 + C_2}}} \quad (4.1-8)$$

In general,  $C_2 \gg C_1$  over the entire working range ( $V_1 = 0.01 V_2$  minimum), thus Equation 4.1-8 is essential independent of  $C_2$  as it reduces to

$$f_3 \approx \frac{1}{2\pi} \sqrt{\frac{1}{\frac{m_2}{A_2^2} C_1}} \quad (4.1-9)$$

which for the selected design parameters is

$$f_3 \approx \frac{1}{2\pi} \sqrt{\frac{1}{\frac{0.1}{386} \times \frac{0.003 \times 1728}{1.6667 \times 250}}} = 88.5 \text{ cps}$$

It should be noted that this is an order of magnitude larger than maximum value of the anti-resonant frequency  $f_o = 8.85 \text{ cps}$ , corresponding to the minimum value of  $V_3 = 0.3 \text{ ft}^3$  and thus will not distort the anti-resonant characteristics at  $f_o$ . As  $V_3$  increases, the difference between  $f_o$  and  $f_3$  becomes even greater.

### Computer Studies

An evaluation of the transfer function  $P_1/x_1$  (Equation B-65) to determine the amplitude and phase shift was implemented on the GE On-Line Time-Shared Digital Computer utilizing the frequency response program previously discussed in Section 4.1.1.

### Selection of Parameters

The weight/area<sup>2</sup> ratio ( $w_2/A_2^2 = 0.1 \text{ lb/in}^4$ ) was selected to keep the anti-resonant frequency determined from Equation 4.1-4

in the range of 1 to 10 cps, as the void volume  $V_2$  varied over a range of 0.3 to 12 ft<sup>3</sup>. The volume of the driver cavity ( $V_1 = 0.003$  ft<sup>3</sup>) was selected to make the corresponding spring/mass resonant frequency approximately an order of magnitude above the highest anti-resonant frequency. This is done in order to avoid any interaction effects which could cause a discrimination problem (in either amplitude or phase shift measurements) between the anti-resonant low frequency that is to be measured, and the additional resonant high frequency which is a characteristic of this system and is predominated by  $V_1$ .

### Sensitivity Studies

The effect of increasing the void volume in the propellant tank on the frequency response of the amplitude ratio  $|P_1/x_1|$  was evaluated for values of  $V_2$  of 0.3, 0.8, 2, 4, and 12 ft<sup>3</sup>, over a frequency range of 1 to 100 cps. The corresponding results are presented in Figure 4-13. The effect of the acoustic radiation term  $R_2'$  is seen to be negligible at the low frequencies involved and as a result, the indicated anti-resonant frequency is in agreement with the calculated result presented in Figure 4-12.

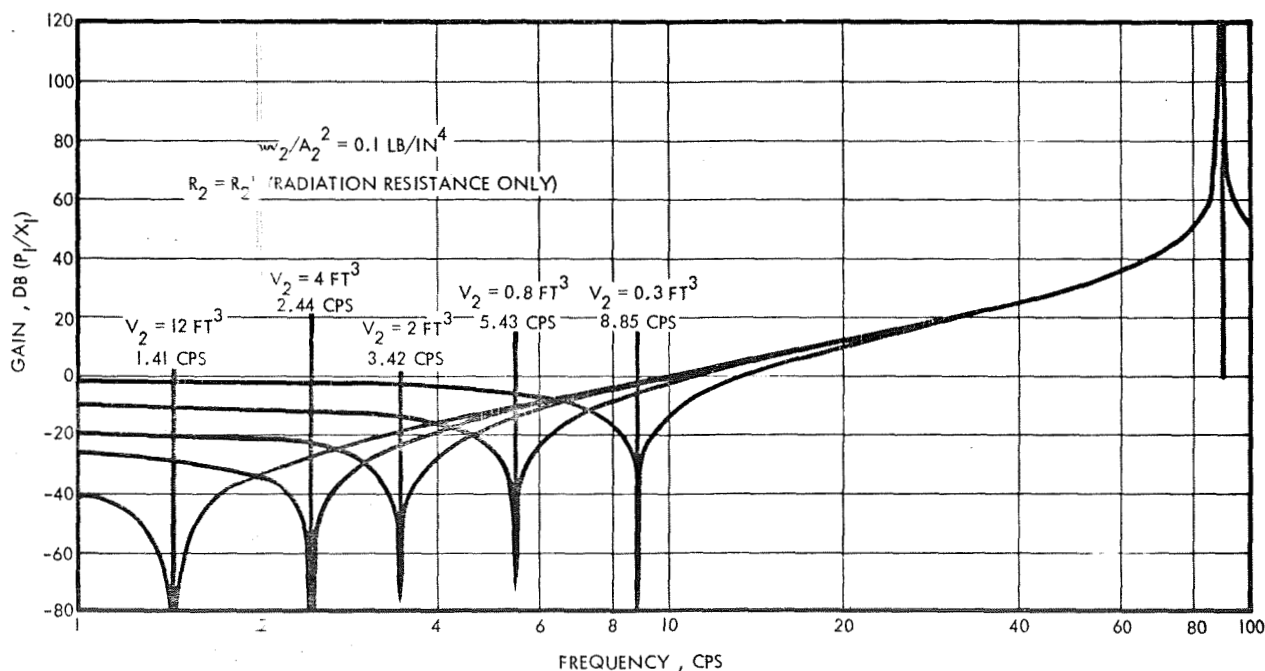


Figure 4-13. RIGS System Response as a Function of Volume

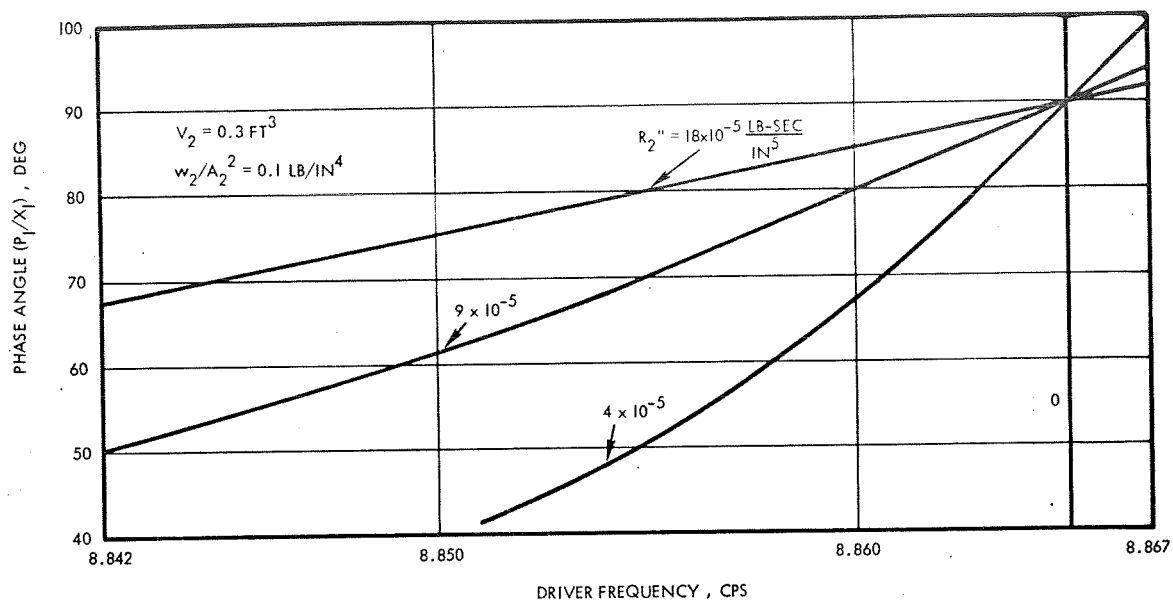


Figure 4-14. Effect of Resistance on Phase Angle,  $V = 0.3 \text{ ft}^3$

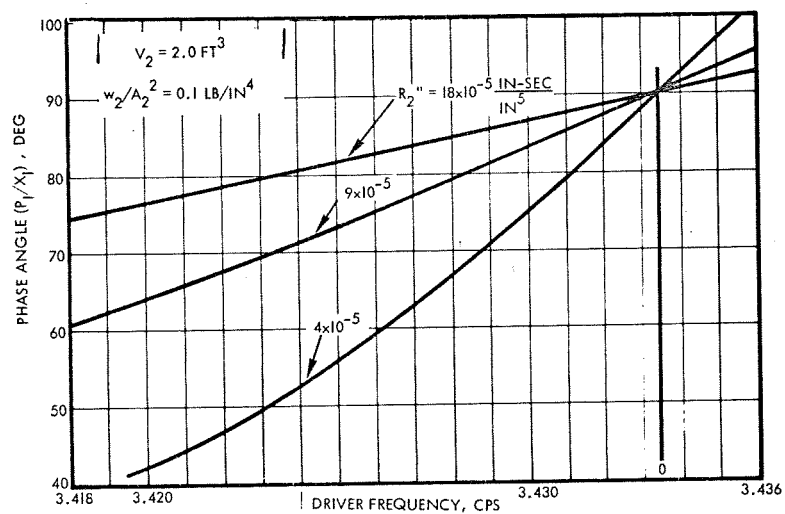


Figure 4-15. Effect of Resistance on Phase Angle,  $V = 2 \text{ ft}^3$

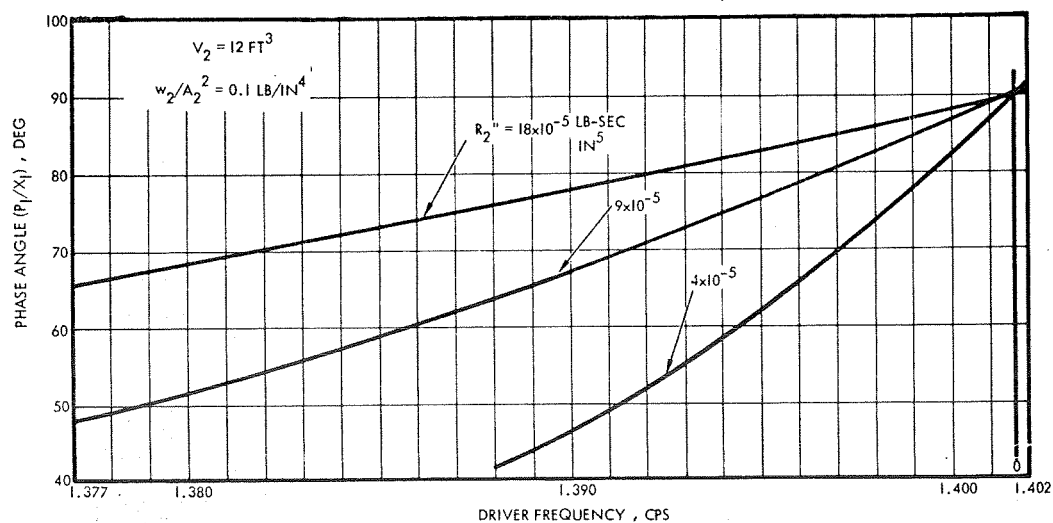


Figure 4-16. Effect of Resistance on Phase Angle,  $V = 12 \text{ ft}^3$

Introduction of additional linear damping, e. g., a dashpot between the diaphragm and the supporting walls, of an amount which still maintains a sufficiently high  $Q$  ( $R_2'' \leq 9 \times 10^{-5}$  lb-sec/in<sup>4</sup>), will have no effect on this anti-resonant frequency and very little on the balance of the frequency response. The corresponding phase shift characteristics will still show a 90 degree phase shift between  $P_1$  and  $x_1$  at this anti-resonant frequency, for the basically second-order dynamic system.

The latter fact is demonstrated by the results presented in Figures 4-14 through 4-16, which were obtained for values of  $V_2$  of 0.3, 2 and 12 ft<sup>3</sup> with various amounts of linear damping ranging from  $R_2''$  of zero to  $4 \times 10^{-5}$  lb-sec/in<sup>5</sup>. It is also seen that the phase shift/frequency characteristics are relatively linear and sufficiently sensitive over the range of interest to make accurate tracking of the 90 degree phase shift frequency feasible. Thus, this phase-shift technique can also be used to establish the anti-resonant condition.

#### 4.1.3 Preliminary Error Analysis of the RIGS System

##### 4.1.3.1 Variation in Specific Heat Ratio

The principal error source for the RIGS discussed in this section is the uncertainty in  $\gamma$ , the ratio of specific heat. It will be noted that both of the infrasonic systems actually measure the gas compliance,  $C$ , which is equal to the gas volume divided by the product of  $\gamma$  and the static pressure. Thus a given error in  $\gamma$  will cause an equivalent error in the gas volume and hence in the liquid quantity.

For a pure gas such as helium, the specific heat ratio is constant over a wide range of temperatures and pressures. Unfortunately the gas contained in the ullage space above the propellant is not a pure gas, but a mixture of gas and propellant vapor. The propellant vapor concentration is dependent upon the equilibrium vapor pressure (and thus propellant temperature) as shown in Figure 3-3, as well as departures from equilibrium. At equilibrium, the propellant vapor concentration (and thus  $\gamma$ ) is defined by the propellant temperature.

To understand why there is a departure from equilibrium, let us consider the following case. A propellant tank 95 percent full has been in space for a sufficient period of time that the ullage space is saturated

with propellant vapor. It is desired to fire the engine, and thus empty the tanks so that only 20 percent of the propellant remains. As the propellant is depleted, pure helium is used to pressurize the propellant. A saturated vapor layer forms on top of the propellant and slowly mixes with the incoming helium. As the mixing is relatively slow, a stratified condition exists immediately before the end of the engine firing with the vapor primarily in a layer immediately on top of the propellant, and the remainder of the tank is filled primarily with helium. As the propellant slowly reorients itself, the propellant vapor diffuses throughout the ullage space until, finally, the ullage gas is saturated with propellant vapor. If the mixing during this period is solely by diffusion without convection, the process has a time constant of about 20 minutes, and the specific heat ratio assumes the shape shown in Figure 4-17. Actually, this is a somewhat pessimistic assumption as the energy imparted by acceleration during firing will be slowly dissipated by local convection currents with appreciable improvement in the mixing process. In addition, no mixing is assumed during firing when the helium actually enters the propellant tank at relatively high velocity which tends to increase the mixing. However, the diffusion-limited case represents an upper limit to this error source and was used in the absence of actual data.

#### 4.1.3.2 Error Analysis

Table 4-1 shows a typical error analysis for the RIGS system. The electronic volume and density errors were obtained by comparison with similar systems such as the Apollo SPS PUGS system (Reference 4-1). The primary assumption made was that at equilibrium, the variation in the propellant vapor pressure from equilibrium would be less than 1 psi. In Figure 4-18, the error caused by the  $\gamma$  variation for the diffusion-limited case is shown as a function of time. This curve represents a "worst case" situation. The two curves shown represent two different possible schemes for measurement of the specific heat ratio,  $\gamma$ . In one scheme, the  $\gamma$  is calculated by measuring the propellant temperature and assuming saturation; in the second case, the  $\gamma$  is calculated by measurement of a local gas property, such as acoustic velocity, near the top of the tank.

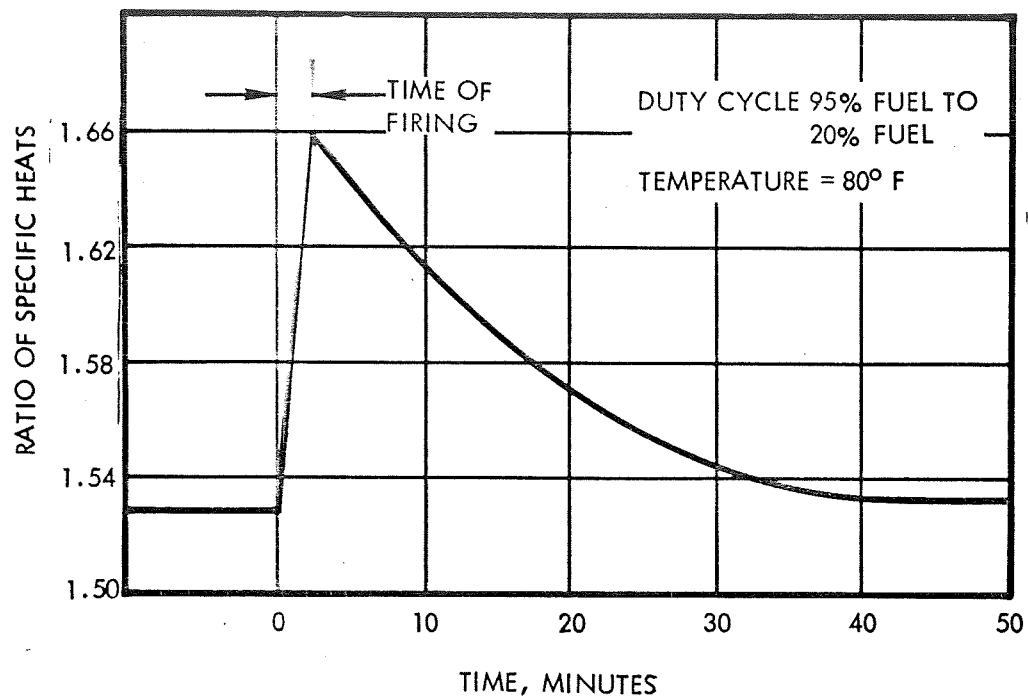


Figure 4-17. Variation of  $\gamma$  With Firing Time

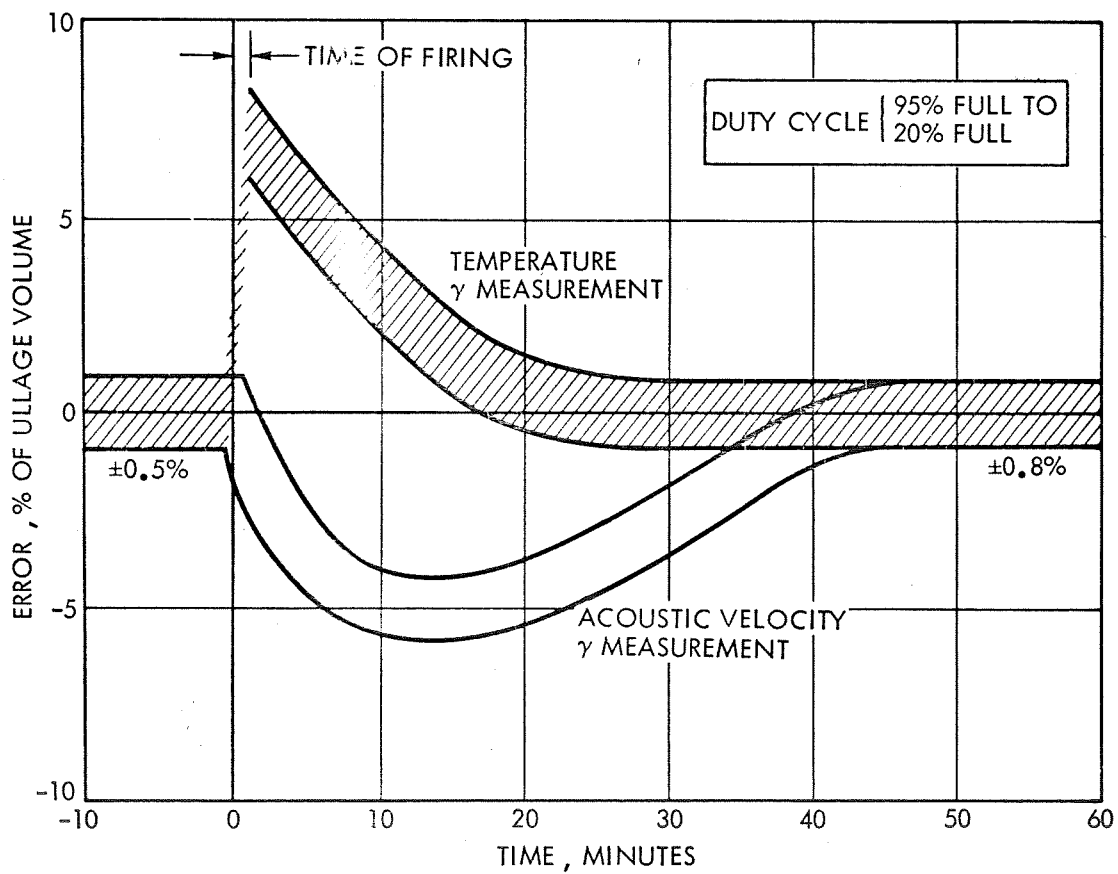


Figure 4-18. Effect of Firing on  $\gamma$  Correction



Table 4-1. RIGS Error Analysis Estimate

DEAD BAND OF PHASE NETWORK	± 0.2%
SETTING OF FULL REFERENCE	± 0.2%
SETTING OF EMPTY REFERENCE	± 0.1%
ACCURACY OF VOLTAGE TO OUTPUT POT.	± 0.1%
LINEARITY OF OUTPUT POT.	± 0.1%
MISC ELECTRONICS	± 0.2%
NET ERROR IN $V_u/\gamma P$	± 0.39%
$V_u/\gamma P$	± 0.39%
GAMMA AT EQUILIBRIUM*	± 0.41%
PRESSURE	± 0.2%
ELECTRONIC	± 0.2%
NET ERROR IN $V_u$	± 0.63%
$V_u$	± 0.63%
TEMPERATURE (DENSITY)	± 0.4%
EMPTY VOLUME	± 0.35%
ERROR (EMPTY TANK)	± 0.8% OF FULL TANK LOAD
ERROR (FULL TANK)	± 0.56% OF FULL TANK LOAD

\* ASSUMED ±1 PSI VARIATION IN LOCAL  $N_2O_4$  CONCENTRATION

## 4.2 HELIUM BALANCE SYSTEM

As shown in Section 3.5, it is possible to gauge the quantity of propellant by keeping track of the quantity of helium in both the pressurant and propellant tanks assuming a single pressurant tank for each propellant tank. Knowing the density of the helium in the propellant tank, and both the volume and the density of the helium in the propellant tank, and barring helium leakage, the gas volume (and thus the liquid volume) may be obtained. A number of systems have been proposed using the helium mass balance approach. The simplest Pressure, Volume, Temperature (PVT), measures the temperature and pressure in the pressurant and propellant tanks to calculate the propellant quantity. As shown in the error analysis in Section 4.2.2, pressure and temperature measurements are inadequate to perform the gauging under typical space conditions with the high vapor pressure oxidizer  $N_2O_4$ .

One simple improvement on the PVT system uses a beta-ray attenuation technique to accurately determine the helium density in the pressurant tank (Reference 4-2). This technique is called the  $\rho V$  system and is sufficiently accurate that this quantity is no longer a major error source. The remaining large error source becomes the density of the helium gas in the propellant tank. However, as shown in Section 4.2.1, a technique using both beta- and X-ray sources, called the RHO gauge system, appears capable of measuring the helium density in the tank to a high degree of accuracy.

### 4.2.1 Analysis of the RHO Gauge System

The feasibility of using measurements of unattenuated betas and low energy photons to uniquely determine the partial densities of a binary mixture of gases with significantly different atomic numbers was investigated. The specific application studied was for a mixture of helium with an atomic number ( $Z$ ) of 2 and a propellant vapor consisting of compounds of atoms ranging in atomic numbers ( $Z$ ) between 1 (for hydrogen) and 8 (for oxygen). This condition is representative of that in the ullage vapor of a zero gravity storable propellant tank. Accurate determination of the partial density of the helium is required for use in the helium balance propellant gauges. The technique exploits the fact that beta attenuation is dependent on only the bulk density of the gas mixture, whereas the low

energy photon attenuation, which is predominated by the photoelectric effect, discriminates against helium since the photoelectric attenuation coefficient is approximately proportional to the 5th power of the atomic number, (Z). The strong dependence of photon attenuation on Z results in the propellant or oxidizer being the controlling factor for attenuation over a range of partial densities. Thus, two attenuation measurements performed on the same sample of gas yield the respective densities of the helium and the other constituent with a high degree of accuracy.

#### 4.2.1.1 Attenuation of Beta Particles by Gas Mixtures

The attenuation of a beta spectrum by an arbitrary element, i, is characterized by the maximum beta energy  $E_{\max}$  through the mass attenuation coefficient  $\mu_{\beta, i}$ . For an element with atomic number  $Z_i$  and atomic weight  $A_i$ ,  $\mu_{\beta, i}$  is given as

$$\mu_{\beta, i} = \frac{35 Z_i}{E_{\max}^{1.14} A_i} \text{ cm}^2/\text{gm} \quad (4.2-1)$$

In the case where a mixture\* of the elements O, C, N and He is the attenuating medium, the attenuation coefficient for each is the same. For these elements this is given as

$$\mu_{\beta, i} = \frac{17.5}{E_{\max}^{1.14}} \text{ cm}^2/\text{gm} \quad (4.2-2)$$

since for each  $Z_i/A_i = 1/2$ . Thus, the fraction of unattenuated radiation through a sample of the mixture of thickness  $x(\text{cm})$  can be expressed as a function of the bulk density,  $\rho_T$ , through

$$\frac{C_{\beta}}{C_{o, \beta}} = A_{\beta} = \exp \left\{ -(\mu_{\beta, 1} \rho_1 + \dots + \mu_{\beta, n} \rho_n) x \right\} = \exp (-\mu_{\beta} \rho_T x) \quad (4.2-3)$$

---

\* Compounds are assumed to behave as a mixture since their binding energy is usually of the order of a few ev, and hence negligible when energies involved in the attenuation mechanism are considered.

where  $\mu_\beta = \mu_{\beta,i}$  and  $C_\beta/C_{o,\beta}$  is the normalized number of counts observed. A simple beta attenuation experiment is therefore sufficient to determine the bulk density,  $\rho_T$ , when the product of  $\mu_\beta x$  is known.

As will be shown below, the total density of compounds containing hydrogen with a  $Z/A$  of 1 (e. g., UDMH and  $N_2H_4$ ) can also be calculated as the ratio of hydrogen to other atoms is known from the chemical formula.

#### 4.2.1.2 Attenuation of Low Energy Photons by Gas Mixtures

For the energy range of photons between the K electron binding energy and the energy at which the Compton effect is important, the photoelectric effect is the predominant mode of interaction of the photons with the attenuating media. Depending on the reference consulted, various expressions are found to describe the attenuation coefficient for this process. From Price (Reference 4-3), the expression for the photoelectric attenuation coefficient for an element with an atomic number  $Z$  is given as

$$\mu = \frac{K Z^5}{(E_\gamma)^{3.5}} \text{ cm}^2/\text{gm} \quad (4.2-4)$$

where  $K$  is a constant and  $E_\gamma$  is the photon energy. It can be seen from Equation 4.2-4 that the attenuation coefficient varies greatly for different values of  $Z$ . This is also shown in Figure 4-19, where the coefficients for the elements H, He, O, N, and C are presented.

For a mixture of materials of densities  $\rho_i$ ,  $i = 1, \dots, n$ , the fraction of unattenuated gamma rays through a thickness  $t(\text{cm})$  is given by

$$A_\gamma = \frac{C_\gamma}{C_{o,\gamma}} = \exp \left[ -(\mu_1 \rho_1 + \mu_2 \rho_2 + \dots + \mu_n \rho_n) t \right] \quad (4.2-5)$$

where the attenuation coefficients,  $\mu_i$ , are determined from Equation 4.2-4 or Figure 4-19. The ratio  $C_\gamma/C_{o,\gamma}$  is again the normalized total number or counts. In the case where a mixture of helium and

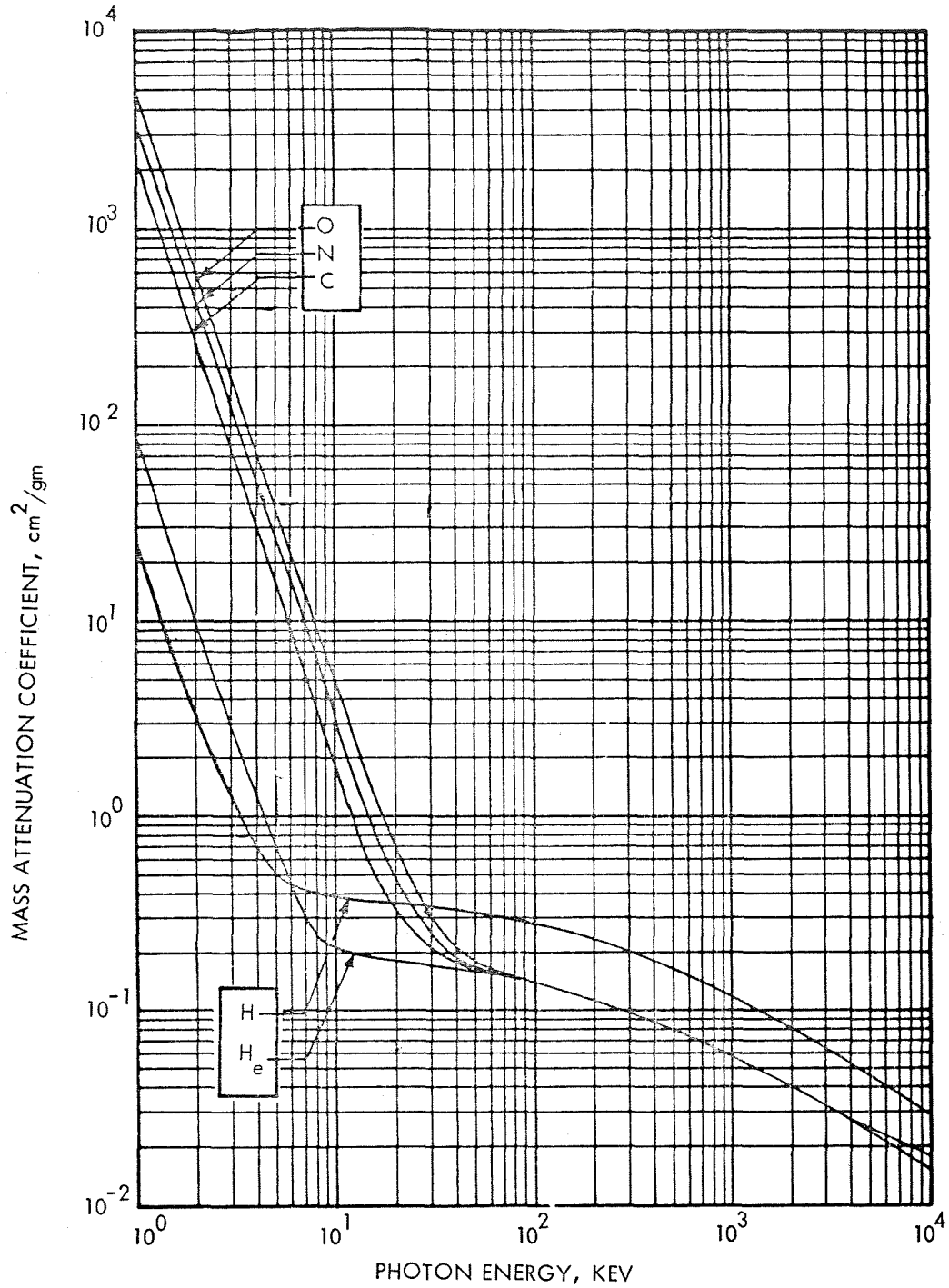


Figure 4-19. Mass Attenuation Coefficients for the Elements - H, He, O, N, and C

another gas ( $N_2O_4$  or Aerozine-50 vapor) with densities of  $\rho_1$  and  $\rho_2$ , respectively, is the attenuating medium, then Equation 4.2-5 may be reduced to

$$\frac{C_Y}{C_{o,Y}} = A_Y = \exp \left\{ -(\mu_1 \rho_1 + \mu_2 \rho_2)t \right\} \quad (4.2-6)$$

If the energy of the photons is sufficiently low ( $< 20$  kev), and if the Z's of the He and the other constituent are sufficiently different, then the measurement of the unattenuated photons will be relatively insensitive to the helium constituent as can be seen by the difference in attenuation coefficients for  $N_2O_4$  and Aerozine-50 of Figure 4-20. This is true only for a limited range of densities since the sensitivity to variations in either density will be somewhat reduced if a relatively large partial density of helium exists.

#### 4.2.1.3 Calculation of Constituent Densities

The results of the two measurements described above can now be combined to determine the respective densities of He and the other constituents. From Equation 4.2-3, it follows that the bulk density of the mixture

$$\rho_T = - \frac{\ln A_\beta}{\mu_\beta x} = \rho_1 + \rho_2 \quad (4.2-7)$$

which, in conjunction with Equation 4.2-6, gives the helium density expressed as

$$\rho_1 = \frac{1}{\left[ 1 - \frac{\mu_1}{\mu_2} \right]} \cdot \left\{ \frac{\ln A_Y}{\mu_2 t} - \frac{\ln A_\beta}{\mu_\beta x} \right\} \quad (4.2-8)$$

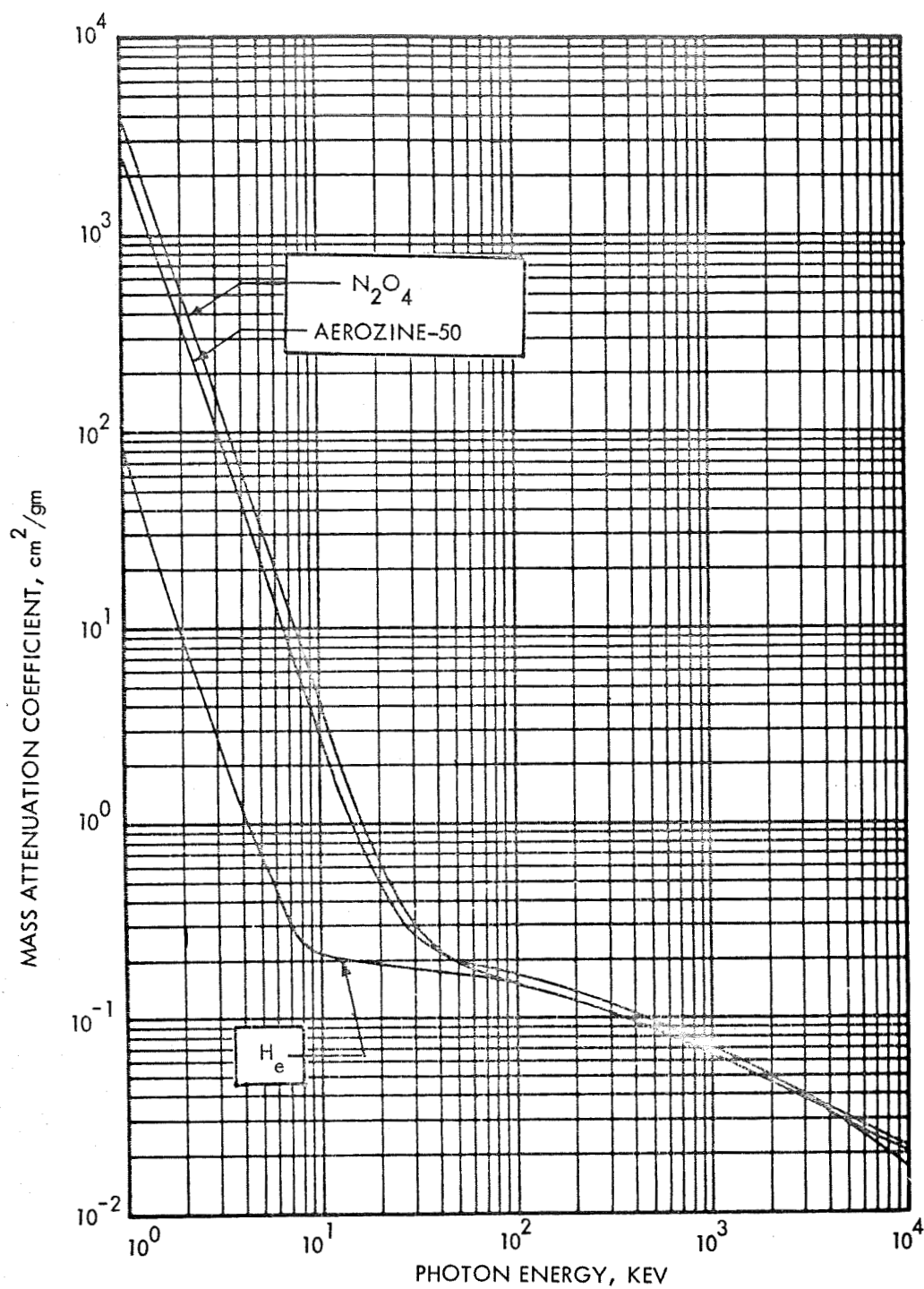


Figure 4-20. Mass Attenuation Coefficients for  $\text{He}$ ,  $\text{N}_2\text{O}_4$ , and Aerozine-50

Using Equation 4.2-1 in conjunction with Equation 4.2-10, the attenuation coefficient of the fuel for the beta particles can be expressed in terms of the partial densities of C, N, H, and H<sub>e</sub> as

$$\begin{aligned}\mu_{\beta \text{ Fuel}} &= \frac{35}{E_m^{1.14}} \left\{ \frac{Z_C}{A_C} \cdot \rho_C + \frac{Z_N}{A_N} \cdot \rho_N + \frac{Z_H}{A_H} \cdot \rho_H \right\} \cdot \frac{1}{\rho_T} \\ &= \frac{19.76}{E_m^{1.14}} \text{ cm}^2/\text{gm}\end{aligned}$$

and from equations 4.2-2 and -3.

$$\frac{C_{\beta}}{C_{o,\beta}} = \exp \left\{ - \frac{17.5}{E^{1.14}} \times \left( \frac{19.76}{17.5} \rho_{\text{fuel}} + \rho_{\text{He}} \right) \right\} \quad (4-2-11)$$

The gamma ray mass attenuation coefficient can be obtained using Equation 4.2-10 in a manner similar to that used for N<sub>2</sub>O<sub>4</sub> which leads to

$$\mu_2 = 0.2 \mu_C + 0.1292 \mu_H + 0.6708 \mu_N \quad (4.2-12)$$

This result is shown in Figure 4-20 as a function of photon energy, along with the corresponding values for N<sub>2</sub>O<sub>4</sub> and as in the previous case, the partial densities of the two constituents are again uniquely defined.

#### 4.2.1.5 Sensitivity Studies

The achievable sensitivity of measurements to variation in the densities of the gases depends primarily on the selection of the maximum beta energy, E<sub>max</sub>, the photon energy, and the separation distances between the sources and detectors. The optimum combination of these factors is subject to constraints such as the space in which the sensing device is to be placed, which fixes the maximum distance permissible between detector and source.



A large source-detector separation distance is desirable since with an increased distance, the radiation is attenuated through a larger sample resulting in more representative measurements. In addition, a reduction in both the maximum beta energy,  $E_{\max}$ , and the photon energy leads to increased sensitivity. However, all these factors must be considered along with the source energies and intensities available. The latter is of particular importance since the accuracy with which a measurement within a given time can be made depends on the amount of unattenuated radiation measured. This aspect will be discussed later.

Before estimating attenuation characteristics, the defined range of typical conditions under which the gas mixture would be expected to exist must be known. The assumed conditions are given in Figure 4-21, where the respective densities of helium and the other constituent were determined from a specified overpressure of 200 psia and the known vapor pressure characteristics of  $N_2O_4$  and Aerozine-50. The range presented describes the anticipated variation of the ullage temperature under typical conditions. This information was then used to obtain an estimate of the sensitivity possible for a system which might be characterized by a 10-cm source-detector separation distance for  $N_2O_4$ , a 20-cm separation for Aerozine-50, using photons of both 5 and 10 kev. It was also assumed that a beta source with  $E_{\max}$  of 1 Mev and a separation distance of 10 cm would be used. The resulting attenuation characteristics were computed using Equations 4.2-3 and 4.2-6 and are presented in Figures 4-22 and 4-23 for  $N_2O_4$  and Aerozine-50, respectively.

The increased separation distance for Aerozine-50 appears necessary since the relatively smaller amount of this propellant in the mixture results in a less sensitive measurement than in the case of the  $N_2O_4$ . This separation distance could be reduced and still maintain the same sensitivity by reducing the photon energy. However, an increase in source strength would probably be necessary to assure consistent measurement accuracy. The results also show that a greater separation distance or reduced  $E_{\max}$  for the beta attenuation measurement is necessary for Aerozine-50 than for  $N_2O_4$  to obtain a consistent sensitivity in the two cases.

The objective of the above discussion was to present the results of preliminary sensitivity studies and to suggest the type of considerations

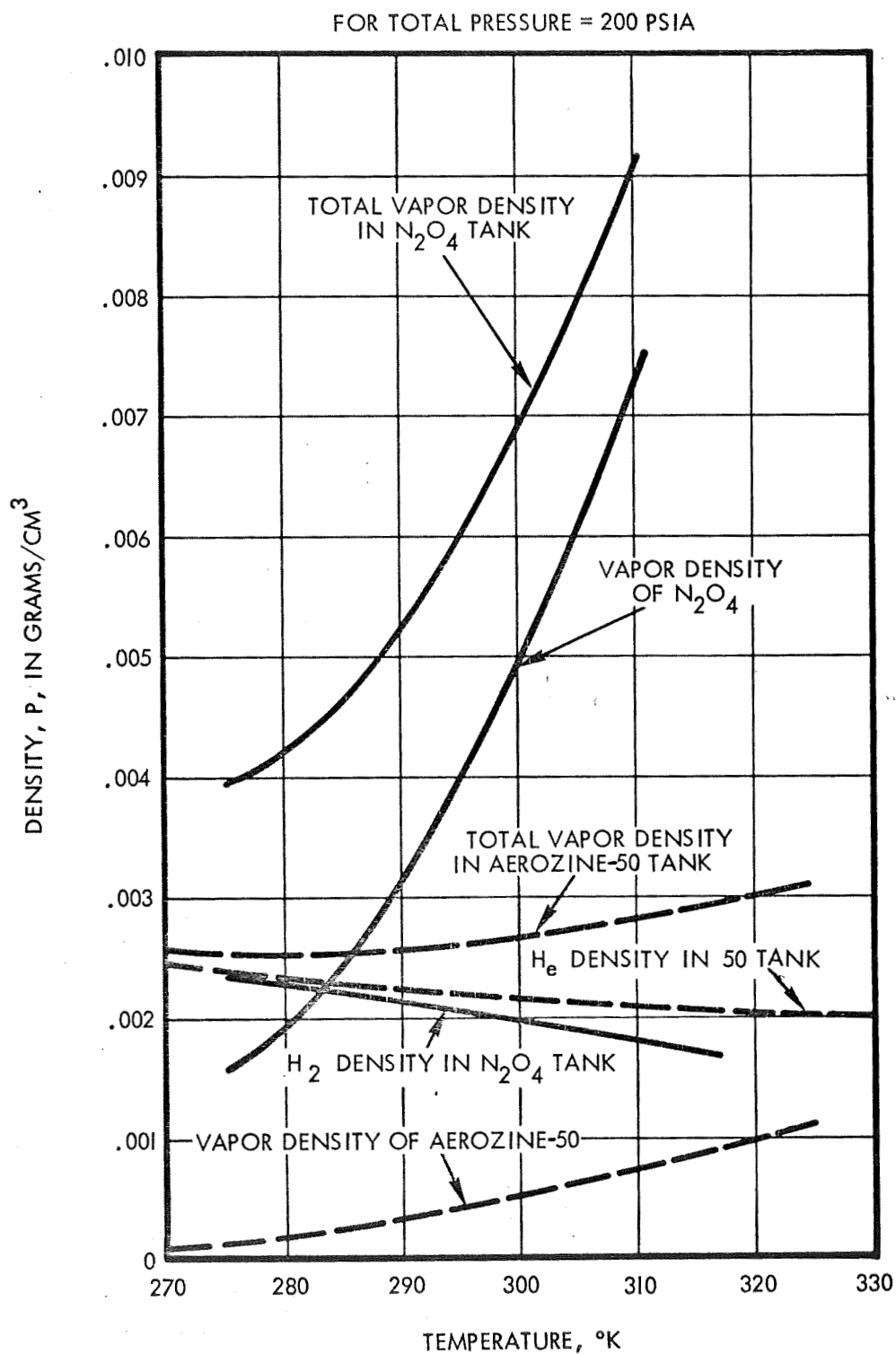


Figure 4-21. Assumed Gas Mixture Characteristics

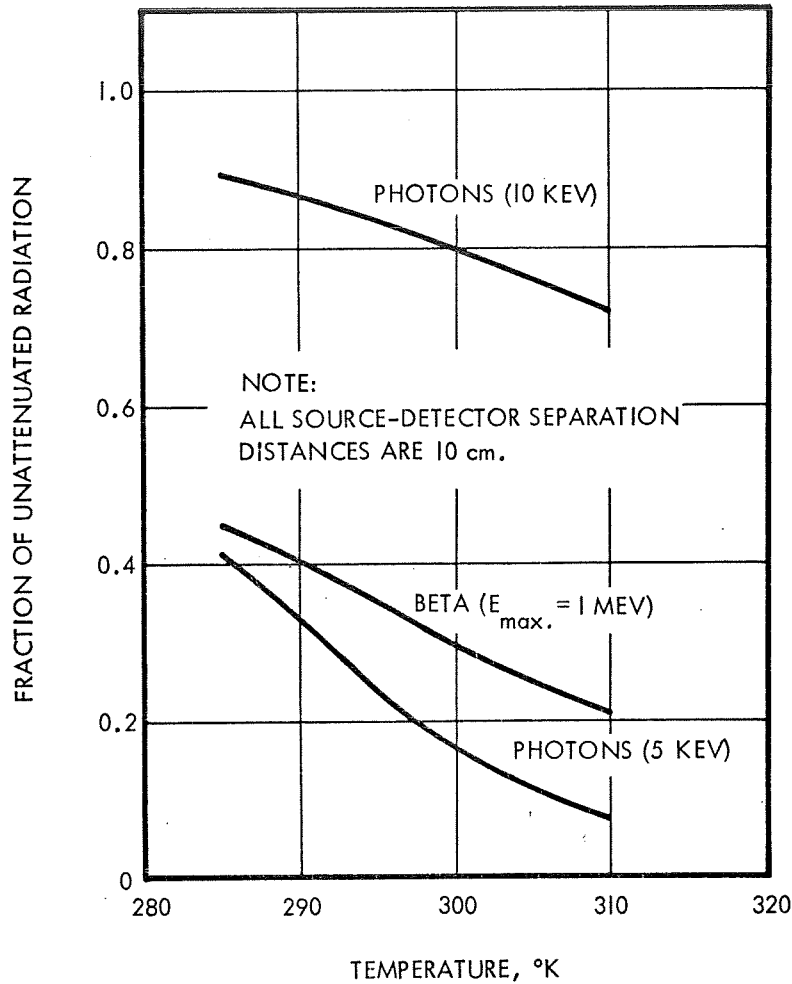


Figure 4-22. Effect of Temperature on the Attenuation of Radiation by the He-N<sub>2</sub>O<sub>4</sub> Ullage at a Constant Pressure of 200 psi

necessary to obtain design guidelines. Before the latter may be accomplished a detailed analysis which entails an investigation of the availability of sources, source energies, half-lives and intensities must be conducted and reviewed in light of specific application constraints and accuracy requirements.

#### 4.2.1.6 Measurement Accuracy

Although several factors can influence the accuracy with which the densities of the constituent gases can be measured, the most significant and obvious error can result from the counting statistics.

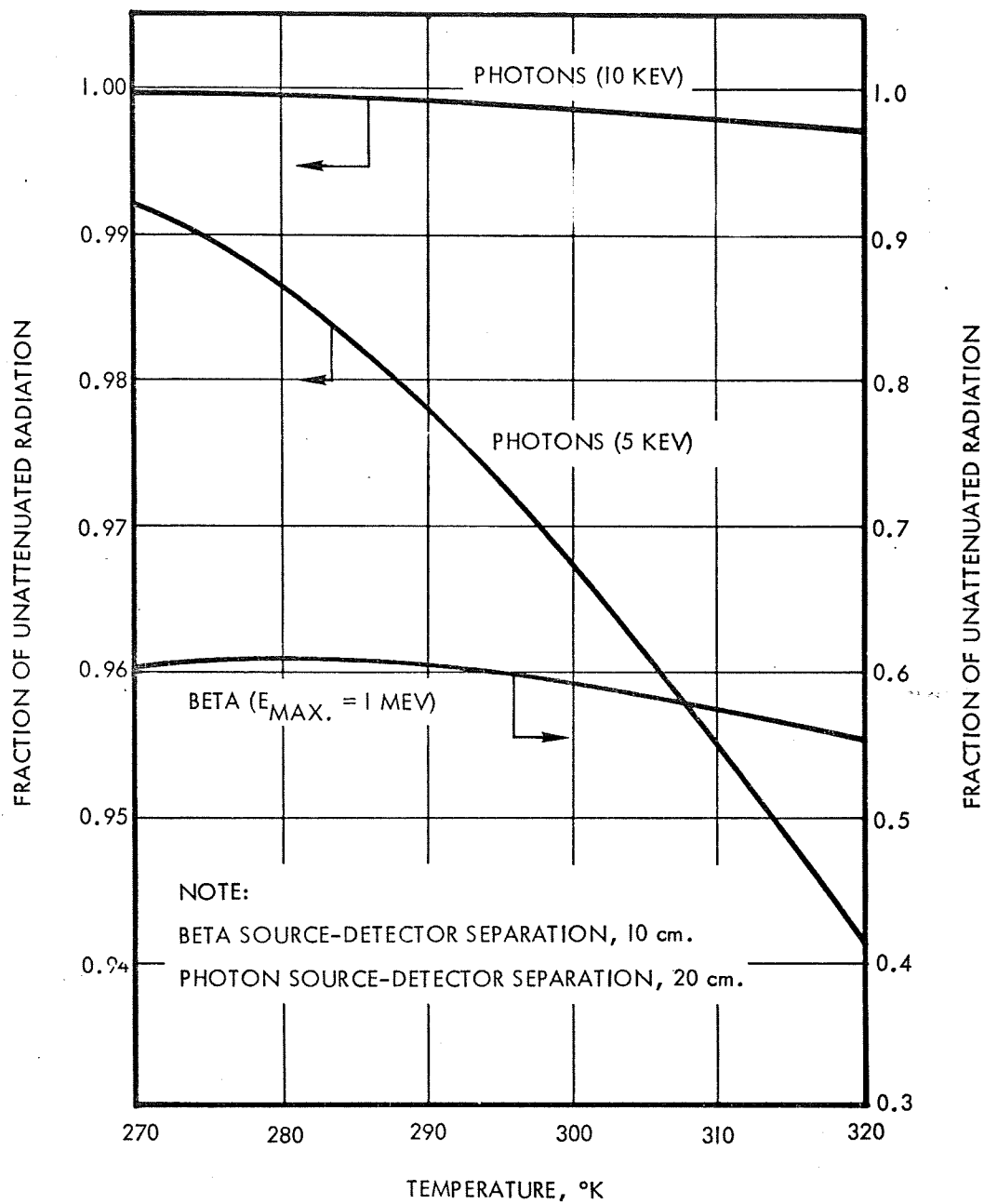


Figure 4-23. Effect of Temperature on Attenuation of Radiation by the Assumed He-Aerazine-50 Ullage at a Constant Pressure of 200 psi

Assuming this to be the major consideration, then the square of the fractional error in the helium density,  $\rho_1$ , can be estimated from

$$\frac{\sigma^2(\rho_1)}{\rho_1^2} = \left( \frac{\partial \rho_1}{\partial A_\beta} \right)^2 \cdot \frac{\sigma^2(A_\beta)}{\rho_1^2} + \left( \frac{\partial \rho_1}{\partial A_\gamma} \right)^2 \cdot \frac{\sigma^2(A_\gamma)}{\rho_1^2} \quad (4.2-13)$$

for which the partial derivatives may be determined from Equation 4.2-8. The quantities  $\sigma^2(A_\beta)$  and  $\sigma^2(A_\gamma)$  are the variances in the ratios of the quantities  $A_\beta$  and  $A_\gamma$ , respectively. If the initial calibration of the counting system has been precisely accomplished, the variances in the ratios  $A_\beta$  and  $A_\gamma$  are simply

$$\frac{\sigma^2(A_\beta)}{A_\beta^2} = \frac{1}{C_\beta} \quad (4.2-14)$$

and

$$\frac{\sigma^2(A_\gamma)}{A_\gamma^2} = \frac{1}{C_\gamma} \quad (4.2-15)$$

where  $C_\beta$  and  $C_\gamma$  are counts accumulated during the prescribed counting period for the betas and photon measurements respectively. (The variance includes the efficiency of the detection system since the total observed counts are considered.)

From Equation 4.2-9,

$$\frac{\partial \rho_1}{\partial A_\beta} = - \left( \frac{1}{1 - \mu_1/\mu_2} \right) \cdot \frac{1}{\mu_\beta^x A_\beta} \quad (4.2-16)$$

and

$$\frac{\partial \rho_1}{\partial A_\gamma} = - \left( \frac{1}{1 - \mu_1/\mu_2} \right) \cdot \frac{1}{\mu_2^t A_\gamma} \quad (4.2-17)$$

which, in Equation 4.2-13 results in

$$\frac{\sigma(\rho_1)}{\rho_1} = \frac{1}{\rho_1 \sqrt{C}} \left( \frac{(\delta_2^2 + \delta_3^2)^{1/2}}{(1 - \delta_2/\delta_1)} \right) = \frac{(\delta_2^2 + \delta_3^2)^{1/2}}{\rho_1 \sqrt{C} (1 - \mu_1/\mu_2)} \quad (4.2-18)$$

where  $\delta_1 = (\mu_1 t)^{-1}$ ,  $\delta_2 = (\mu_2 t)^{-1}$  and  $\delta_3 = (\mu_\beta x)^{-1}$  and the accumulated counts  $C_\gamma$  and  $C_\beta$  were assumed equal to  $C$ . An important aspect of the proposed technique is readily apparent from Equation 4.2-18. If the attenuation coefficients for helium ( $\mu_1$ ) and the propellant ( $\mu_2$ ) are such that  $\mu_1 \leq \mu_2$  then the error is much smaller than if  $\mu_1 \approx \mu_2$ , for which a large error can result. This points up the requirement that a low energy photon be used since this satisfies the conditions that  $\mu_1 \ll \mu_2$  (Figure 4-20). If the latter condition is indeed the case, the  $\mu_1/\mu_2$  from Figure 4-20 can be seen to be small relative to 1 for energies in the kev range. Then Equation 4.2-18 can be written as

$$\frac{\sigma(\rho_1)}{\rho_1} = \frac{1}{\rho_1 \sqrt{C}} \left( \delta_2^2 + \delta_3^2 \right)^{1/2} \quad (4.2-19)$$

This expression may be employed to determine the count rate (and hence the source strength) and measurement time necessary to achieve a given accuracy once the radiation source energies and geometric parameters have been defined.

#### 4.2.1.7 Summary

A method to determine the constituent densities of a binary mixture of gases has been discussed, and some preliminary analyses were performed to show its applicability to a ullage mixture of He -  $N_2O_4$  and He - Aerozine-50 over a typical range of density variations that might exist in a zero gravity propellant and oxidizer storage system. The technique exploits the fact that the attenuation of beta particles can be characterized by only the bulk density of the mixture, whereas the attenuation of low energy photons is sensitive to the variation in the constituent with the higher Z.

For measurements performed under the appropriate conditions, the calculations resulted in a very simple expression for the helium density,  $\rho_1$ , which, in terms of the unattenuated fraction of betas and photons given respectively as  $A_\beta$  and  $A_\gamma$  can be expressed as

$$\rho_1 = \text{constant} \cdot \ln(A_\beta/A_\gamma) \quad (4.2-20)$$

The density of the other gas constituent can also be determined from equations presented in the text.

Preliminary sensitivity and accuracy studies were conducted to define the important factors which must be considered in a design study once the required counting accuracy and the geometric relationships for an actual system have been established.

#### 4.2.2 Application of the RHO Gauge to Zero Gravity Gauging

The RHO gauge described in Section 4.2.1 provides a measurement of the density of helium in the ullage gas. This information can be used for zero-gravity gauging in a number of different ways. The RHO gauge can be used in conjunction with a beta attenuation gauge in the pressurant tank to measure pressurant density (the  $\rho_V$  system described in Section 3.5). This approach is capable of a fair degree of accuracy when a single pressurant tank is used for a single propellant tank. It consists simply of a helium balance as shown below.

$$\begin{aligned} m_{\text{He}_p} &= m_{\text{He}_{g_o}} - m_{\text{He}_g} = V_g (\rho_{\text{He}_{g_o}} - \rho_{\text{He}_g}) \\ V_p &= V_{p_o} - V_{\text{He}_g} = V_{p_o} - \frac{m_{\text{He}_p}}{\rho_{\text{He}_p}} \\ &= V_{p_o} - V_g \frac{(\rho_{\text{He}_{g_o}} - \rho_{\text{He}_g})}{\rho_{\text{He}_p}} \end{aligned}$$

In the more common situation, a single pressurant tank is used to pressurize both the fuel tank and the oxidizer tank. This leads to

additional errors in determining the quantity of propellant remaining in the individual tanks. If information is available from a high gravity gauge, the error from this source can be somewhat reduced. However, in this situation a somewhat simpler approach seems more desirable, namely, to lock off the individual propellant tanks from the pressurant tanks and simply monitor the helium density in the propellant tank. If the helium density does not change, the helium volume is the same as that shown by the high gravity gauge at termination of the last firing. This technique serves as a zero g gauging system by detecting any leakage. It will be noted that the helium density could also be determined by a simple measurement of the pressure and temperature (the familiar PVT system). In Table 4-2 an error analysis of the RHO and the pressure and temperature system is presented. The analysis shows that as the tank depletes, the RHO gauge accuracy degrades more slowly than does the PVT system.



Table 4-2. Helium Balance Error Estimate\*

	<u>Percent</u>	<u>Total</u>
<u>RHO Gauge</u>		
Sensitivity of Beta-Ray	±0.1	
Sensitivity of X-Ray	±0.1	
Miscellaneous Electronics	<u>±0.2</u>	
Net error in local helium density measurement	±0.5	
Variation in Helium Partial Pressure in Ullage*	±0.5	
Liquid Density	±0.4	
Dissolved Helium	±0.2	
Net error in measurement		±0.84
Error - Empty Tank		±0.84
Error - Full Tank		±0.55
<u>Pressure, Temperature Measurement</u>		
Sensitivity of Temperature Measurement (±0.5°F)	±0.75	
Sensitivity of Pressure Measurement (±0.2%)	<u>±0.2</u>	
Total Temperature and Pressure Measurement	±0.78	
Variation in Helium Partial Pressure	±0.5	
Variation in Local Temperature (±2°F)	±3.0	
Dissolved Helium	±0.2	
Liquid Density	±0.4	
Net error in measurement		±3.2
Error - Empty Tank		±3.2
Error - Full Tank		±0.8

---

\* Assumes ±1 psi variation in local N<sub>2</sub>O<sub>4</sub> concentration.

### 4.3 ANALYSIS OF AN ULLAGE GAS RADIOTRACER GAUGE IN A BLADDERLESS TANK

The ullage gas radiotracer gauge described in Section 3.5.2 has been shown as an effective gauging system in those systems incorporating bladders. In this section, an analysis is made which demonstrates that significant errors will occur when this system is used in a bladderless tank.

#### 4.3.1 System Description

In the ullage gas radiotracer gauge, a quantity of inert tracer gas is introduced into the ullage volume. As propellant is consumed, the ullage volume increases and the tracer gas concentration decreases. This reduction in tracer gas concentration is directly related to the change in the ullage volume and, hence, the propellant volume. The above description assumes that all of the tracer gas remains in the ullage gas. When the propellant is not contained in a bladder, an appreciable portion of the tracer gas will dissolve in the propellant with resulting errors as described below.

#### 4.3.2 Discussion

The radiotracer gas system considered in this study consists of a storable propellant tank ( $V = 4.25 \times 10^6 \text{ cm}^3$ ) containing either  $\text{N}_2\text{O}_4$  or Aerozine-50 propellant with an initial ullage fraction  $\times$  of 0.07. The pressure in the propellant tank is maintained at 200 psi by introducing He gas from a pressurant tank through a regulator. The tracer gas concentration in the ullage space is assumed to be measured after each firing to determine the fraction of propellant remaining.

In this preliminary analysis, it was assumed that the temperature and pressure are constant and that deviations from ideal gas behavior can be neglected. It has also been assumed that the concentration of the gases in the propellant remain constant during firing. That is, the firing time is much less than the effective time constant of the various mechanisms restoring equilibrium (e.g., diffusion, mixing, etc.).

The equations which describe the system performance are as follows:

$$\text{Ideal gas relationship} \quad P_k V_{u_k} = n_{gk} RT \quad (4.3-1)$$

$$\text{Henry's laws} \quad \bar{p}_j = x_{j\ell} K_j(T) \quad (4.3-2)$$

$$\bar{p}_{jg} \cong x_{jg} P_k \quad (4.3-3)$$

and component mass balances

$$n_{ji} = n_{jg} + n_{j\ell} + n_{jo} \quad (4.3-4)$$

where

$K_j(T) \equiv$  Henry's constant for jth component, atm/mole fraction

$n_{gk} \equiv$  total number of moles in gas after kth firing

$n_j \equiv$  number of moles of jth component

$P_k \equiv \bar{p}_{1k} + \bar{p}_{2k} + \bar{p}_{3k} \equiv$  total pressure in propellant tank, atm

$\bar{p}_j \equiv$  partial pressure of jth component, atm

$R \equiv 82.06 \equiv$  gas constant,  $\text{cm}^3\text{-atm/gm-mole-}^\circ\text{K}$

$T \equiv$  temperature,  $^\circ\text{K}$

$V_{uk} \equiv$  ullage volume after kth firing,  $\text{cm}^3$

$x_j \equiv$  mole fraction of jth component

Subscripts

$g =$  gas

$i =$  initial value

$j =$  component; 1 - helium, 2 - tracer, 3 - propellant

$k =$  conditions after kth firing

$\ell =$  liquid

$o =$  expelled with propellant

$u =$  ullage

In addition, define:

$f_k = n_{3k}/n_{3i}$  = fraction of fuel remaining after kth firing

$\chi = V_{ui}/V$  = initial ullage fraction

and the ullage volume may be expressed as

$$V_{uk} = V \left[ 1 - f_k(1 - \chi) \right] \quad (4.3.5)$$

Combining Equations 4.3-1 through 4.3-5 yields the ratio of tracer gas concentration after the kth firing to the initial concentration:

$$\frac{C_k}{C_i} = \frac{\chi \left( 1 - \frac{n_{2o}}{n_{2i}} \right) \left[ 1 + \frac{R T n_{3i}}{V K_2(T)} \right]}{\left\{ 1 - f_k \left[ 1 - \chi \left( 1 + \frac{R T n_{3i}}{V K_2(T)} \right) \right] \right\}} \quad (4.3-6)$$

where  $C$  = count rate

Another equation required to account for the tracer gas expelled with the propellant is the relationship:

$$\frac{n_{2o}}{n_{2i}} = \left[ \frac{R T n_{3i}}{\chi V K_2(T) \left( 1 + \frac{R T n_{3i}}{\chi V K_2(T)} \right)} \right] \sum_{r=1}^k \frac{C_{r-1}}{C_i} \Delta f_r \quad (4.3-7)$$

The initial value of the ratio of the total number of moles of tracer gas in the propellant tank to the moles in the ullage space is given by:

$$\frac{n_{2i}}{n_{2gi}} = 1 + \frac{R T n_{3i}}{\chi V K_2(T)} \quad (4.3-8)$$

Clearly, this ratio will be unity when  $K_2(T) \approx \infty$  which characterizes an insoluble tracer gas. In this case, the system performance will duplicate the results of past studies where an impermeable bladder was considered. For decreasing values of  $K_2(T)$  the ratio will increase indicating that more of the tracer gas initially present is dissolved in the propellant. For large values of the ratio (i. e., greater than two) there is more tracer in the propellant than in the ullage volume.

Using the solubility data in Figure 4-24 for Aerozine-50 and Reference 4-4 for  $N_2O_4$ , the performance of three tracer gases was studied. The tracers studied were  $^{39}A$ ,  $^{85}Kr$  and a hypothetical isotope with the solubility of helium. Henry's constant for  $^{85}Kr$  was obtained by extrapolation as indicated in Figure 4-24. The variation of the concentration ratio with the fraction of propellant expelled, 1-f, for the three tracers with  $N_2O_4$  and Aerozine-50 is shown in Figures 4-25 through 4-27. The performance of the helium tracer gas does not deviate significantly from that of a system incorporating an impermeable bladder. However, for  $^{39}A$  and, particularly,  $^{85}Kr$  there is a considerable difference. Under the ideal conditions of constant temperature and pressure throughout the mission, the performance of the soluble gases does not appear particularly undesirable since a greater sensitivity near the tank empty conditions is achieved than is realized in the bladder system. In Figure 4-28 the difference in system performance of  $^{39}A$  with  $N_2O_4$  for two temperatures, both assumed constant throughout the mission, is small indicating that the temperature dependence of Henry's constant is not an important consideration. However, in Figure 4-29 it is seen that the propellant usage rate (i. e., fraction expelled during each firing) affects the system performance rather significantly. The reasons for this behavior are discussed in the following paragraph.

The ullage gas measures the change in concentration of tracker in the ullage space. The quantity measured is in turn related to the change in ullage volume. When the tracer gas is insoluble in the propellant or if there is an impermeable bladder present, the mass of tracer gas in the ullage volume is constant and a change in concentration is due only to expulsion of propellant or, to a much lesser degree, any change in ambient temperature or pressure. However, when the tracer gas is

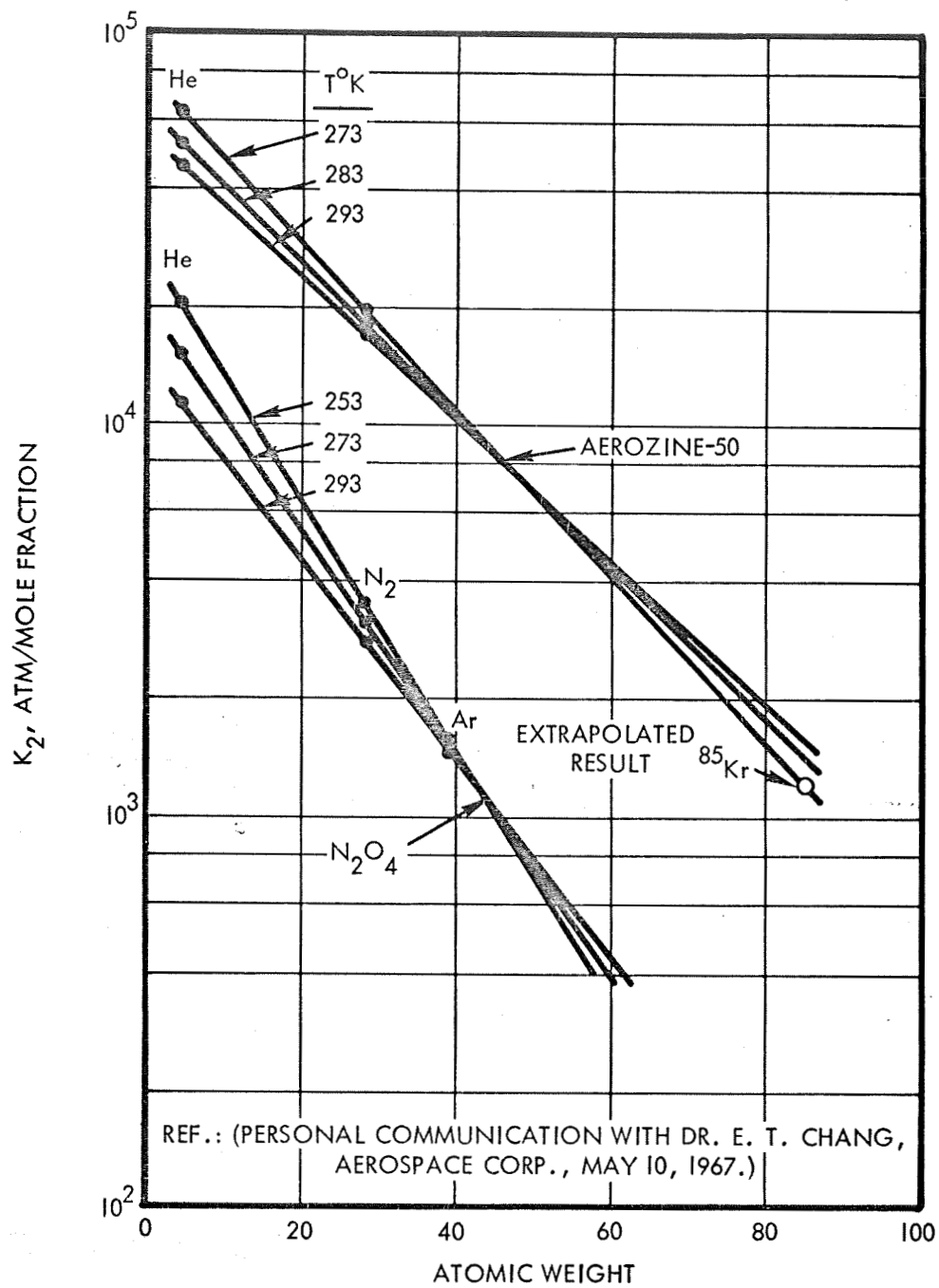


Figure 4-24. Henry's Constant for Aerozine-50 and Nitrogen Tetroxide

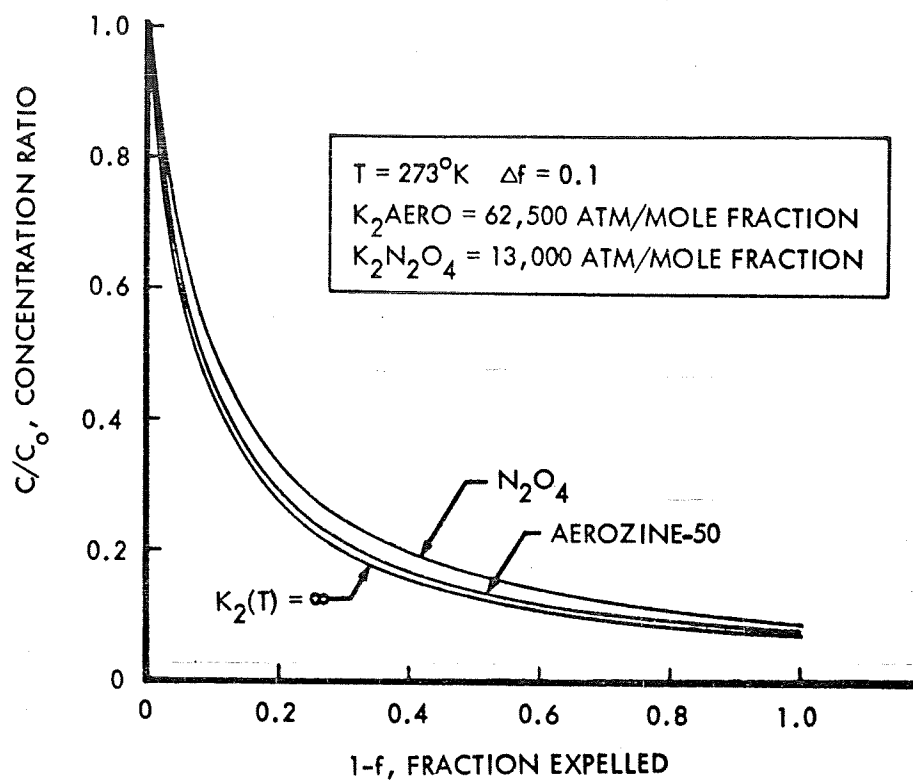


Figure 4-25. Performance of Hypothetical Helium Radiotracer Propellant Gauging System

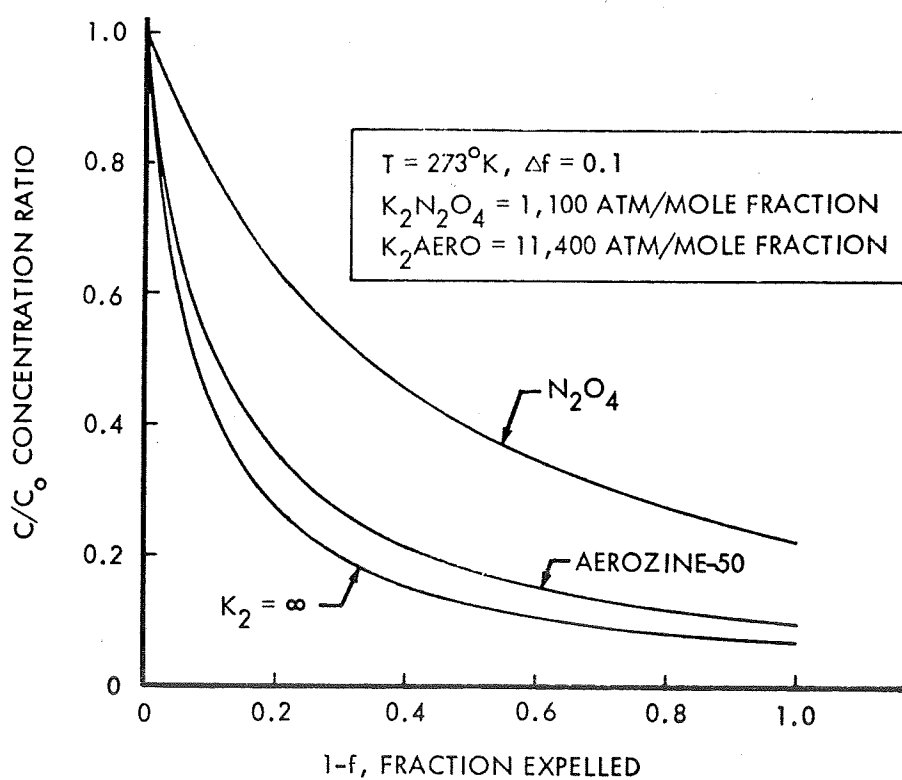


Figure 4-26. Performance of  $^{39}A$  Radiotracer Propellant Gauging System

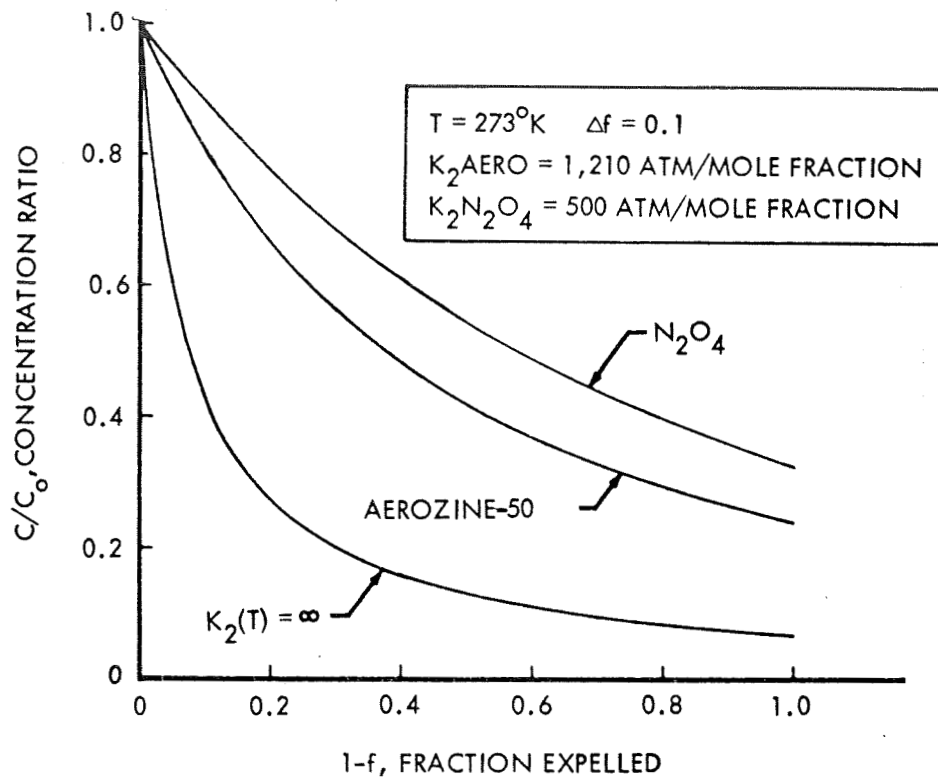


Figure 4-27. Performance of  $^{85}\text{Kr}$  Radiotracer Propellant Gauging System

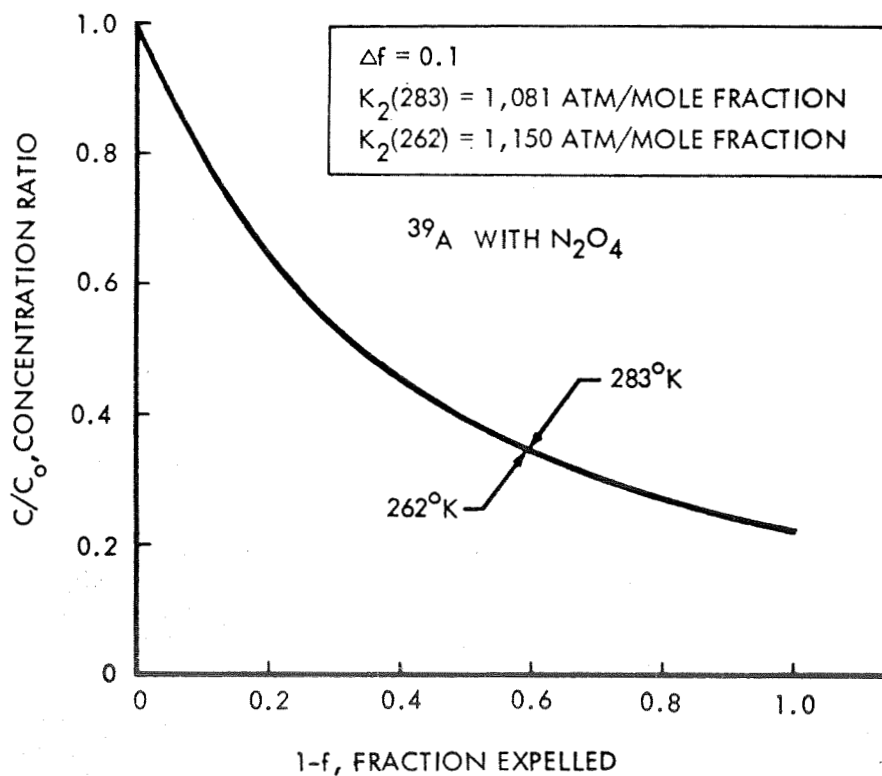


Figure 4-28. Performance of  $^{39}\text{A}$  Radiotracer System for Different Temperatures



soluble in the propellant, the amount of tracer gas in the ullage space is not constant and will depend upon how much tracer gas has been expelled in previous firings and what proportion of that remaining is dissolved in the propellant. This is not necessarily undesirable as long as the relationship between ullage volume and tracer concentration is not altered during the mission life. Unfortunately, when the tracer gas is soluble in the propellant, the tracer concentration is dependent on both the liquid and gas volumes. As the propellant is depleted, the partial pressure of the tracer gas is reduced. This changes the equilibrium between the tracer in the ullage and the propellant gas previously dissolved in the propellant, and some of this tracer gas comes out of solution. The gas in the propellant that is expelled during a firing does not have time to come to equilibrium, and a greater quantity of tracer is removed from the system than equilibrium would predict.

It is apparent that solubility effects become more important as the ratio of the number of moles of tracer gas dissolved in the propellant to the number of moles in the ullage volume increases. The value of this ratio for the conditions shown in Figures 4-25, 4-26, and 4-27 is presented in Table 4-3.

Table 4-3. Ratio of Moles in Liquid vs Gas

Tracer gas	$\frac{\text{Weight of Tracer in Liquid}}{\text{Weight of Tracer in Ullage Gas}}$	
	Aerozine-50	N <sub>2</sub> O <sub>4</sub>
He (Hypothetical)	0.0973	0.367
<sup>39</sup> A	0.534	4.15
<sup>85</sup> Kr	5.03	9.54

#### 4.3.3 Conclusions

The solubility of the tracer gas in the propellant is sufficient to cause appreciable error in interpreting data from ullage gas radiotracer systems. The resulting measurement is exceedingly sensitive to the usage rate of the propellant, as shown in Figure 4-29.

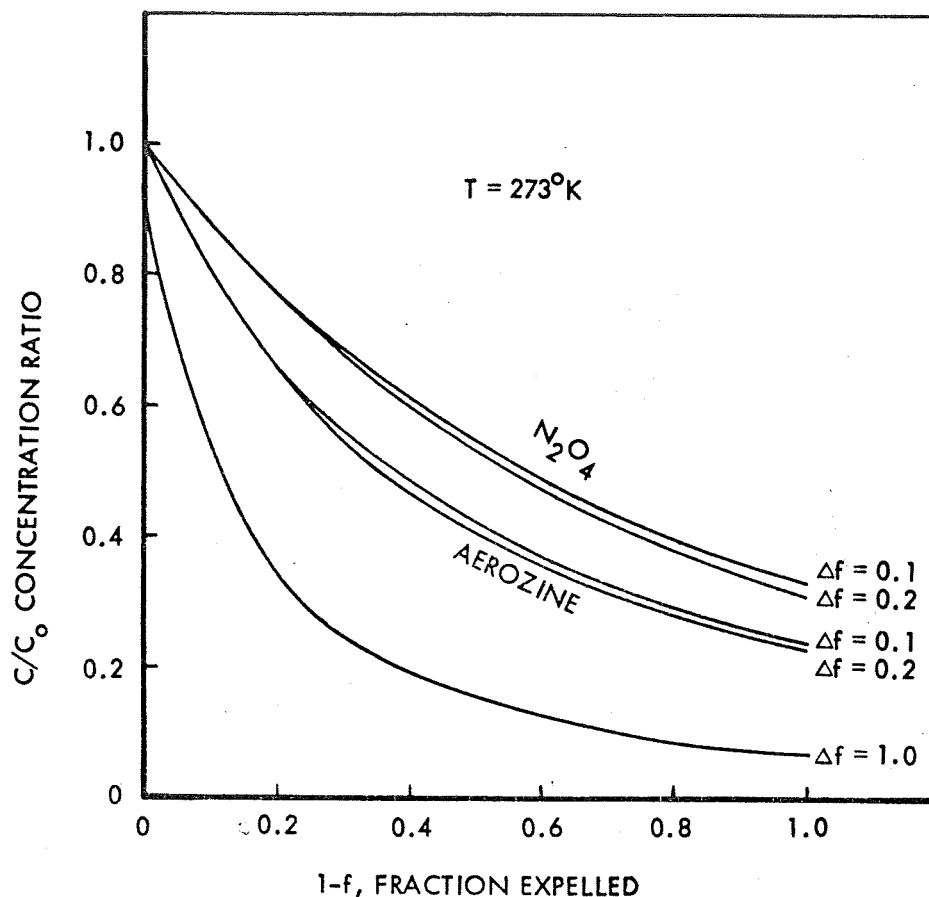


Figure 4-29. Effect of Increment Size on Gauging System Performance, Fuel Expelled in Equal Increments

From this preliminary analysis, it is concluded that a Radiotracer Propellant Gauge based upon measuring the concentration of tracer gas in the ullage space of a bladderless tank is not feasible unless a new tracer gas is found with a considerable lower solubility in propellants than those presently under consideration (e. g.,  $^{85}\text{Kr}$ ,  $^{39}\text{Ar}$ ,  $^{36}\text{Cl}$ ,  $^{14}\text{Se}$ , etc.).

## 5. SUMMARY AND RECOMMENDATIONS

### 5.1 INTRODUCTION

During the Phase I portion of this study, a large number of different concepts were examined for possible application to propellant gauging. One new system, the Resonant Infrasonic Gauging System (RIGS) is recommended for further study in the Phase II portion of this study. A second system, a helium balance system (the RHO Gauge) also appears to justify further study.

This section of the report summarizes the results of the Phase I study and indicates the reasons for the selection of the RIGS system.

### 5.2 RESULTS OF GENERAL SURVEY

The initial task in this study was to undertake a general survey to determine both existing and new techniques in the field of propellant gauging in the zero gravity environment. Two methods were used in the attempt to delineate new and novel techniques for propellant gauging. A morphological survey of propellant properties was performed to determine which, if any, of the propellant properties might form the basis of a new gauging concept.

A second approach was to organize brainstorming sessions to bring together TRW technical specialists from diverse fields to discuss, originate, screen, and evaluate proposed ideas. Personnel for these sessions were selected on the basis of proven inventiveness and discussion among participants was greatly encouraged. A total of seven such sessions was held. The hope was that the combination of a systematic survey of potential gauging techniques and a group of creative specialists would result in the identification of useful new concepts. Approximately 60 different concepts were proposed during the survey and a summary of the more promising techniques is presented in Table 5-1. The systems were evaluated on the basis of the requirements presented in Table 2-1 with particular emphasis on the capability to gauge propellants under zero gravity and in a bladderless tank. For the specified propellants, Aerozine-50 and  $N_2O_4$ , none of the systems studies appear to be capable of  $\pm 0.5\%$  accuracy during all phases of the flight profile but a number indicated potential achievement of this goal during the zero gravity portion

Table 5-1. Summary of Gauging Principles

Type	Method	Problems
Light Attenuation*	Measure attenuation through propellant.	Affected by propellant location. Refraction at interfaces.
Light Extinction*	Pulse with multiple light sources. Measure time for light to decay.	Requires highly reflective walls, highly transparent propellant. Refraction at interfaces.
Light Phase Shift (Transmission Time)*	Scan with coherent light source. Measure phase shift caused by variation in speed of light.	Refraction at interfaces, pulse analysis difficult. High power requirements.
Light Phosphorescence*	Add a phosphor to the propellant, pulse with light source that activates phosphor and measures emitted light.	Refraction at interfaces. Requires two transparent windows. Slightly sensitive to propellant location.
RF Phase Shift, VLF-LF	Capacitance between RF coil and tank.	Conductivity of fuel. Requires uniform field. Sensitive to propellant location.
RF Resonance, VHF	Lowest resonant mode	Conductivity of fuel. Sensitive to propellant location.
RF Mode Counting, UHF-Microwave	Number of modes in frequency band.	Conductivity of fuel. Symmetry in tank leads to position sensitivity. Sweep rate may distort peaks. Location of pickup.

\*Note: No sufficiently transparent windows are present in nitrogen tetroxide and therefore none of these techniques can be used.

Table 5-1. Summary of Gauging Principles (Continued)

Type	Method	Problems
RF Loss Measurement, VHF	Measure loss tangent.	Variation in conductivity. Requires uniform field. Sensitive to propellant position.
Inertial	Vibrate tank. Measure frequency.	Only propellant against the wall will react
Paddle	Sweep the tank with rotating paddle, measure force required.	Viscosity variation with temper- ature. Causes motion of vehicle. Requires extensive tank modifica- tion. Sensitive to external g field.
Flowrate	Integrate flowrate	Does not detect leakage.
Acoustical Resonance	Measure fundamental frequency in tank.	Sensitive to position of propellant. Cannot detect gas pockets.
Acoustical Mode Counting	Count resonant modes over fixed frequency range.	Sensitive to position of propellant. Cannot detect gas pockets.
Infrasonic	Measure ullage gas com- pliance with low frequency pressure perturbation.	Sensitive to gas composition. Most inaccurate during engine firing. Can be temporarily dis- abled by liquid against diaphragm.
Helium Balance	Keep track of helium used. Calculate ullage volume.	Requires separate pressurant tank for each propellant tank. Cannot distinguish between propellant and pressurant leak. Requires high gravity gauge to maintain accuracy.

Table 5-1. Summary of Gauging Principles (Continued)

Type	Method	Problems
γ-Rays X-Rays	Attenuation	Sensitive to propellant location. External radiation. Cross-talk between tanks.
Neutrons	n, γ activation Pulse thermalization Attenuation	External radiation. Sensitive to position.
Nuclear Magnetic Resonance	Measure NMR	Requires very large fields, hence high weight.
Capacitance	Multiple plates Wire network	Conductivity of fuel.
Gravitation	Measure attraction of mass.	Extremely difficult to detect. R <sup>2</sup> effect results in position sensitivity. Small movements give noise.
Dielectrophoresis	Position propellant with electric field.	Conductivity of fuel.
Heat Titration	Add heat, measure temperature rise.	Low time constant. Needs good mixing. High power requirements.
Magnetometer	Dope propellant with ferric salt, measure field.	R <sup>2</sup> effect results in position sensitivity.
Ullage Gas Tracer	Radio tracer. Infrared tracer.	Solubility of tracer in propellant.

of the flight. These systems were then studied in more detail. It is important to realize, however, that the conclusion as to gauging system accuracy and applicability could be substantially different for other propellant combinations, such as cryogenics.

### 5.3 RESULTS OF PRELIMINARY ANALYSIS

The objective of the preliminary analysis was to determine the major problem areas, advantages, and limitations of each candidate system. Systems which were studied during this phase may be classified as light interaction, infrasonic, helium balance, and gas tracer systems.

#### 5.3.1 Light Interaction Systems

Three versions of light interaction systems were studied. All three were dropped when the results of an experimental determination of the transmission characteristics of the propellant indicated that no sufficiently transparent windows were present in the range between far-infrared to the ultraviolet. A brief summary of the advantages and other problem areas of each is presented below.

##### 5.3.1.1 Light Attenuation System

This approach was similar to the gamma ray attenuation system developed by Giannini for propellant gauging. Since light was used rather than gamma or X-rays, no external radiation was present. Its primary disadvantages were sensitivity to refraction of the light, and sensitivity to propellant location within the tank.

##### 5.3.1.2 Light Transmission Time System

This system used the difference in speed of light in the ullage gas and the propellant to measure the propellant quantity in the tank. Reduced sensitivity to propellant location, due to the linear nature of the measurement, was the primary advantage of this system. The system could be self-calibrating and effects of refraction could be minimized by time sequencing the light rays. The system could provide an accurate measurement under boost and loading conditions. Primary disadvantages other than lack of transparent windows were that a large number of sensors would be required in order to minimize the effect of propellant location under zero gravity and refraction of the light beams could result in errors (particularly for the highly refractive fuel).

#### 5.3.1.3 Light Phosphorescent System

In this system a phosphor was added to the propellant and activated with a light source. If the propellant was highly transparent the measurement would be quite insensitive to propellant location. Problem areas are the availability of suitable phosphors and the salting out of the phosphors.

#### 5.3.2 Infrasonic Systems

Two infrasonic systems were examined. Since both systems measured the compliance of the ullage gas, they were both quite sensitive to the composition of ullage gas (see Section 4.1). Both systems, therefore, suffer an appreciable loss of accuracy during and immediately after a major system transient such as an engine firing. Another common problem was the sensitivity of both systems to liquid directly impinging upon the diaphragm. While techniques are available to insure that this will not occur during zero gravity, both systems would be temporarily disabled during periods of high reverse thrust.

##### 5.3.2.1 Phase Sensitive Infrasonic System

This system measures the phase shift across an acoustical resistance and relates the phase shift to the gas compliance, then to the ullage, and finally to the liquid volume (see Section 4.1.1). The system is light, compact, requires little power, and should not be very costly to produce. Major problem areas of the system, in addition to those listed above, include a variation of the acoustical resistance with changes in temperature, and the sensitivity to small changes in phase angle resulting from nonlinearities or noise in the system. Because one of the phase measurements is made in the propellant tank, it is sensitive to noise generated by the propellant motion, pressure regulator, etc.

##### 5.3.2.2 Resonant Infrasonic System

This system employs a resonant mass to determine the compliance and hence the ullage volume (see Section 4.1.2). By eliminating the acoustical resistance the system is made insensitive to the temperature; and by employing a resonant circuit the system is made insensitive to nonlinearities. The system is light, compact, requires little power, and should not be costly to produce. The only measurements required are in the gauge itself, not in the propellant tank. Major problem areas



include the necessity for detecting the phase angle of a signal varying over a wide (100:1) range and the stability of the resonant mass under vibration.

### 5.3.3 Helium Balance System

A number of different helium balance gauging systems were studied in this phase. These systems are all based on the determination of the ullage volume from the mass of helium in the propellant tank and the helium density. One major failing of all proposed helium balance systems is their inability to distinguish between a propellant or a helium leak. Any helium lost to the system is assumed to correspond to a liquid volume change.

#### 5.3.3.1 PVT and $\rho V$ Systems

In this system the quantity of helium entering the propellant tank is determined by measuring the density change in the helium tank. In the case of the PVT system it is determined by measurement of the pressure and temperature in the helium tank. Helium density in the pressurant tank is measured by either pressure and temperature measurements or by the RHO gauge discussed below. The  $\rho V$  system uses a beta-ray attenuation technique to provide more accurate density measurement. In either case, when a common pressurization system is used for both oxidizer and fuel no information is available to determine into which tank the pressurant went. This can result in appreciable errors. While a high gravity system can provide recalibration points, the somewhat simpler RHO gauge seems preferable in this case.

#### 5.3.3.2 RHO Gauge

The RHO gauge uses the attenuation of both an X-ray and beta-ray source to determine the density of helium in the presence of propellant vapor. This measurement, in a tank which is isolated from the pressurant source, acts as a zero gravity gauging system. If the helium density in the propellant tank remains constant during an extended zero gravity coast no leakage has occurred and the quantity of propellant is the same as when the engine last fired. If the helium density decreases, assuming no helium loss, the quantity of propellant lost can be calculated. Thus the RHO gauge, in conjunction with a standard high gravity gauge, performs the total gauging function. Note that if the propellant vapor pressure were

sufficiently low, a simple pressure transducer and thermocouple could perform the same task.

The RHO gauge is simple, light, and should not be very costly. External radiation is completely negligible. Output from the system is digital. Major problem areas, in addition to requiring a high gravity gauge, include the requirement of maintaining a liquid-free area, the inability of the system to distinguish between liquid and gas leakage, and the difficulties of obtaining a good sample of the ullage gas.

#### 5.3.4 Ullage Gas Tracer Systems

The approach was similar to the radiotracer technique developed by TRW for propellant gauging in bladder-containing tanks. A quantity of an inert beta-emitting tracer gas is added to the ullage gas and the concentration measured by a beta-ray counter. As propellant is depleted the volume occupied by the gas increases, diluting the tracer gas. By measuring the tracer gas concentration, the ullage volume and thus the liquid volume can be measured. The analysis presented in Section 4.3 showed that sufficient tracer gas would be dissolved in the propellant to invalidate this technique for use with a bladderless tank.

#### 5.4 RECOMMENDATIONS

On the basis of the results of the preliminary analysis the Resonant Infrasonic Gauging System (RIGS) is recommended for the Phase II study. This selection was made by evaluating the systems on their ability to measure propellant quantity under zero gravity, simplicity of the concept, and the character of the unresolved problem areas. The RHO gauge, because of its inherent simplicity, was also considered worthy of further study. These conclusions were specific for Aerozine-50 and  $N_2O_4$ . Significantly different conclusions might be reached for other propellant combinations.

## 6. REFERENCES

- 2-1 G. C. K. Yeh and R. E. Hutton, "Static Configurations of the Liquid-Vapor Interface in an Axisymmetric Tank in Various Gravitational Fields," EM 15-2, TRW Systems, March 1965. To be published in the Proceedings of the 9th Midwestern Mechanics Conference (1965) Madison, Wisconsin.
- 2-2 W. C. Reynolds, M. A. Saad and H. M. Satterlee, "Capillary Hydrostatics and Hydrodynamics at Low g," Tech. Rept. LG-3, Mechanical Engineering Dept., Stanford University, September 1964.
- 2-3 G. C. K. Yeh, "Forced Oscillations of a Liquid in a Cylindrical Tank at Low Gravity Environments," EM 16-8, TRW Systems, September 1966.
- 3-1 Cohn, Irving H., Space/Aeronautics, "Gas Laws Provide New Method of Zero-G Gravity," March 1966, P. 102.
- 3-2 Rod, Robert L., Knox, Dr. Cammeron, and Doshi, Navih H., "Propellant Utilization and Control for Spacecraft," Air Force Rocket Propulsion Laboratory Research and Technology Division, Technical Report AFRPL-TR-65-115, Edwards, California, September 1965.
- 3-3 Fontana, A., Gunny, E., Doshi, N., Lee, L., et al, "Development of a Zero-Gravity Propellant Gaging Flight Experiment for MOL-HSQ Program," Acoustica Associates, Inc., July 1967.
- 3-4 Kinsler, L. E., Frey, A. R., "Fundamental of Acoustics," 2nd Edition John Wiley and Sons, 1962.
- 3-5 Morse, "Vibration and Sound," McGraw-Hill, 1958.
- 3-6 Raytheon Mft. Co., "Investigation of Fuel Quantity Measuring Techniques, for USAF, Air Material Command, Wright-Patterson Air Force Base, Ohio, Waltham 54, Massachusetts, June 1952.
- 3-7 Terman, "Radio and Electronics Engineering," McGraw-Hill, 1962.
- 3-8 General Dynamics Convair Division, "Large Scale Model Evaluation of Propellant Mass Quantity, Air Force Flight Dynamics Laboratory Research and Technology Division WPAFB, Technical Documentary Report No. RTD-TDR-65 Part I, June 1965.

## REFERENCES (Concluded)

- 3-9 General Dynamics Convair Division, Stored Propellant Measuring Techniques Investigation, Air Force Flight Dynamics Laboratory and Technology Division, WPAFB, Technical Documentary Report No. RDT-TDR-65 Part II, November, 1965.
- 3-10 Lockheed Missiles and Space Company, "RF Liquid Level Sensing Technique", LMSC-A 785006, February, 1966.
- 3-11 Ramo, S., Whinnery, J.R., Van Duzer, T., "Fields and Waves in Communication Electronics", John Wiley and Sons, 1965.
- 3-12 Miller, Barry, Aviation Week and Space Technology, "Nucleonic Sensor to Gage Spacecraft Fuel," May 5, 1964, P. 74.
- 3-13. Pfeifer, R.J., Cho, B.Y., Evans, H.J., "Nuclear Techniques for Measuring Propellant Mass Aboard Orbiting Space Vehicles", Industrial Nucleonics Corporation, Columbus, Ohio
- 3-14 Bhuta, P.G., Koval, L.R., "Dynamics of a Gyrogenic Liquid in an Electric Field", Advances in Cyrogenic Engineering, Vol. 12, 1966.
- 3-15 Blackmon, J.B., "Collection of Liquid Propellants in Zero Gravity with Electric Fields," Journal of Spacecraft and Rockets, May-June, 1965, P. 391-398.
- 3-16 Bell Aerosystems Company, "Development of Expulsion and Orientation Systems for Advanced Liquid Rocket Propulsion Systems", for USAF, Rocket Research Laboratory, Space Systems Division, Air Force Systems Command, Edwards, California, Technical Documentary Report No. SSD-TDR-62-172, Phase I, December, 1962.
- 4-1 TRW Systems Report 05952-6116-T000. "Final Report, Service Propulsion System, Propellant Utilization and Gauging System Simulation," January 1967.
- 4-2 TRW Systems Report No. 02831-J008-R0-000, "Exploratory Development of the pV Propellant Gauge," Monthly Progress Report, July 1967.
- 4-3 Price, W.J., "Nuclear Radiation Detection," McGraw-Hill Book Co., Inc., New York, 1958.
- 4-4 McGrath, E.J., "An Analytical Investigation of a Radioactive Tracer Leak Detection Technique", TRW Systems Report No. 07991-6362-R000 January 1967.

## APPENDIX A

This appendix presents a brief description of the brainstorming sessions held during the general survey portion of the Phase I survey. The purpose of these sessions was to efficiently use in-house technical specialists from diverse fields to originate, screen and evaluate proposed ideas. Personnel for these sessions were selected on the basis of demonstrated inventiveness in a variety of fields.

A total of seven sessions was held. At the first session all of the specialists were invited. A survey of known techniques for propellant gauging was presented along with a general discussion of the problems of zero gravity gauging. The system goals, summarized in Table 2-1, were also presented. Five of the remaining six sessions were designed to cover specific areas. Two sessions each were held to discuss electromagnetic radiation and mechanical systems while one session was held on nuclear and chemical systems. However, no attempt was made to limit the discussion to a particular field, as evidenced by the fact that the genesis of the RIGS system occurred during a session on electromagnetic radiation. Approximately 50 new systems were discussed and the more promising are included in Table 5-1. It became apparent that one primary advantage of the brainstorming sessions was the immediate availability of specialists to answer questions concerning feasibility of newly originated concepts. Systems were proposed, analyzed, and critiqued immediately without the need to search out specialists who had the particular knowledge required. As a result, appreciably less time was required for the system evaluation. Between sessions the individual participants critiqued and originated new systems for presentation. The final session was general and those systems which seemed most promising were summarized.

Table A-1 contains a list of most of the participants and their backgrounds.

Table A-1. General Survey Participants and Backgrounds

Name	Current Position	Degree	Specialty	Years of Experience
Ai, D. K.	MTS	PhD	Fluid Dynamics	12
Artusio, T. W.	MTS	BS	Volatile liquids positive expulsion systems, zero-gravity vent system and reaction control propellant feed systems design, development, and analysis	16
Burns, E. A.	Assistant Manager Chemistry Department	PhD	Applied chemistry and propellant technology	23
Bhuta, P. G.	Manager, Advanced Technology Department	PhD	Fluid mechanics, zero gravity problems	16
Decker, R.	MTS	PhD	Acoustics, electromagnetics	14
Grunt, A.	MTS	BS	Chemistry	6
Haefl, A. V.	Director, Physical Electronics Laboratory	PhD	Electronics, acoustics	25
Howell, G. W.	Head, Fluid Component Section	MS	Fluid components and propellants	14
Jones, I. R.	Associate Manager, Nuclear Technology Department	PhD	Radioisotope technology	10
Kane, T. R.	MTS	PhD	Electroptics, radio frequency transmission	18
Kliegel, J. R.	Manager, Propulsion Analysis Department	PhD	Propulsion analysis and technical management	11
Lieberman, S.	MTS	BS	Propulsion and propellant utilization systems performance analysis, and control system component analysis	14
Lipow, M.		BS	Reliability	16
MacLeod, G. J.	Assistant Manager, Propulsion Analysis Department	MEE	Propulsion systems and propellant utilization, and propellant loading systems performance analysis	17
McGrath, E. J.	MTS	PhD	Physics	5
Plebuch, R. K.	Section Head, Nuclear Analysis Section	ScD	Systems analysis, nuclear physics	6
Rudolpi, F.	MTS	MS	Radiation shielding	5
Rusch, R. J.	MTS	MS	Radioisotope applications and nuclear instrumentation	5
Siegel, B.	Project Manager, Propulsion Analysis Department	BS	Propulsion systems design, including hardware development, system analysis, and program management	14
Solomon, L. A.	MTS	PhD	Acoustic wave propagation	5
Spencer, R. B.	MTS	MS	Gauging and propulsion system analysis	4
Vernon, D. W.	Assistant Manager Systems Analysis Department	MS	Systems analysis	11
Wakeman, J. F.	Head, Nuclear Gauging Section	MS	Radioisotope and nuclear applications	9
Webb, R.	MTS	PhD	Heat and mass transfers	5
Wohlwill, H. E.	Associate Manager Electromagnetics and Acoustics Department	PhD	Electromagnetics	21
Zivi, S. M.	Manager, Applied Thermodynamics Depart Department	MS	Acoustics, thermodynamics	20

## APPENDIX B

### MATHEMATICAL MODELS OF THE PHASE SENSITIVE AND RESONANT INFRASONIC SYSTEMS

In this appendix, equations are derived for the behavior of two infrasonic systems. In Section 1 the analysis is performed for the phase sensitive infrasonic system. Section 2 presents the analysis for the resonant infrasonic systems. Descriptions of the two systems can be found in Section 4.1 of this report.

#### 1. MATHEMATICAL MODEL OF THE PHASE SENSITIVE INFRASONIC SYSTEM

##### 1.1 Analysis

The basic dynamic equations for the Phase Sensitive Infrasonic System, illustrated schematically in Figure B-1, are derived below. The nomenclature is defined in Table B-1.

##### 1.1.1 Driver Cavity (No. 1)

From the basic definition of the bulk modulus ( $\beta$ ) of a fluid

$$\beta = \frac{dP}{\left(\frac{dV}{V}\right)} \quad (B-1)$$

For adiabatic gas compression or expansion, we have

$$PV^\gamma = \text{a constant} \quad (B-2)$$

thus

$$\frac{dP}{P} = -\gamma \left(\frac{dV}{V}\right) \quad (B-3)$$

or

$$\beta = -\frac{dP}{\left(\frac{dV}{V}\right)} = \gamma P \quad (B-4)$$

which reduces to the following expression when differentiated with respect to time.

$$-\frac{V}{\gamma P} \frac{dP}{dt} = \frac{dV}{dt} \quad (B-5)$$

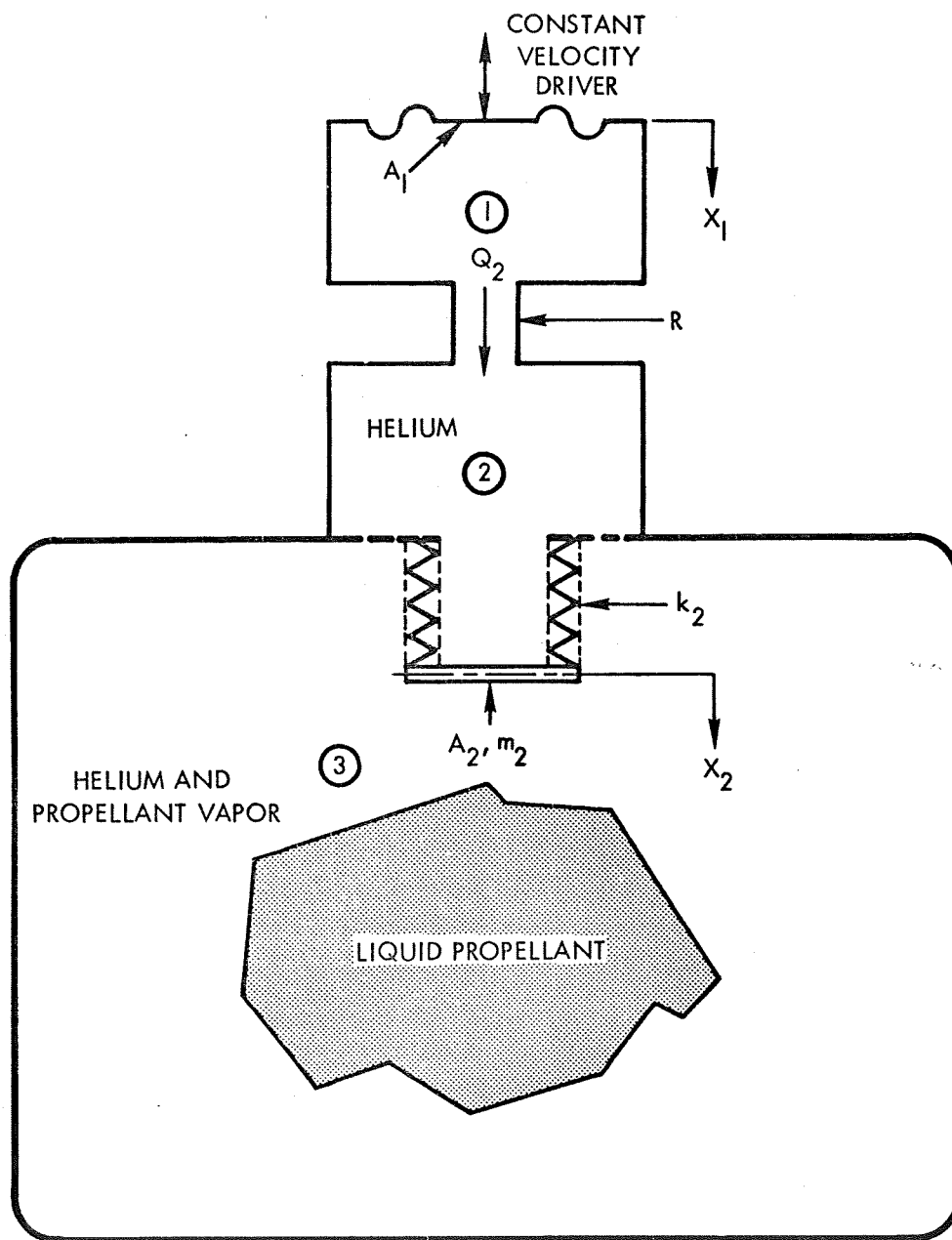


Figure B-1. Schematic of Infrasonic Propellant Gauge



Table B-1. Nomenclature for Appendix B

<u>Symbol</u>	<u>Description</u>	<u>Unit</u>
P	Pressure	psi
V	Volume	in <sup>3</sup>
C	Fluid capacitance	in <sup>5</sup> /lb
Q	Volumetric flowrate	in <sup>3</sup> /sec
Q <sub>o</sub>	Figure of merit for tuned resonant systems	dimensionless
γ	Specific heat ratio	dimensionless
A	Area	in <sup>2</sup>
x	Displacement	in.
$\dot{x}$	Velocity	in/sec
R	Gas flow resistance	lb-sec/in <sup>5</sup>
m	Mass	lb-sec <sup>2</sup> /in.
m'	m/A <sup>2</sup>	lb-sec <sup>2</sup> /in <sup>5</sup>
k	Spring rate	lb/in.
k <sup>1</sup>	K/A <sup>2</sup>	lb/in <sup>5</sup>
w	Weight	lb
s	Laplace notation = $\left(\frac{d}{dt}\right)$	sec <sup>-1</sup>
ω	Angular velocity	radian/sec
f	Frequency	cycles/sec
ρ	Density	lb/in <sup>3</sup>
g	gravitational constant	in/sec <sup>2</sup>
c	Acoustic velocity	in/sec
MW	Molecular weight	lb/mol
T	Absolute temperature	°R

#### Subscripts

- 0 - low frequency anti-resonant condition
- 1 - related to Volume No. 1
- 2 - related to Volume No. 2
- 3 - high frequency resonant condition or Volume No. 3

#### Superscripts

- $\bar{x}$  - nominal quasi-steady-state value of x
- <sup>1</sup> - due to acoustic radiation
- <sup>11</sup> - due to linear damping

This is equivalent to

$$C \frac{dP}{dt} = Q_{in} - Q_{out} \quad (B-6)$$

where

$$C = \frac{\bar{V}}{\gamma \bar{P}}$$

$$Q_{in} - Q_{out} = \text{net flowrate into the cavity}$$

$$\bar{V}, \bar{P} = \text{nominal volume and pressure, respectively, under small perturbations}$$

For cavity No. 1, we can thus write (in Laplace transform notation)

$$C_1 s P_1 = Q_1 - Q_2 \quad (B-7)$$

where

$$C_1 = \frac{\bar{V}_1}{\gamma_1 \bar{P}_1} \quad (B-8)$$

$$Q_1 = A_1 \dot{x}_1 \quad (B-9)$$

and  $Q_2$  is the flowrate through the resistance  $R$  connecting cavities No. 1 and No. 2.

### 1.1.2 Resistance (R)

For small perturbations in  $Q_2$ , the pressure drop across resistance ( $R$ ) can be assumed proportional to the flowrate through it, thus

$$P_1 - P_2 = R Q_2 \quad (B-10)$$

Equation B-15 becomes, by substitution of Equations B-16 and B-17,

$$\frac{m_2}{A_2^2} \frac{dQ_3}{dt} = (P_2 - P_3) - \frac{k_2}{A_2^2} \int Q_3 dt \quad (B-18)$$

Letting

$$m_2' = \frac{m_2}{A_2^2} = \frac{w_2}{gA_2^2} \quad (B-19)$$

$$k_2' = k_2/A_2^2 \quad (B-20)$$

Equation B-18 in Laplace transform notation becomes:

$$\left( m_2' s + \frac{1}{C_{k_2} s} \right) Q_3 = P_2 - P_3 \quad (B-21)$$

where

$$C_{k_2} = 1/k_2' \quad (B-22)$$

#### 1.1.5 Cavity Being Measured (No. 3)

For the propellant cavity No. 3, the net flow in can be expressed as:

$$C_3 s P_3 = Q_3 \quad (B-23)$$

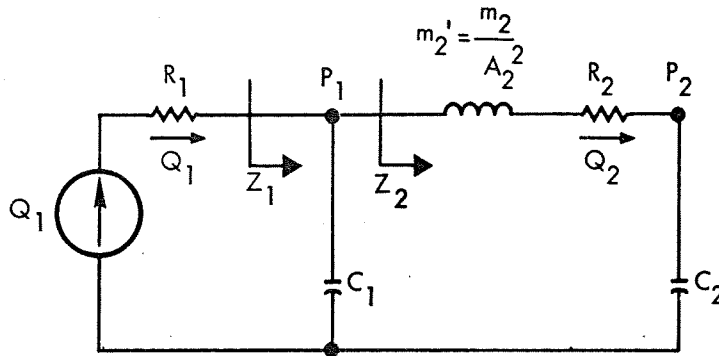
where

$$C_3 = \frac{\bar{V}_3}{\gamma_3 \bar{P}_3} \quad (B-24)$$

and  $Q_3$  has been previously defined in Equation B-13.

### 1.1.6 Derivation of $P_3/P_1$ Transfer Function

The equivalent pressure/flow circuit diagram for the Phase Sensitive Infrasonic System is based on Equations B-7 through B-24. The electric circuit analogy ( $m' = L$ ,  $1/k' = C$ ,  $R = R$ ,  $P = V$ , and  $Q = i$ ) is as follows (Section 3.1):



In order to establish the desired phase relationship between  $P_3$  and  $P_1$ , it is necessary to establish the corresponding transfer function. This derivation follows, based on the combined impedance characteristics of the various circuit loops.

From the circuit diagram above, we can write

$$P_1 = Q_2 Z_1 \quad (B-25)$$

$$P_3 = Q_3 \frac{1}{C_3 s} \quad (B-26)$$

Thus,

$$\frac{P_3}{P_1} = \frac{Q_3}{Q_2} \frac{1}{s C_3 Z_1} \quad (B-27)$$

but

$$Q_2 = Q_3 + C_2 s P_2 \quad (B-28)$$

and

$$P_2 = Q_3 Z_3 \quad (B-29)$$

where

$$Z_3 = s m_2' + \frac{1}{s C_{k_2}} + \frac{1}{s C_3}$$

or

$$Z_3 = \frac{s^2 m_2' C_3 + \frac{C_3}{C_{k_2}} + 1}{s C_3} \quad (B-30)$$

thus,

$$C_2 s P_2 = s C_2 Q_3 \frac{s^2 m_2' C_3 + \frac{C_3}{C_{k_2}} + 1}{s C_3} \quad (B-31)$$

and

$$Q_2 = Q_3 + Q_3 \frac{C_2}{C_3} \left( s^2 m_2' C_3 + \frac{C_3}{C_{k_2}} + 1 \right)$$

which gives

$$\frac{Q_2}{Q_3} = 1 + \frac{C_2}{C_3} \left( s^2 m_2' C_3 + \frac{C_3}{C_{k_2}} + 1 \right)$$

or

$$\frac{Q_2}{Q_3} = \frac{s^2 m_2' C_2 C_3 + C_2 \frac{C_3}{C_{k_2}} + C_2 + C_3}{C_3} \quad (B-32)$$

Equation B-27 becomes:

$$\frac{P_3}{P_1} = \frac{1}{sC_3 Z_1} \frac{C_3}{s^2 m_2' C_2 C_3 + \frac{C_2 C_3}{C_{k_2}} + C_2 + C_3} \quad (B-33)$$

where, from the circuit diagram above,

$$Z_1 = R + Z_2 \quad (B-34)$$

and

$$Z_2 = \frac{1}{Y_2}$$

where

$$Y_2 = sC_2 + \frac{1}{Z_3} \quad (B-35)$$

Thus,

$$Y_2 = sC_2 + \frac{sC_3}{s^2 m_2' C_3 + \frac{C_3}{C_{k_2}} + 1}$$

$$Y_2 = \frac{s^3 m_2' C_2 C_3 + s \left( \frac{C_2 C_3}{C_{k_2}} + C_2 + C_3 \right)}{s^2 m_2' C_3 + \frac{C_3}{C_{k_2}} + 1} \quad (B-36)$$

Now

$$Z_1 = R + \frac{s^2 m_2' C_3 + \frac{C_3}{C_{k_2}} + 1}{s^3 m_2' C_2 C_3 + s \left( \frac{C_2 C_3}{C_{k_2}} + C_2 + C_3 \right)}$$

or

$$Z_1 = \frac{s^3 m_2' R C_2 C_3 + sR \left( \frac{C_2 C_3}{C_{k_2}} + C_2 + C_3 \right) + s^2 m_2' C_3 + \frac{C_3}{C_{k_2}} + 1}{s^3 m_2' C_2 C_3 + s \left( \frac{C_2 C_3}{C_{k_2}} + C_2 + C_3 \right)} \quad (B-37)$$

Equation B-33 finally reduces to the following transfer function between  $P_3$  and  $P_1$ .

$$\frac{P_3}{P_1}(s) = \frac{1}{s^3 m_2' R C_2 C_3 + s^2 m_2' C_3 + sR \left( \frac{C_2 C_3}{C_{k_2}} + C_2 + C_3 \right) + \frac{C_3}{C_{k_2}} + 1} \quad (B-38)$$

which is of the form:

$$\frac{P_3}{P_1}(s) = \frac{\frac{1}{a_o}}{\left( \frac{a_3}{a_o} \right) s^3 + \left( \frac{a_2}{a_o} \right) s^2 + \left( \frac{a_1}{a_o} \right) s + 1} \quad (B-39)$$

where:

$$a_o = 1 + \left( \frac{V_3}{\gamma_3 P_3} \right) \left( \frac{k_2}{A_2} \right) \quad (B-40)$$

$$a_1 = R \left[ \frac{V_2}{\gamma_3 P_2} + \frac{V_3}{\gamma_3 P_3} + \left( \frac{V_2}{\gamma_2 P_2} \right) \left( \frac{V_3}{\gamma_3 P_3} \right) \left( \frac{k_2}{A_2} \right) \right] \quad (B-41)$$

$$a_2 = \left( \frac{w_2}{g A_2} \right) \left( \frac{V_3}{\gamma_3 P_3} \right) \quad (B-42)$$

$$a_3 = \left( \frac{w_2}{g A_2} \right) R \left( \frac{V_2}{\gamma_2 P_2} \right) \left( \frac{V_3}{\gamma_3 P_3} \right) \quad (B-43)$$

#### 1.1.6.1 P<sub>3</sub>/Q<sub>1</sub> Transfer Function

The transfer function between Q<sub>1</sub> and P<sub>3</sub> is derived using similar techniques as above extended to Z<sub>eq</sub>, where

$$Z_{eq} = \frac{1}{Y_{eq}} \quad (B-44)$$

and

$$Y_{eq} = sC_1 + \frac{1}{Z_1}$$

From Equation B-37,

$$Y_{eq} = sC_1 + \frac{s^3 m_2' C_2 C_3 + s \left( \frac{C_2 C_3}{C_{k_2}} + C_2 + C_3 \right)}{s^3 m_2' R C_2 C_3 + s^2 m_2' C_3 + sR \left( \frac{C_2 C_3}{C_{k_2}} + C_2 + C_3 \right) + \frac{C_3}{C_{k_2}} + 1} \quad (B-45)$$



$$\frac{1}{Z_{eq}} = \frac{s^4 m_2' R C_1 C_2 C_3 + s^3 m_2' C_3 (C_1 + C_2) + s^2 R C_1 \left( \frac{C_2 C_3}{C_{k_2}} + C_2 + C_3 \right) + s \left( \frac{C_1 C_3}{C_{k_2}} + \frac{C_2 C_3}{C_{k_2}} + C_1 + C_2 + C_3 \right)}{s^3 m_2' R C_2 C_3 + s^2 m_2' C_3 + s R \left( \frac{C_2 C_3}{C_{k_2}} + C_2 + C_3 \right) + \frac{C_3}{C_{k_2}} + 1}$$

(B-46)

Now,

$$\frac{P_3}{Q_1} = \left( \frac{P_3}{P_1} \right) \left( \frac{P_1}{Q_1} \right) = \left( \frac{P_3}{P_1} \right) Z_{eq}$$

Thus from Equations (B-38) and (B-46)

$$\frac{P_3}{Q_1} = \frac{1}{s \left[ s^3 m_2' R C_1 C_2 C_3 + s^2 m_2' C_3 (C_1 + C_2) + s R C_1 \left( \frac{C_2 C_3}{C_{k_2}} + C_2 + C_3 \right) + \frac{C_1 C_3}{C_{k_2}} + \frac{C_2 C_3}{C_{k_2}} + C_1 + C_2 + C_3 \right]}$$

(B-47)

#### 1.1.7 $Q_3/Q_1$ Transfer Function

The transfer function of  $Q_3$  to  $Q_1$  is easily derived from the previously derived transfer function  $P_3/Q_1$  as follows:

$$\frac{Q_3}{Q_1} = \left( \frac{P_3}{Q_1} \right) \left( \frac{Q_3}{P_3} \right) \quad (B-48)$$

From Equations B-23 and B-47 this reduces to

$$\frac{Q_3}{Q_1} = \frac{1}{s^3 m_2' R C_1 C_2 + s^2 m_2' (C_1 + C_2) + s R \frac{C_1}{C_3} \left( \frac{C_2 C_3}{C_{k_2}} + C_2 + C_3 \right) + \frac{C_1}{C_{k_2}} + \frac{C_2}{C_{k_2}} + \frac{C_1 + C_2 + C_3}{C_3}}$$

(B-49)

## 2. MATHEMATICAL MODEL OF THE RESONANT INFRASONIC SYSTEM

### 2.1 Analysis

The basic dynamic equations for the resonant infrasonic gauging system, illustrated schematically in Figure B-2, are derived below. The nomenclature is defined in Table B-1.

#### 2.1.1 Driver Cavity

For cavity No. 1 (in linearized Laplace transform notation for relatively small perturbations):

$$C_1 s P_1 = Q_1 - Q_2 \quad (B-50)$$

where:

$$C_1 = \bar{V}_1 / \gamma_1 \bar{P}_1$$

$$Q_1 = A_1 \dot{x}_1$$

$$Q_2 = \text{flowrate corresponding to displacement of flexible diaphragm}$$

$$\bar{V}_1, \bar{P}_1 = \text{nominal volume and pressure}$$

$$P_1 = Q_1 R_1 \quad (B-51)$$

where

$$R_1 = \text{effective resistance seen by the driver}$$

#### 2.1.2 Force Balance on Mass ( $m_2$ )

From Newton's equation of motion

$$m_2 \ddot{x}_2 = (P_1 - P_2) A_2 + R_2 Q_2 \quad (B-52)$$

By suitable manipulation, this can be reduced to

$$(m_2' s + R_2) Q_2 = P_1 - P_2 \quad (B-53)$$

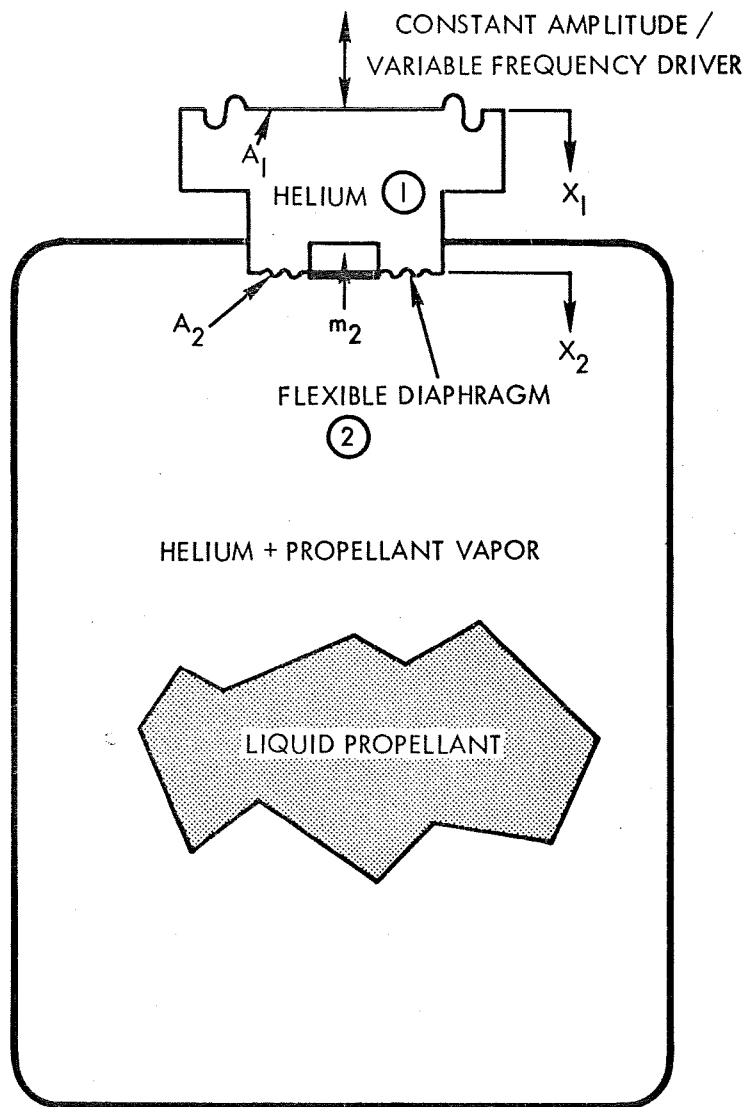


Figure B-2. Schematic of RIGS

where

$$m_2' = \frac{m_2}{A_2} = \frac{w_2}{gA_2}$$

$$Q_2 = A_2 \dot{x}_2 \quad (B-54)$$

### 2.1.3 Cavity Being Measured (No. 2)

For the propellant cavity No. 2, the flow in can be expressed as:

$$C_2^s P_2 = Q_2 \quad (B-55)$$

where

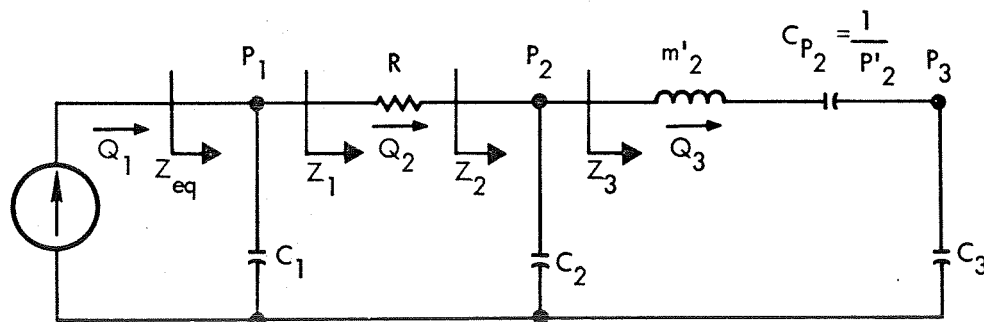
$$C_2 = \frac{\bar{V}_2}{\gamma_2 \bar{P}_2}$$

$$\bar{V}_2, \bar{P}_2 = \text{nominal volume and pressure}$$

## 2.2 Derivation of Transfer Functions

### 2.2.1 $P_1/x_1$ Transfer Function

The equivalent electrical circuit analog corresponding to Equations B-50 through B-55 is sketched below.



In order to establish the amplitude or phase relations between  $P_1$  and  $x_1$ , it is necessary to establish the corresponding transfer function. Based on the impedance characteristics of the above circuit diagram, we can write:

$$\frac{P_1}{Q_1} = Z_1 \quad (\text{B-56})$$

where

$$\frac{1}{Z_1} = s C_1 + \frac{1}{Z_2} \quad (\text{B-57})$$

Now

$$Z_2 = s \frac{m_2}{A_2^2} + R_2 + \frac{1}{s C_2}$$

which can be modified to

$$Z_2 = \frac{\frac{s^2 m_2 C_2}{A_2^2} + s R_2 C_2 + 1}{s C_2} \quad (\text{B-58})$$

Substituting Equation B-58 in B-57, we get

$$\frac{1}{Z_1} = s C_1 + \frac{s C_2}{\frac{s^2 m_2}{A_2^2} C_2 + s R_2 C_2 + 1}$$

which can then be modified by suitable algebraic manipulation to

$$\frac{P_1}{Q_1} = Z_1 = \frac{s^2 \frac{m_2}{A_2} C_2 + s R_2 C_2 + 1}{s(C_1 + C_2) \left( s^2 \frac{m_2}{A_2} \frac{C_1 C_2}{C_1 + C_2} + s R_2 \frac{C_1 C_2}{C_1 + C_2} + 1 \right)} \quad (B-59)$$

but

$$Q_1 = A_1 s x_1$$

Thus, Equation B-59 can be reduced to:

$$\frac{P_1}{x_1} = \left( \frac{A_1}{C_1 + C_2} \right) \left( \frac{s^2 \frac{m_2}{A_2} C_2 + s R_2 C_2 + 1}{s^2 \frac{m_2}{A_2} \frac{C_1 C_2}{C_1 + C_2} + s R_2 \frac{C_1 C_2}{C_1 + C_2} + 1} \right) \quad (B-60)$$

If the system contains no built-in or inherent linear damping, there will still be a frequency sensitive acoustic radiation resistance loss associated with the acoustic pumping. This resistance was evaluated from the following expression obtained from Reference 3-4.

$$R_2 = R_2' = \frac{\rho}{2\pi g c} \omega^2 \quad (B-61)$$

where

$\rho$  = gas density

$c$  = acoustic velocity in the gas =  $\sqrt{\gamma g \frac{1545}{MW} T}$  (B-62)

$\omega$  = angular velocity of the oscillations

MW = molecular weight of gas

For Laplace notation,  $s = j\omega$  for sinusoidal oscillations and Equation B-61 can be equivalently expressed as:

$$R_2' = -\frac{\rho}{2\pi gc} s^2 \quad (B-63)$$

Substituting Equation B-63 into B-60, we get

$$\frac{P_1}{x_1} = \left( \frac{A_1}{C_1 + C_2} \right) \left( \frac{-\frac{\rho}{2\pi gc} C_2 s^3 + \frac{m_2}{2} C_2 s^2 + 1}{-\frac{\rho}{2\pi gc} \frac{C_1 C_2}{C_1 + C_2} s^3 + \frac{m_2}{2} \frac{C_1 C_2}{C_1 + C_2} s^2 + 1} \right) \quad (B-64)$$

This is of the form

$$\frac{P_1}{x_1} = \left( \frac{A_1}{C_1 + C_2} \right) \left( \frac{a_3 s^3 + a_2 s^2 + a_1 s + 1}{b_3 s^3 + b_2 s^2 + b_1 s + 1} \right) \quad (B-65)$$

where

$$a_3 = -\frac{\rho}{2\pi gc} C_2 \quad (B-66)$$

$$a_2 = \frac{m_2}{2} C_2 \quad (B-67)$$

$$a_1 = 0 \quad (B-68)$$

$$b_3 = -\frac{\rho}{2\pi gc} \left( \frac{C_1 C_2}{C_1 + C_2} \right) \quad (B-69)$$

$$b_2 = \frac{m_2}{A_2^2} \left( \frac{C_1 C_2}{C_1 + C_2} \right) \quad (B-70)$$

$$b_1 = 0 \quad (B-71)$$

For any built-in or inherent linear damping, we can express the total damping as:

$$R_2 = R_2' + R_2''$$

where  $R_2'$  is defined in Equation B-61 and  $R_2''$  is the equivalent resistance due to any linear damping on the flexible diaphragm. Equation B-65 still holds in this case; however,  $a_1$  and  $b_1$  are no longer zero, but now become

$$a_1 = R_2'' C_2 \quad (B-68a)$$

$$b_1 = R_2'' \frac{C_1 C_2}{C_1 + C_2} \quad (B-71a)$$

### 2.2.2 Additional Transfer Functions

The following additional derived transfer functions are summarily presented (without derivation) to help in giving further insight into the operation of this system:

$$\frac{x_2}{x_1} = \frac{\left( \frac{C_2}{C_1 + C_2} \right) \left( \frac{A_1}{A_2} \right)}{s^2 \frac{m_2}{A_2^2} \frac{C_1 C_2}{C_1 + C_2} + s R_2 \frac{C_1 C_2}{C_1 + C_2} + 1} \quad (B-72)$$



$$\frac{P_2}{x_1} = \frac{\frac{A_1}{C_1 + C_2}}{s^2 \frac{m_2}{A_2^2} \frac{C_1 C_2}{C_1 + C_2} + s R_2 \frac{C_1 C_2}{C_1 + C_2} + 1} \quad (B-73)$$

$$\frac{x_2}{P_1} = \frac{\frac{C_2}{A_1}}{s^2 \frac{m_2}{A_2^2} C_2 + s R_2 C_2 + 1} \quad (B-74)$$

$$\frac{P_2}{P_1} = \frac{1}{s^2 \frac{m_2}{A_2^2} C_3 + s C_3 R_3 + 1} \quad (B-75)$$

$$\frac{x_2}{Q_1} = \frac{1}{A_2 s} \frac{\frac{C_2}{C_1 + C_2}}{s^2 \frac{m_2}{A_2^2} \frac{C_1 C_2}{C_1 + C_2} + s R_2 \frac{C_1 C_2}{C_1 + C_2} + 1} \quad (B-76)$$

$$\frac{P_2}{Q_1} = \frac{1}{s(C_1 + C_2)} \left( \frac{1}{s^2 \frac{m_2}{A_2^2} \frac{C_1 C_2}{C_1 + C_2} + s R_2 \frac{C_1 C_2}{C_1 + C_2} + 1} \right) \quad (B-77)$$

$$\frac{P_1}{Q_1} = \frac{1}{s(C_1 + C_2)} \frac{\left( s^2 \frac{m_2}{A_2^2} C_2 + s R_2 C_2 + 1 \right)}{\left( s^2 \frac{m_2}{A_2^2} \frac{C_1 C_2}{C_1 + C_2} + s R_2 \frac{C_1 C_2}{C_1 + C_2} + 1 \right)} \quad (B-78)$$